

**SURFACE MODIFICATION OF STIMULI RESPONSIVE POLYMERS BY  
WRINKLING METHOD: SURFACE MORPHOLOGY AND BACTERIAL  
ADSORPTION STUDIES**

by  
Rıdvan Demiryürek

Submitted to the Graduate School of Engineering and Natural Sciences

in partial fulfillment of

the requirements for the degree of

Master of Science

Sabancı University

January, 2014

© Rıdvan Demiryürek 2014

All Rights Reserved

SURFACE MODIFICATION OF STIMULI RESPONSIVE POLYMERS BY  
WRINKLING METHOD: SURFACE MORPHOLOGY AND BACTERIAL  
ADSORPTION STUDIES

Rıdvan Demiryürek

MAT, Master of Science Thesis, 2014

Thesis Supervisor: Assis. Prof. Gözde Özaydın İnce

Keywords: Stimuli responsive polymers, Initiated chemical vapor deposition,  
Surface wettability, Buckling, Bacterial attachment

## Abstract

Stimuli responsive polymers are the great candidates to engineer the surfaces that can switch between different states of surface energy. Integration of those responsive polymers to the systems, where filtration or a controlled adsorption of the microscopic organisms are targeted, offers a very practical and functional pathway. Topographical modifications of these polymers may improve the wettability limits of the smart surfaces and the control over the adhesion of microscopic organisms. In this work, we present a useful method to form 2 distinct sets of surface modified thin films: Poly(N-isopropylacrylamide) [PNIPAAm] and poly(hydroxyethylmethacrylate-co-perfluorodecylacrylate) [poly(HEMA-co-PFA)]. Surface modifications of the thin films are achieved by the initiated chemical vapor deposition (iCVD) of the polymers on stretched poly(dimethylsiloxane) (PDMS) molds in order to provide simultaneous chemical and morphological treatment. The surface properties of the flat and wrinkled thin films are analyzed. Wrinkled PNIPAAm surfaces are also investigated for bacterial attachment activity.

UYARIYA DUYARLI POLİMERLERİN KIRIŞIKLIK METODU İLE YÜZEY  
MODİFİKASYONLARI: YÜZEY MORFOLOJİSİ VE BAKTERİYEL  
BAĞLANMA ÇALIŞMALARI

Rıdvan Demiryürek

MAT, Yüksek Lisans Tezi, 2014

Tez Danışmanı: Yar. Doç. Dr. Gözde Özaydın İnce

Anahtar kelimeler: Uyarıya duyarlı polimerler, Kimyasal buhar çökeltme metodu,  
Yüzey ıslanırılığı, Kırışıklanma, Bakteriyel bağlanma

## Özet

Uyarıya duyarlı polimerler, değişken enerjili yüzeyler oluşturmak için oldukça uygundurlar. Uyarıya duyarlı polimerlerin mikroskopik canlıların filtrasyonu veya kontrollü yapışmalarını amaçlayan sistemlerde kullanılması pratik ve fonksiyonel bir yol sunar. Yüzey modifikasyonları ile bu tarz malzemelerin ıslanma limitleri ve dolayısıyla mikroskopik canlıların yapışmalarının kontrolü geliştirilebilir. Bu çalışmada, poly(N-isopropylacrylamide) [PNIPAAm] ve poly(hydroxyethylmethacrylate-co-perfluorodecylacrylate) [poly(HEMA-co-PFA)] ince filmlerinin yüzey topografilerini modifiye etmek amacıyla kullanışlı bir metot sunulmaktadır. Eşzamanlı kimyasal ve topografik modifikasyonu mümkün kılmak amacıyla, polimer filmler kimyasal buhar çökeltme yöntemi (iCVD) ile önceden gerilmiş poly(dimethylsiloxane) (PDMS) kalıplar üzerine kaplanmıştır. Düz ve kırışık ince filmlerin yüzey özellikleri analiz edilmiştir. Ayrıca, düz ve kırışık PNIPAAm yüzeyleri bakteriyel bağlanma aktivitesi çalışmalarında test edilmiştir.

## Acknowledgements

I would like to thank to **Gözde Özaydın-İnce** as my advisor and **Zehra Sayers** as my co-advisor,

My reading committee **Yusuf Menceloğlu, Fevzi Çakmak Cebeci** and **Burç Mısırhoğlu,**

**TÜBİTAK-BİDEB** MSc scholarship program for funding my graduate education for two years,

**Hazal Büşra Köse** for her extensive biology-related contributions to this thesis,

**My colleagues at our laboratory;** Ali Tufani, Parveen Qureshi, Mariamu Kassim Ali, Efe Armağan, Ömer Karakoç, İlhan Yeşilyurt and Fikri Ege Şengün,

**My friends at Sabancı University;** Çağatay Yılmaz, Fatih Fazlı Melemez, Esat Selim Kocaman, Ataman Deniz, Murat Gökhan Eskin, Dilek Çakıroğlu, Mustafa Baysal, Canhan Şen, Mohammadreza Khodabakhsh, Zeynel Harun Alioğulları, Zekiye Pelin Güven, Shalima Shawuti, Omid Akhlaghi Baghoojari, Oğuzhan Oğuz, Melike Mercan Yıldızhan, Hasan Kurt, Gülcan Çorapcıoğlu, Güliz İnan Akmehmet, Ezgi Dünder Tekkaya, İnanç Arın, Hasan Azgın, Alper Yıldırım, Tolga Yıldırım, Ömer Kemal Adak, Yaşar Tüzel, Furkan Aytugan, Amin Rahmat, Gergely Czukor, Taner Aytun, Ece Alpaslan, Gökay Çoruhlu, Hamidreza Khassaf, Alim Solmaz, Alihan Kaya, Yeliz Ekinci, Çınar Öncel and all those friends from my undergraduate education in Sabancı University,

**My family** for their limitless support and courage during my whole life,

To all of you, Thank you.

Rıdvan Demiryürek

# Contents

<b>Abstract</b> .....	<b>i</b>
<b>Özet</b> .....	<b>ii</b>
<b>Acknowledgements</b> .....	<b>iii</b>
<b>Contents</b> .....	<b>iv</b>
<b>List of Figures</b> .....	<b>vii</b>
<b>List of Tables</b> .....	<b>xii</b>
<b>Abbreviations</b> .....	<b>xiii</b>
<b>Symbols</b> .....	<b>xiv</b>
<b>Introduction</b> .....	<b>1</b>
1.1 Motivation .....	1
1.2 Thesis Outline .....	3
<b>Background and Literature Review</b> .....	<b>4</b>
2.1 Introduction .....	4
2.2 Stimuli Responsive Polymers .....	4
2.3 Material Form .....	5
2.4 Stimuli Responsive Polymers: Applications and Types .....	6
2.4.1 pH Responsive .....	7
2.4.2 Ionic strength .....	8
2.4.3 Field responsive polymers .....	8
2.4.4 Thermoresponsive Polymers .....	9
2.4.5 “Water responsive” Polymer: PHEMA .....	14
2.5 Wettability Studies .....	17
2.6 Buckling as a Surface Modification Method .....	20
2.7 Anti-Fouling Studies .....	25

2.8	Initiated Chemical Vapor Deposition (iCVD).....	28
<b>Experimental Procedure and Characterization .....</b>		<b>32</b>
3.1	Introduction.....	32
3.2	iCVD synthesis .....	32
3.3	Synthesis of PDMS .....	36
3.4	Characterization details .....	40
<b>Analysis of the Flat Thin Films .....</b>		<b>45</b>
4.1	Introduction.....	45
4.2	Flat PNIPAAm Thin Films.....	46
4.2.1	FTIR Discussion.....	46
4.2.2	Surface Topography Analysis .....	47
4.2.3	Contact Angle Studies .....	48
4.3	Flat HEMA-PFA Thin Films .....	51
4.3.1	FTIR results.....	51
4.3.2	Surface Roughness.....	54
4.3.3	Contact angle studies .....	54
4.3.4	Swelling properties .....	56
<b>Wrinkled PNIPAAm and HEMA-PFA Films .....</b>		<b>58</b>
5.1	Introduction.....	58
5.2	Control Experiments: Understanding the Reason of Wrinkle Formation .....	58
5.3	Wrinkling Patterns on PNIPAAm Films .....	60
5.3.1	Uniaxial Wrinkling .....	60
5.3.2	Random Wrinkling Patterns on PNIPAAm Films.....	66
5.4	Wrinkling Patterns on HEMA-PFA Thin Films .....	73
5.4.1	Elastic Modulus Calculations of HEMA-PFA Copolymers .....	73
5.4.2	Elastic Modulus Calculations by SIEBIMM Method.....	73
5.4.3	Uniaxial Wrinkling of HEMA-PFA Copolymers.....	74
5.5	Temperature Response of Uniaxially Wrinkled PNIPAAm Films.....	77
<b>Bacterial Adhesion Studies .....</b>		<b>83</b>
6.1	Introduction.....	83
6.2	Comparing Bare Si wafer and Flat PNIPAAm Films .....	83
6.3	Effect of PNIPAAm Chemical Composition on Bacteria Attachment.....	86
6.4	Comparing Flat PNIPAAm Film and Uniaxially Wrinkled PNIPAAm Films .....	87

6.5	Investigation of the Bacteria Behavior on Uniaxially Wrinkled PNIPAAm Surfaces.....	88
6.6	Investigation of the Bacteria Behavior on Randomly Wrinkled PNIPAAm Surfaces.....	91
6.7	Effect of the Temperature on the Bacterial Attachment Behavior of Wrinkled PNIPAAm Films .....	93
	<b>Conclusion .....</b>	<b>95</b>
	<b>Bibliography .....</b>	<b>97</b>

## List of Figures

Figure 1	Degree of dimensional changes for stimuli responsive polymeric systems in the form of solution, surface, gel and solid.....	6
Figure 2	Water-polymer chain interactions for thermoresponsive polymers in the form of a) solution and b) brush .....	9
Figure 3	Chemical structures of a) poly(N-isopropylacrylamide) and b) ethylene glycol dimethacrylate.....	12
Figure 4	A schematic representation of PNIPAAm thin film coated on Si substrate; a) below LCST and b) above LCST. Red lines, orange arrows and blue dots represent PNIPAAm chains, EGDMA crosslinking and water molecules, respectively.....	12
Figure 5	Molecular structures of HEMA and PFA. ....	15
Figure 6	Surface contact angle on PNIPAAm grafted surface, for low and high temperatures, with respect to different nominal sizes .....	19
Figure 7	Schematic representing the wrinkles forming due to a thin rigid film on an elastic foundation. ....	22
Figure 8	Different types of surface patterns obtained by a) plasma oxidation of heated PDMS sheets, b) zigzag pattern formation through biaxial stretch and release mechanism and c) a simple strain set up and uniaxial wrinkle formation.....	24
Figure 9	Surface patterns on a) a shark's skin and b) PDMS (replicated). ....	27
Figure 10	Schematic representing the polymerization reaction on iCVD stage.....	29
Figure 11	Total picture of iCVD system with important tools indicated. ....	33
Figure 12	An example of the laser-thickness data. The estimated film thickness is approximately 370 nm and the real thickness measured by ellipsometer is 385 nm .....	35

Figure 13	Pictures of a) bare Si wafer, b) conformal PNIPAAm film, and c) heterogeneous thickness over PNIPAAm film. The clear reflections on the surfaces indicate absence of condensation.....	36
Figure 14	Pictures from the different steps of PDMS production; a) agent addition, b) base addition, c) pouring the solution over petri dish, d) bubbles in the solution and e) rigid PDMS mold after baking.....	38
Figure 15	Crosslinking of siloxane oligomer with siloxane crosslinker to form hardened PDMS.....	39
Figure 16	Preparation of PDMS bars for iCVD deposition. For 20% strain the lengths of PDMS sticks a) 4 cm (unstrained) and b) 4.8 cm. ....	39
Figure 17	Schematic showing the wrinkle formation steps on PDMS bars.....	39
Figure 18	Calculation of the film thickness over Si wafer. The thickness for this example is 94 nm.....	41
Figure 19	Ellipsometer system used for swelling experiments.....	43
Figure 20	FTIR spectra for PNIPAAm films of different EGDMA proportions.....	46
Figure 21	An example of the surface scan on a representative PNIPAAm film.....	47
Figure 22	Static contact angle results for PNIPAAm films of various EGDMA ratios (a). Also a representative illustration for the contact angle change by temperature is provided (b). ....	48
Figure 23	Dynamical contact angle results of PNIPAAm films of various EGDMA ratios.....	50
Figure 24	FTIR spectra of poly(HEMA-co-PFA) with varying PFA ratios.....	52
Figure 25	Positions of the bands associated with the O-H stretching frequency of PHEMA as PFA ratio is changed.....	52
Figure 26	Surface roughness results of the copolymer thin films.....	54
Figure 27	Contact angle results of the copolymers.....	55
Figure 28	Swelling degrees of the copolymers for different PFA proportions (a) and the dynamical thickness change for a representative sample having 47% PFA (b).....	56
Figure 29	Optical microscopy images of the PDMS sticks after iCVD treatment. No monomer vapor is fed during the treatment. The surfaces of 2.5% crosslinked PDMS surfaces with the strains a) 10% and b) 0%. ....	59
Figure 30	IR spectrum of PNIPAAm films on Si substrate and PDMS substrate.....	60

Figure 31	Optical microscopy images of uniaxially wrinkled PNIPAAm surfaces. (Film thickness: 130 nm, Film EGDMA ratio: 20%). The crosslink ratios for PDMS samples are a) 2.5%, b) 5%, c) 10%, d) 20% and e) 30%, and i) a representative 3-D image of uniaxial wrinkling.....	61
Figure 32	Wavelength of the uniaxial wrinkles with respect to changing PDMS crosslink ratios. For each film; thickness is 130 nm and EGDMA ratio is 20%.....	62
Figure 33	Wavelength of the uniaxial wrinkles with respect to changing film crosslink ratios. For each film; thickness 130 nm and PDMS crosslinking 2,5 %.....	63
Figure 34	Elastic modulus values of PNIPAAm films calculated by AFM nanoindentation method. The films thickness for each sample is 130 nm. ....	64
Figure 35	Optical microscopy images of the random wrinkling patterns observed on PNIPAAm surfaces (Film thickness 130 nm and EGDMA ratio 20%). PDMS crosslinking ratios; a) 2.5% (20x), b) 2.5 % (100x), c) 5% (100x) and d) 20% (100x).....	66
Figure 36	Wavelength data for randomly wrinkled PNIPAAm surfaces with respect to varying PDMS crosslinking ratio. The films thickness for each sample is 130 nm.....	68
Figure 37	Surface wrinkling patterns at different deposition temperatures; a) 100 °C, b) 113 °C and c) 120 °C. ....	70
Figure 38	Effects of the surface defects on wrinkle distribution; a) disturbance of the wrinkles and b) no effect of the defects. ....	71
Figure 39	Wrinkling pattern of PNIPAAm on a surface modified PMDS mold.....	72
Figure 40	Reduced elastic modulus values of HEMA-PFA copolymers with varying PFA ratios. ....	73
Figure 41	Optical microscopy images of wrinkled copolymers coated on 2.5% crosslinked PDMS sticks. (Film thickness: 200 nm, PFA ratio: 14%, and strain: 5%). a) 20x magnification and b) 100x magnification. White arrows show the direction of strain .....	75
Figure 42	Optical microscopy images of wrinkled copolymers deposited on 2.5% crosslinked PDMS sticks. (Film thickness:1500 nm, PFA ratio: 15%, and strain: 10%). a) 20x magnification, b) 50x magnification and c) 100x magnification. White arrows show the direction of strain.....	75

Figure 43	Wavelength data for wrinkled copolymer films with respect the varying PFA ratio. Film thickness is 300 nm for each sample. ....	76
Figure 44	Contact angle results on uniaxially wrinkled PNIPAAm films; a) topographical effect and b) effect of film EGDMA ratio. ....	77
Figure 45	Hot water treatment on wrinkled PNIPAAm films. FTIR spectra of a) control sample and b) treated sample; optical microscopy images of c) control sample and d) treated sample. ....	79
Figure 46	Elemental nitrogen percentage profile detected by XPS depth etching. ....	80
Figure 47	Imaging of bacteria on microscope glass slides at 2 different magnifications; a) 927.9 x 698.8 $\mu\text{m}^2$ scanning area and b) 155.5 x 84.6 $\mu\text{m}^2$ scanning area. ....	83
Figure 48	Inverted fluorescent microscope images of the surfaces. Washed by NaCl for 1 min a) bare Si wafer and b) 15% crosslinked PNIPAAm flat film; washed by NaCl for 5 min c) bare Si wafer and d) 15% crosslinked PNIPAAm flat film; and e) bacteria accumulation around defects. All measurements are conducted at room temperature. ....	84
Figure 49	Inverted fluorescent microscope images of flat PNIPAAm surfaces; a) 5% crosslinking and b) 20% crosslinking. All measurements are conducted at room temperature. Thickness of each film is around 200 nm ....	86
Figure 50	Inverted fluorescent microscope images of a) 10% crosslinked flat PNIPAAm film and b) wrinkled ( $\sim 5 \mu\text{m}$ wavelength) PNIPAAm thin film (10% crosslinked). All measurements are performed at room temperature. Thickness of each film is around 200 nm. ....	87
Figure 51	Images of bacterial attachment of the surfaces of a) 5% crosslinked bare PDMS, c) uniaxially wrinkled PNIPAAm thin films (10% crosslinked) on 20% crosslinked PDMS, the corresponding the light intensity graphs b) for a and d) for c. Each peak on light intensity graphs represents a single bacterium. All measurements are conducted at room temperature. ....	90
Figure 52	Images of the bacterial attachment on randomly wrinkled PNIPAAm thin film of a) 10 % crosslinking and b) 28% crosslinking. All measurements are performed at room temperature. ....	91
Figure 53	Schematic showing the geometrical considerations regarding bacterial adhesion on a) uniaxially wrinkled and b) randomly wrinkled surfaces. ....	93

Figure 54 Light intensity graphs for bacterial attachment on the surfaces of a) RTTHT sample (0.9  $\mu\text{m}$  wavelength), b) RT sample (0.9  $\mu\text{m}$  wavelength). Film thickness and EGDMA ratio for each film is 130 nm and 15%, respectively ..... 94

## List of Tables

Table 1	List of some of the important thermoresponsive homopolymers and their corresponding LCSTs. [28] .....	10
Table 2	Relationship between the surface roughness and EGDMA ratio for PNIPAAm films.....	48
Table 3	Reduced elastic modulus of PDMS molds.....	60
Table 4	Comparison chart including the elastic modulus values calculated by SIEBIMM method and measured by AFM nanoindentation technique. ...	65
Table 5	Comparison chart including the elastic modulus values calculated by SIEBIMM method and measured by AFM nanoindentation technique. ...	74
Table 6	Swelling fractions for uniaxially wrinkled PNIPAAm films.....	81
Table 7	List of the sample parameters to be studied in this section.....	89

## Abbreviations

<b>PNIPAAm</b>	Poly(N-isopropylacrylamide)
<b>PHEMA</b>	Poly(2-hydroxyethylmethacrylate)
<b>LCST</b>	Lower Critical Solution Temperature
<b>EGDMA</b>	Ethylene glycol dimethacrylate
<b>PFA</b>	Perfluorodecylacrylate
<b>iCVD</b>	Initiated Chemical Vapor Deposition
<b>PDMS</b>	Poly(dimethylsiloxane)
<b>SIEBIMM</b>	Strain-Induced Elastic Buckling Instability for Mechanical Measurement
<b>FTIR</b>	Fourier Transform Infrared Spectroscopy
<b>XPS</b>	X-ray Photoelectron Spectroscopy
<b>AFM</b>	Atomic Force Microscope

## Symbols

$E_s$	Substrate elastic modulus	MPa
$E_f$	Film elastic modulus	MPa
$\bar{E}_f$	Reduced elastic modulus of film	MPa
$\bar{E}_s$	Reduced elastic modulus of substrate	MPa
$\lambda$	Wrinkle wavelength	$\mu\text{m}$
$A$	Wrinkle amplitude	$\mu\text{m}$
$\nu_s$	Substrate Poisson's ratio	
$\nu_f$	Film Poisson's ratio	
$h$	Thickness	nm
$\varepsilon$	Strain	
$\sigma$	Stress	MPa
$P_m$	Monomer vapor pressure	mTorr
$P_{\text{sat}}$	Monomer saturation pressure	mTorr
$\alpha_f$	Film linear thermal expansion coefficient	$^{\circ}\text{C}^{-1}$
$\alpha_s$	Substrate linear thermal expansion coefficient	$^{\circ}\text{C}^{-1}$

*To my family*

# Chapter 1

## Introduction

### 1.1 Motivation

It has always been a great desire that engineering systems maintain the stability of their application-specific properties. Basically many systems are supposed to not to be affected by the environmental changes. A composite component of an aircraft is expected to preserve the mechanical strength against harshest climate conditions and not be broken into pieces in a strong storm. However the great development of science has opened the gate of many brilliant discoveries which motivated scientists to deal with smarter systems and materials. Unlike the body component of an aircraft some systems require a functional transformation under changing environmental conditions. For example; the biological transformation of human lungs in water medium to consume dissolved oxygen would have been a great case. The idea of the functional transformation of a system has resulted in building of engineering designs that can respond differently under different conditions. In this regard a huge work and literature have been gathered in the past decades and especially stimuli responsive-smart polymer systems gained an extensive interest.

Stimuli sensitive polymers are those which can change their properties under a specific trigger such as pH or temperature. Imagining a fiction, a polymeric system would transform from being superhydrophilic to superhydrophobic with a slight change of temperature in the environment. The fascinating point could be that this polymer does not need an external sensor to detect the change and act accordingly. Basically the sensor and the transformation mechanism would be the polymer itself. Polymeric chains can sense the external environmental change and energetic considerations may push the

polymer system to a complete configurational change. With the today's scientific knowledge this imagination becomes real.

Since the discovery of the Lotus leaf it has been possible to create superhydrophobic polymeric surfaces. Hence these surfaces have been widely studied and used especially in self-cleaning systems. However those studies correspond to stable states of the materials and do not satisfy the requirements of a smart system. One would like to have full control over the surface properties of those kinds of materials to design multifunctional and responsive ones. Especially for wettability studies, specifically bacteria adsorption cases, stimuli responsive polymers are the great candidates to have fully anti-biofouling surfaces or a surface that would provide a controlled microscopic organism attachment. In a desalination membrane system one would expect it to filter different kinds of proteins and organisms in different temperature scales. Thinking the variety of the microscopic organisms in water a smart system rather than a stably functioning one would be much more beneficial. Formation of those kinds of systems requires both chemical and morphological modifications. The chemical aspect of the job can be handled with one of the most famous temperature responsive polymers: Poly(N-isopropylacrylamide) (PNIPAAm). The surface energy of this polymer is found to be tuned by temperature change around a characteristic temperature so called lower critical solution temperature (LSCT). The polymer undergoes a phase transition from being hydrophilic to hydrophobic upon temperature change. Another strategy to create smart polymer surfaces is to form molecular level surface heterogeneities. Addition of hydrophobic monomers to hydrophilic ones forms the amphiphilic surfaces. This task can be achieved by the copolymerization of hydroxyethylmethacrylate (HEMA) and perfluorodecylacrylate (PFA). In this regard PHEMA offers a smart polymer which can swell-deswell according to the medium, and PFA can be used as the co-monomer to tune the properties of PHEMA.

Unfortunately it is very difficult, most of the time impossible, to obtain a superhydrophobic or superhydrophilic surface (or a transition between them) with only chemical considerations. Besides, the attachment of the microscopic organisms to surfaces is not only a matter of chemical interaction between them. That brings out the necessity of topographical modifications for these two reasons. For example a sphere shaped bacterium of diameter 100  $\mu\text{m}$  cannot fit into the desalination membrane holes of 10  $\mu\text{m}$  opening. In this regard incorporation of chemistry and morphology can be

achieved in several ways. One would create a patterned surface with one of the many available lithography techniques, and next form a chemical layer on top of that. Another strategy could be the surface modification on an existing layer. Obviously both approaches usually compel two different jobs to be operated one after another. As a more practical method the smart thin film polymers, PNIPAAm and poly(HEMA-co-PFA) in our case, can be coated on specific substrates which also provides a simultaneous morphology change. At this point one would take advantage of the soft elastomeric polymer which has been widely used for topography studies: Poly(dimethylsiloxane) (PDMS). This silicon-based organic polymer can be easily synthesized, controlled and manipulated further to design specific patterns at the surface of the material. Once synthesized the surface modification of PDMS can be achieved simply by a mechanical stretching and following plasma oxidation operation to create a wrinkled surface structure, with no need of lithographic methods. Using the physical reasoning behind this mechanism the same wavy surface structure can be achieved by the mechanical stretching and following polymeric deposition instead of plasma oxidation. This novel method creates the opportunity to deposit polymeric thin films and form a surface topography at the same time.

In light of the above provided information, the motivation behind this work is to synthesize wrinkled polymeric thin films by initiated chemical vapor deposition (iCVD) technique. In regard to the motivation three goals are set: successful deposition of the polymeric thin films, analysis of films and wrinkling patterns, and finally investigation of the wrinkled films for bacteria adsorption studies.

## **1.2 Thesis Outline**

The rest of the thesis is developed as follows. Chapter 2 gives literature summary and state of the art for the chemical and topographical aspects of the study. In chapter 3 the detailed methodology of iCVD technique and PDMS synthesis, and the characterization tools/techniques are described. Chapter 4 deals with the analysis results of the polymeric thin films from chemical perspective. In chapter 5 the wrinkling patterns are presented both numerically and visually in detail. Chapter 6 evaluates the bacterial attachment studies and comparative results are presented. The present thesis provides a concluding summary in chapter 7.

## Chapter 2

# Background and Literature Review

### 2.1 Introduction

In this chapter background information on stimuli-responsive polymers, thermoresponsive polymers, PHEMA based polymers and PNIPAAm will be given. Later on wettability studies related to PNIPAAm will be provided. The surface modification studies for PDMS molds and wrinkling theory are going to be presented. Finally some of the major bacteria-protein adhesion studies regarding PNIPAAm are going to be given.

### 2.2 Stimuli Responsive Polymers

Stimuli responsive polymers can be defined as the type of polymers which can switch their physiochemical properties with respect to an environmental factor. Small external changes may lead to rapid and major changes in molecular level and suddenly polymer's response to the new medium may become drastically different than before. Due to this smart act such polymers are also named intelligent or stimuli sensitive. The signal that triggers the polymer to behave in a different manner can be chemical (pH, ionic concentration, type of chemical agent) or physical (temperature, mechanical stress, light, electrical field, magnetic field) and polymers are named after the type of stimuli such as temperature responsive polymers. Besides the fact that stimuli responsive polymers show an alteration in their conformation, surface state, surface energy or charge state those transitions are mostly recognized as completely reversible [1]. The reversible and smart characteristics of stimuli responsive polymers can also be

combined in different ways. Recent studies have focused on the fabrication and synthesis of polymer systems which are able to respond to more than one external stimulus. Especially combination of temperature sensitive polymers with pH sensitive polymers have given rise to the idea of dual (or multiple) responsive polymeric systems.

### **2.3 Material Form**

An important point regarding stimuli responsive polymers is the form of materials that have been utilized. Mostly usage of stimuli responsive polymers is thought only in the context of polymeric solutions. This assumption is nothing but the demolition of the superior properties of this class of polymers. Many application fields require the use of such polymers as surfaces, micelles, interfaces, gels, films, coatings and even solids [2]. The energetic and entropic mechanisms leading to polymeric response are different for each form.

The basic response mechanism of typical stimuli responsive polymers is the conformational change of the polymer chains. A responsive polymer is expected to show reaction to the proper signal by changing its conformation, as well as maintaining the structural and chemical integrity [3]. The degree and ease of the conformational change are directly related to the mobility of the chains in x, y and z axes. Figure 1 shows the possible dimensional changes for different forms of smart polymers: solutions, surfaces, gels and solids. The degree of freedom for chain mobility is expressed by the length of the axes. Solution polymer systems apparently have the biggest segmental mobility for polymeric chains. Due to the spatial restrictions the chain mobility drastically lowers for the case of polymeric surfaces and becomes even worse for solids [4]. Therefore the energetic requirements and the capacity of the response are all different for each case. Although the work subjected to this thesis deals with the thin film form of the polymers some examples of the solution polymerized responsive polymers are also provided throughout this chapter. Therefore one should always keep in mind the differences highlighted in Figure 1.

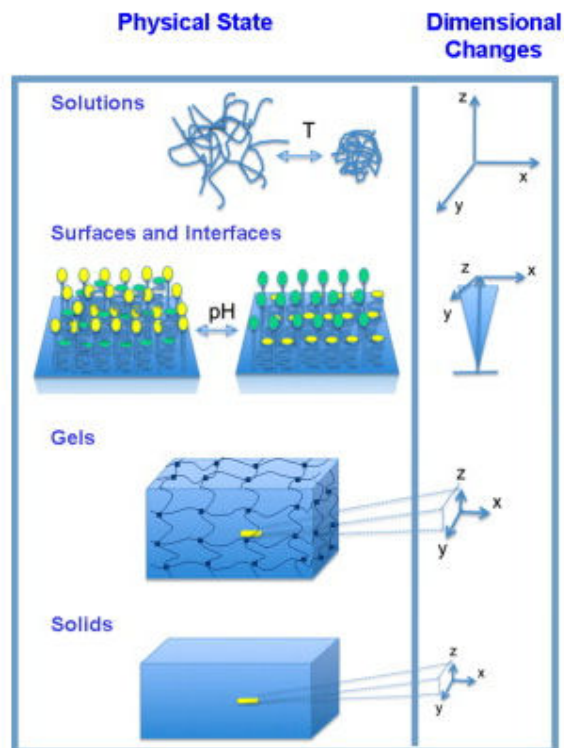


Figure 1: Degree of dimensional changes for stimuli responsive polymeric systems in the form of solution, surface, gel and solid [5].

## 2.4 Stimuli Responsive Polymers: Applications and Types

The classification of stimuli responsive polymers according to the type of stimulus was previously described. Because of the vast variety of the smart polymers many studies related to biological, micromechanical and microelectrical bases have been successfully accomplished. Drug delivery systems [6], separation processes [7], sensors [8], actuators [9], tissue engineering [10], micro fluidic systems [11] and textile products [12] are only a small fraction of existing and potential application areas of stimuli responsive polymers. In the following sections some of the important smart polymer types are going to be discussed together with the major applications and physicochemical mechanisms.

### 2.4.1 pH Responsive

As the name implies pH responsive polymers are able to exhibit different responses under changing environmental pH levels due to the ionizable pendant group in the molecular structure. These weakly ionizable groups can accept or donate proton with respect to the pH degree. At the critical point called  $pK_a$  overall molecular structure undergoes a transition from collapsed state to expanded state and volume of the molecule is increased due to the osmotic pressure. This volumetric expansion occurs because of the change in the net charge of the side groups [13]. In this regard pH sensitive polymers can be classified as polyelectrolytes containing weak acidic or basic pendant groups. The primary difference between pH responsive polymers and strong acids/bases is the difficulty of the ionization of the pendant groups because of the electrostatic forces imposed by adjacent ionized groups [14].

pH-responsive polymers are classified according to type of the pendant groups: weak polyacids and weak polybases. The mechanisms of pH response for two types work oppositely. Weak polyacids are able to show a pH response because of the carboxylic group which can accept protons at low pH and donate protons at high pH level. Therefore at low pH levels ( $<7$ ) the polymer becomes unswollen while it releases the encapsulated water at high pH due to electrostatic repulsion forces exerted by the change of the pendant groups' charge. The most widely studied weak polyacids are poly(acrylic acid) (PAAc), poly(methacrylic acid) (PMAAc) and polysulfonamides [15]. On the other hand weak polybases mostly contain amino and amine functional groups which make the polymer swollen and extended under acidic conditions. Poly(N,N'-dimethyl aminoethyl methacrylate) (PDMAEMA) and poly(2-vinylpyridine) (PVP) are the most well known polybases [16]. High pH conditions lead to strong hydrophobic interactions at the long pendant amine group. Therefore at high pH levels PDMAEMA-like pH responsive polymers transform to hypercoiled conformations. It is also interesting to recognize that PDMAEMA shows also temperature response like PNIPAAm and PDMAEMA is one of the few dual-responsive homopolymers [17].

pH responsive polymers have been widely used for biomedical and chemo-mechanical applications especially in gene carriers, drug delivery systems and glucose sensors. These polymers are very suitable for biomedical applications since the pH value of the human body can vary drastically along with a specific path [18]. Bellomo et al. [19] proposed a new sort of synthetic vesicle that carriers amphiphilic block polypeptides.

Lysine and leucine peptide create the hydrophilic and hydrophobic nature of the system, respectively. This new polymer system have exhibited excellent performance in the drug delivery actuator system and, showed precise and high sensitivity to environmental pH.

As well as the biomedical applications pH responsive polymers have been extensively studied in wettability researches. Yu et al. [20] covered a mixed monolayer of  $\text{HS}(\text{CH}_2)_2\text{CH}_3$  and  $\text{HS}(\text{CH}_2)_{10}\text{COOH}$  over a rough gold surface which is modified by electrodeposition technique . The surface showed excellent superhydrophobic and superhydrophilic character under different pH levels: complete wetting with basic water and contact angle of  $154^\circ$  with acidic water.

#### **2.4.2 Ionic strength**

Due to the changing concentration of the ions some type of polymers can exhibit a phase transition. Since the type of the ion that triggers the phase transition could be numerous there is no specific physical mechanism for ionic responsive polymers. Ghosh and his friends utilized a microporous polyvinylidene fluoride (PVDF) membrane with salt-responsive hydrogel. When NaCl concentration is low polymer macrostructures undergo a phase transition from collapsed state to extended state and therefore closing the membrane pores. As a result this situation decreases the protein permeability though the pores. On the other hand as the NaCl concentration is increased the polymer chains collapse and the pores become completely permeable for protein transmission [21].

#### **2.4.3 Field responsive polymers**

Electric or magnetic field of the environment may turn the polymer structure into swollen, shrunk or bended states. Electrically or magnetically driven motility of the polymers is responsible for the field responsive nature. Such polymers have been widely employed in microelectrical applications such as actuators. It was reported that a polythiophene based conductive polymer actuator expands and contracts according to the applied potential [22].

### 2.4.4 Thermoresponsive Polymers

Thermoresponsive polymers can be considered as the most widely studied stimuli responsive polymers since temperature is an easily controllable and applicable type of stimulus. Temperature responsive polymers mostly have a critical point for phase transition. Lower critical solution temperature (LCST) is the commonly observed phenomena for temperature responsive polymer systems. Below this temperature solution and polymer molecules form one single phase while polymer chains collapse above LCST. The opposite case suggests the presence of higher critical solution temperature (HCST): The polymer is dissolved in solvent matrix above HCST and vice versa below HCST [23]. The phase transition mechanism is driven by the interactions between chains and solvents. For LCST type responsive polymers the intermolecular interactions lead to a single phase solution in which the overall polymer volume is increased due to the solvent intake (mostly water) below LCST. Thermodynamically homogeneous phase of solvent and polymers chains are favored ( $\Delta G < 0$ ) because the enthalpy terms associated with the polymer (mostly hydrogen)-solvent bonding is active for polymer dissolution. However if the medium temperature rises above LCST the intramolecular interactions become dominant and polymer chains collapse expelling water out. The collapse of the polymer comes from the fact that entropic term ( $\Delta S$ ) becomes smaller than enthalpic term and the new unfavorable state forces the system to a phase separation [24]. Such two sided transitions (collapsed-extended, coil-globule, swelling-deswelling) (Figure 2) observed by LCST based polymers are mostly reversible which make them very useful for biomedical applications and micromechanical systems such as on-off sensors triggered by temperature changes.

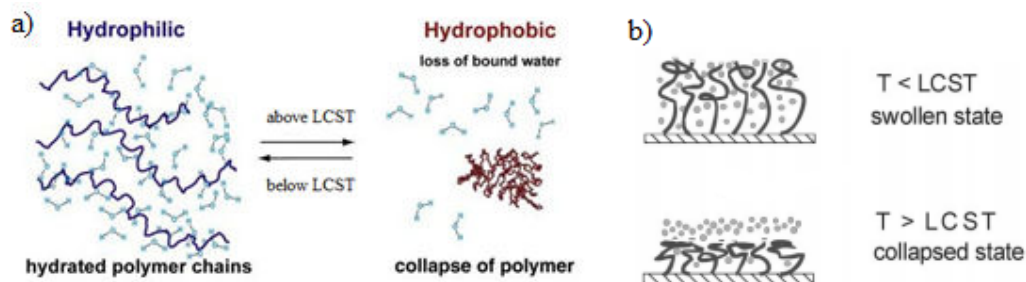


Figure 2: Water-polymer chain interactions for thermoresponsive polymers in the form of a) solution [25] and b) brush [26].

The most famous and extensively studied thermoresponsive polymers based on LCST are in the family of poly(N-substituted acrylamide). Poly(N-isopropyl acrylamide), poly(2-carboxy isopropyl acrylamide), poly(N-(L)-(1-hydroxymethyl) propylmethacrylamide) are some of the thermoresponsive polymers in this group. Mostly amide groups, hydroxyl groups or ether groups are responsible for thermoresponsive nature [27]. Some of the important thermoresponsive polymers and their LCSTs are given in Table 1.

Table 1: List of some of the important thermoresponsive homopolymers and their corresponding LCSTs. [28]

Abbreviation	Name	LCST ( $^{\circ}$ C)
PNIPAAm	Poly(N-isopropylacrylamide)	32
PVCL	Poly(N-vinylcaprolactam)	31
PPO	Poly(propylene oxide)	10-20
PVME	Poly(vinyl methyl ether)	33.8
MC	Methylcellulose	50
EHEC	Ethyl(hydroxyethyl)cellulose	65
PDMA	Poly(2-dimethylamino)ethyl methacrylate)	50
PEMA	Poly(N,N-ethylmethylacrylamide)	70
PNPAm	Poly(N-n-propylacrylamide)	25
PBMEAm	Poly(N,N-bis(2-methoxyethyl) acrylamide)	49
HPC	Hydroxypropylcellulose	42

Type of the functional groups has a big role in response mechanism and the LCST design. Simply LCST of a thermoresponsive polymer can be tuned by the type and number of the functional groups in chain. The balance between hydrophobic and hydrophilic groups determines LCST. If a LCST based thermoresponsive polymer is copolymerized with a hydrophilic polymer the new LCST is commonly observed to be increased and even disappeared. Oppositely, incorporation of a hydrophobic monomer decreases LCST [29]. The physics behind these treatments is related to the balance

between hydrophobic-hydrophilic groups. Apart from copolymerization another technique to tune LCST is to change the end groups of the polymers. This method is especially crucial for polymeric surface applications. Attachment of hydrophilic or hydrophobic moieties to end groups of LCST based polymers can drastically change LCST. For N-substituted poly acrylamides more alkyl groups or more carbon atoms on alkyl side is observed to decrease LCST since attractive intermolecular attractions among alkyl groups overcome hydrogen bonding and polymer becomes insoluble even at room temperature [30]. On the other hand when N-substituted poly(acrylamides) have more ether groups or hydroxyl groups the LCST of the polymer increases due to the increased interaction with polymer and water [31, 32]. Modification of LCST is crucial for biomedical applications. Considering that the body temperature of a healthy human being is 37 °C LCST of PNIPAAm (32 °C) should be modified especially for drug delivery systems.

#### **2.4.4.1 PNIPAAm as a thermoresponsive polymer**

Poly (N-isopropylacrylamide) (PNIPAAm) is one of the well known and widely studied thermoresponsive polymers. Homopolymer and copolymers of PNIPAAm have been successfully integrated into several biomedical, MEMS, wettability applications and separation techniques due to the unique thermoresponsive character. PNIPAAm has LCST of 32 °C at which the polymer molecules change their conformation through a phase transition [33]. Below LCST PNIPAAm amide groups (hydrophilic) form very strong hydrogen bonds with dissociated water molecules. A single phase of the solution undergoes a phase separation above LCST, and precipitation of the polymer molecules create two different phases. The polymer becomes insoluble and hydrophobic in water, forming a collapsed state of the molecules. In this regime single phase solution is energetically found to be unfavorable because the hydrophobic isopropyl groups of the polymer dominate the overall bonding mechanism. Basically the strong intermolecular bonds are replaced with the strong intramolecular hydrophobic interactions above LCST [34]. In literature this change is associated with coil-to-globule transition. The hydrophilic and hydrophobic groups of PNIPAAm are shown at Figure 3-a.

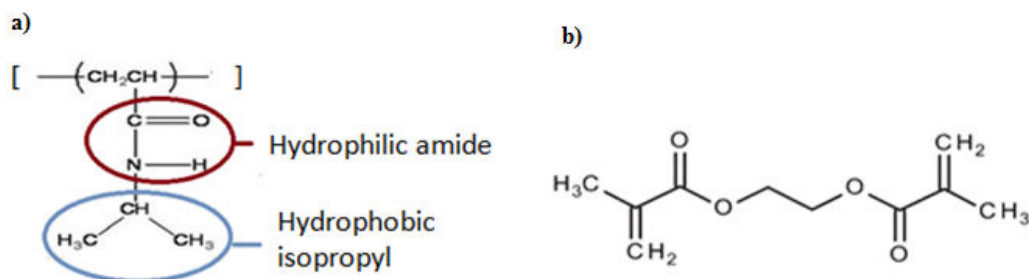


Figure 3: Chemical structures of a) poly(N-isopropylacrylamide) and b) ethylene glycol dimethacrylate.

The coil-to-globule transition is both a thermodynamic and kinetic process. Around LCST the favorable hydrogen bonds between water and amide group of PNIPAAm begin to break. Instead the hydrogen bonding is switched to the molecules between amide groups and carbonyl groups. At the same time the strong interactions between isopropyl groups begin to appear. The molecules in water start entering a new phase in which a continuous dehydration occurs. The decreased pressure inside the molecules due to the intense dehydration causes the PNIPAAm molecules to be entangled. Further heating above LCST causes complete water expelling [35]. The interesting point is that all mechanical and optical properties of the polymer suddenly change. For example the elastic modulus of PNIPAAm micro-gel spheres is calculated as 1.8 and 12.8 MPa below and above LCST, respectively [36].

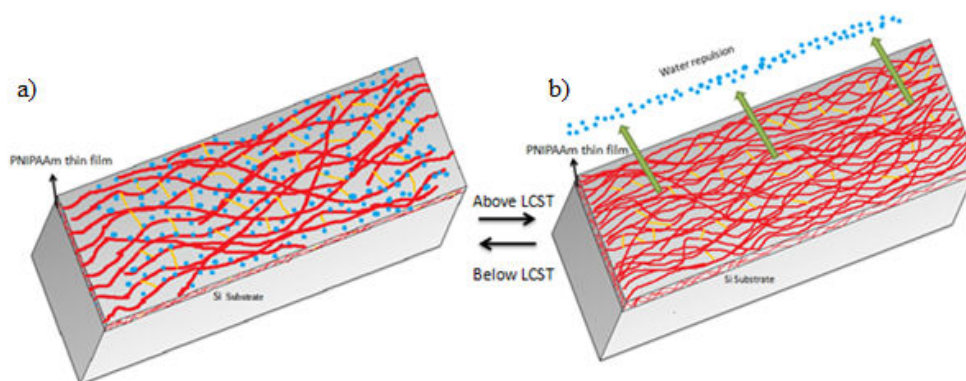


Figure 4: A schematic representation of PNIPAAm thin film coated on Si substrate; a) below LCST and b) above LCST. Red lines, orange arrows and blue dots represent PNIPAAm chains, EGDMA crosslinking and water molecules, respectively.

LCST of pure PNIPAAm (32 °C) is a sharp point where PNIPAAm shows a dramatic volume change. However there exists many ways to manipulate the LCST point and the transition behavior. LCST of PNIPAAm is affected by the molar weight [37], solvent kind, ionic degree of the solution, surfactants and the type of the monomer B for poly(PNIPAAm-co-B) [38]. Very simply any effect which favors the solvent-PNIPAAm interactions increases LCST point and those which supports PNIPAAm-PNIPAAm interactions interrupting the intermolecular bonds decreases LCST. Geever et al. [39] reported that LCST of PNIPAAm hydrogels can be varied between 32 °C and 42 °C by different feeding ratios of 1-vinyl-2-pyrrolidinone (NVP) monomer. A similar study conducted by Xiaomei Ma et al. [40] revealed that LCST of PNIPAAm microgels can be lowered below 20 °C by copolymerization with hydrophobic isopropyl methacrylate (iPMA). A very extensive study published by Patel et al. [41] has shown the effect of the common salts such as NaBr or NaCl and these salts have been reported to be lowering LCST of PNIPAAm hydrogels.

A common problem with PNIPAAm-related applications is the temperature response time of the molecules. Especially for hydrogels response to temperature might be considered as slow [42]. However it is misleading to specify an average time for the sake of reference because the kinetics of coil-to-globule transition is directly related to the chemical nature of the solution and fabrication technique. Nevertheless one can assume that as the size of the hydrogels increases the response rate of the polymer increases as well [43]. Based on this rule several chemical and physical methods can be utilized to tune response time of PNIPAAm. Pore forming agents or porosigen chemicals are observed to be increasing the responsive rate of PNIPAAm. Schild mentioned that incorporation PEG during hydrogel preparation drastically increases the response rate of PNIPAAm since PEG forms a macroporous molecular structure that leads to easier water passage [44]. Formation of mesoporous structure by SiO<sub>2</sub> [45], the freezing technique [46], and incorporation of poly(ethylene oxide) (PEO) as a freely mobile hydrophilic ingredient [47] are just a few of the many methods to increase the response rate of solution polymerized PNIPAAm. Although there are numerous studies related to response rate of solution polymerized PNIPAAm a few published works are present for thin film PNIPAAm's response rate in the literature. Alf et al. [48] reported that a graded PNIPAAm thin film showed extremely fast response. She deposited pure PNIPAAm layer on a PNIPAAm-co-EGDMA thin film by iCVD. QCM-D analysis

showed that the composition variation along the thickness substantially increased the response rate compared to pure PNIPAAm-co-EGMDA thin film.

The discussion given so far has been the general properties of PNIPAAm as a thermosensitive polymer and mostly given within the hydrogel context. Those properties given for hydrogels in water solutions can be applicable to the thin films of PNIPAAm also. Figure 4 provides a schematic on the thermoresponsive mechanism for PNIPAAm thin films. Alf et al. [49] performed a unique study on PNIPAAm thin films which are deposited on silicon wafers. According to the results the LCST of the polymer is measured as 28 °C and swollen film thickness is about 3 times larger than the dry film thickness. Cho et al. [50] deposited a PNIPAAm monolayer on gold surface and transition from hydrophilic to hydrophobic state is observed as a broad peak from 26 °C to 32 °C rather than a sharp point. Another study related to LCST of thin film PNIPAAm showed that the pure PNIPAAm thin film shows a sharp LCST point at 32 °C while copolymerized PNIPAAm (with a vinyl monomer) undergoes the transition within broad peak ( 26 °C-35 °C) [51]. Also in the same study the dry film thickness is found to be approximately 3 times smaller than swollen film thickness.

As a final note PNIPAAm thin films are crosslinked with ethylene glycol dimethacrylate (EGDMA) in order to increase mechanical strength of the films. Having a diester structure EGDMA provides the links between PNIPAAm chains.

#### **2.4.5 “Water responsive” Polymer: PHEMA**

Poly(hydroxyethylmethacrylate) (PHEMA) and PHEMA based hydrogels have been extensively studied and used mostly in biomedical applications such as drug delivery and contact lenses since the first discovery in 1960s [52]. PHEMA and PHEMA based hydrogels provide nontoxic, biocompatible and high swelling properties and therefore functions related to bacteria adhesion, cell growth and molecular separation can be accomplished using thin film form of the polymer [53]. The large scale application areas of PHEMA result from the responsive nature of the polymer. Although it is difficult to put this material into the nomenclature of the commonly used responsive polymers one could name PHEMA a water-stimuli polymer. Basically PHEMA is able to swell in water medium whereas water is expelled in dry medium. Although in the literature PHEMA is considered as hydrophilic monomer the more correct definition

can be expressed in the way that the medium determines the hydrophilicity or hydrophobicity of the monomer.

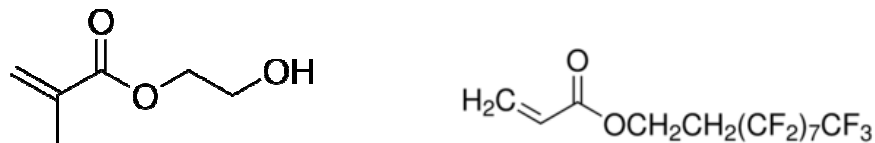


Figure 5: Molecular structures of HEMA and PFA.

PHEMA contains hydrophobic methyl groups and hydrophilic hydroxyl groups in the polymer backbone (Figure 5). Speaking for thin film form of the polymer hydroxyl groups orient outward and make strong hydrogen bonding in water medium. On the other hand when medium is switched from water to air (dry) the outer surface of the film is mostly populated by the hydrophobic groups that are oriented outward. Therefore PHEMA undergoes a transition from being hydrophilic to hydrophobic upon medium change. Chan et al. [54] reported that pure PHEMA thin film shows a contact angle of 37° and 17° in air and water medium, respectively.

Many published studies confirmed that surface properties and swelling characteristics of PHEMA thin films can be tuned by crosslink agents. Generally it has been observed that crosslinking PHEMA thin films decreases the swelling properties while the films are mechanically strengthened [55]. To promote the mechanical strength and engineer the swelling capacity of the polymer crosslinking becomes very essential. In the study conducted by Chan et al. [56] the water content in pure PHEMA is almost 35% while this percentage decreases to 10% after highly crosslinking the polymer with ethylene glycol diacrylate (EGDA). Moreover it has been observed that an opposite relationship is found between crosslinking degree and swelling ratio for different HEMA-EGDA ratios. Besides contact angle results changed in the same manner as well. Another study conducted by McMahon revealed [57] very similar results. Photoinitiated chemical vapor deposition of the PHEMA films crosslinked with EGDA showed poor swelling ratios.

The surface topographies introduced to PHEMA thin films also affects the swelling and contact angle results. The introduction of surface heterogeneities in nano scale is found to improve the swelling properties. Ozaydin-Ince et al. [58] successfully deposited PHEMA thin films crosslinked with EDGA on anodic aluminum oxide (AAO) templates and a nanoforest-type PHEMA thin film structure is obtained. Nanoforest PHEMA thin films provided approximately 70% swelling percentage compared to planar thin films showing 15% water content on average. Also the same study revealed that crosslinking ratio lowers the swelling percentages and increases the overall contact angle. Therefore this study highlights that nano-scale surface structures present on PHEMA thin films may drastically affect the swelling properties. Besides the topographical introductions graded film structures can develop the swelling properties of PHEMA as well. Montero et al. [59] created a graded film composition in which fluorinated monomer pentafluorophenyl methacrylate (PFM) monomer with the thickness of 10-20 nm is deposited above PHEMA thin film layer. This composite structure allows PHEMA to retain its swelling capacity as well as providing PFM to react completely with amines.

It has been a common approach to synthesize copolymers from hydrophilic and hydrophobic monomers. The balance between those monomers showing extremely different surface energies may create an amphiphilic type of film. Besides crosslinking agents and different geometrical implications PHEMA can be copolymerized with hydrophobic or more hydrophilic monomers in order to obtain an amphiphilic copolymer. Ahmad et al. [60] reported that copolymerization of HEMA with N-vinyl-2-pyrrolidone (VP) changes the swelling percentages compared to homopolymer of HEMA. High VP ratio on the copolymer increases the swelling capacity of the copolymer compared to that of low VP ratio (93% to 15%). In another study hydrophobic poly(methylmethacrylate) (PMMA) intraocular lens was modified with HEMA and high contact angle of PMMA ( $76^{\circ}$ ) has been decreased to  $45^{\circ}$  [61]. Also the incorporation of HEMA decreased the concentration of the cell attachment to the contact lens surface due to the hydrophilic nature of PHEMA. That is simply why PHEMA has been widely used for contact lenses and blood cell applications [62, 63, 64] which require hydrophilic-hydrophobic balance.

Choosing a highly hydrophilic and a highly hydrophobic monomer seems pretty reasonable to manipulate amphiphilic type of copolymers. In this regard fluorinated

polymers have very low surface energies [65]. Perfluorodecylacrylate (PFA), which contains a long fluorinated alkyl chain, has a surface contact angle of  $130^{\circ}$  [66]. Therefore copolymerization of HEMA with PFA can be viewed as a wise method to synthesize an amphiphilic type of thin film. It has been shown that the swelling properties and surface morphology of PHEMA thin films can be drastically altered by different proportions of PFA in the copolymer [67].

## 2.5 Wettability Studies

Up until now the general aspects of the thermoresponsive and water-responsive polymers have been analyzed in this thesis. As emphasized many times the idea of stimuli responsive polymeric coatings implies the surfaces that can reversibly change the polymer-specific properties by a triggering signal. The contact angle studies performed for PNIPAAm and PHEMA basically show that the surfaces of these polymers show drastic surface energy changes through environmental changes. In this regard especially PNIPAAm surfaces have been extensively studied for wettability: superhydrophobic surfaces or surfaces that can change between superhydrophilic and superhydrophobic (transitional states between Wenzel and Cassie). Applications related to desalination, self cleaning systems or biofilm prevention may require the polymeric coatings that can vary the surface energy [68]. PNIPAAm polymeric coatings can be considered as one of the most popular candidates to be used in those types of applications.

Before giving some major studies regarding superhydrophobic surfaces and surfaces that can switch between superhydrophobic and superhydrophilic a historical and conceptual background seems beneficial. The wettability studies, specifically self cleaning systems, have been first inspired by Nature's present: Lotus leaf. The presence of microscopical roughness on the surface creates a superhydrophobic structure and the lotus leaf was observed to remain clean [69]. After this great discovery the effect of the surface morphology was better understood and existence of hierarchical or unitary micro/nano scale structures has been considered as the major reason behind the superhydrophobicity. Two basic mechanisms have been proposed in order to engineer the surface morphology: producing a rough surface from a hydrophobic surface or a rough surface being modified as a low surface energy material. For the first category

silicones, fluorocarbons, organic and inorganic material surfaces are being roughened in order to combine morphology and chemistry effects. Teflon (polytetrafluoroethylene) surface was roughened by oxygen plasma and water contact angle of  $168^{\circ}$  was achieved [70]. Lu et al. [71] synthesized a porous superhydrophobic low density polyethylene (LDPE) by controlling crystallization time and nucleation rate. The resulting structure gave a contact angle of  $173^{\circ}$ . For the second category of making superhydrophobic surfaces the mechanism is slightly different. These types of studies require first the creation of roughened surfaces and then the modification of these surfaces by proper materials. Therefore different ways of surface modifications have been predominantly used: Lithography, wet chemical reaction, electrospinning, etching, self assembly by layers, sol gel method, electrospraying, texturing and so on [72]. In a preliminary study polycrystalline metals are etched by acidic or basic solutions. Then these surfaces are treated with fluoroalkylsilane and superhydrophobicity of the surfaces have been achieved [73]. Lithography is a commonly used technique for surface modifications and depending on the patterning mechanism several type of methods are available: e-beam lithography, optical lithography, X-ray soft lithography and so on. Martines and his colleagues performed e-beam lithography on gold surface in order to obtain nanopits and nanopillars. This surface is treated with octadecyltrichlorosilane and water contact angle of  $164^{\circ}$  was achieved [74]. Teashima et al. combined plasma etching and plasma enhanced chemical vapor deposition in order to form a tetramethylsilane coating on nanotextured poly(ethylene terephthalate). The resulting contact angle was about  $150^{\circ}$  [75]. Zen Yoshimitsu et al. [76] fabricated pillar like and groove structures on silicon wafers by simple dicing method. Later on they coated the substrate surface with fluoroalkylsilane. As the roughness factor increased the contact angle of water droplets on the structured polymer surface increased from  $114^{\circ}$  to  $153^{\circ}$ . Öner et al. [77] prepared the topographically structured silicon wafers by optical lithography. Many different size and shapes of posts are created on wafers and the substrate surfaces are coated with hydrocarbon, siloxane and fluorocarbons. The paper suggested that superhydrophobic surfaces can be obtained with this technique and depending on the shape and size of the posts contact angles larger than  $160^{\circ}$  can be achieved. In another study capillary pore membranes of  $240\ \mu\text{m}$  lengths and  $3\ \mu\text{m}$  pore sizes are coated with poly(1H,1H,2H,2H-perfluorodecylacrylate (PPFA). As the porosity and thereby the roughness factor of the surfaces are increased the water contact angle consistently increased from  $121^{\circ}$  to  $151^{\circ}$ . PPFA being already a hydrophobic polymer can behave as a superhydrophobic polymer

on structurally modified surfaces [78]. These studies show that superhydrophobic surfaces can be readily achieved on rough substrates.

Besides superhydrophobic surfaces a limited literature has been built-up for superhydrophilic surfaces and mostly these studies are confined to  $\text{TiO}_2$ . This glass is able to break down the organic materials and impurities by photocatalysis method and due to the superhydrophilicity the broken particles are washed away by water. Many studies have been conducted in order to increase efficiency of  $\text{TiO}_2$  [79, 80].

Those studies given so far basically focus on either superhydrophobic or superhydrophilic surfaces. Depending on the extraordinary results of these studies incorporation of the smart polymeric coatings, which are chemically and topographically modified, can offer smart surfaces that can switch between superhydrophobicity and superhydrophilicity. As PNIPAAm shows drastically different surface energies in low and high temperature regimes one method could be the morphological modification of PNIPAAm surfaces. There have been numerous studies published about the surface energy properties of flat PNIPAAm thin films. Hydrophobic regime contact angle of the polymer can barely exceed  $100^\circ$  [81, 82, 83, 84] and this angle is far beyond to be considered as superhydrophobic. Therefore PNIPAAm surfaces have to be topographically modified in order to increase the hydrophobic contact angle at high temperature scale.

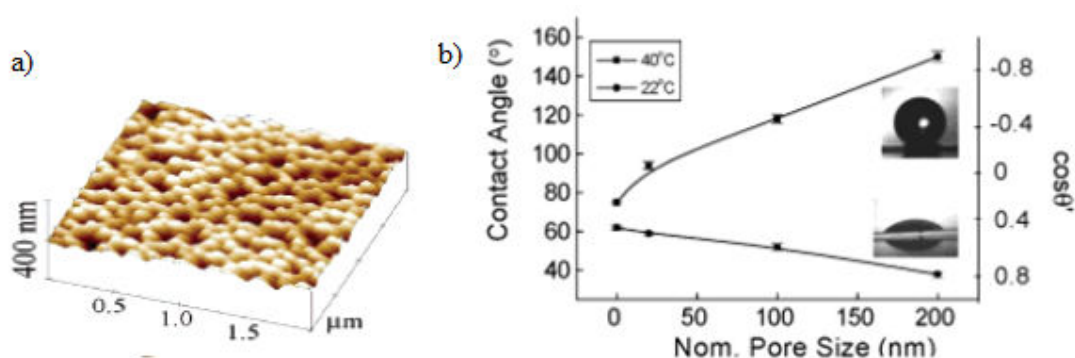


Figure 6: Surface contact angle on PNIPAAm grafted surface, for low and high temperatures, with respect to different nominal sizes [86].

Sun et al. [85] synthesized PNIPAAm on flat and rough silicon substrates using atomic transfer radical polymerization (ATRP) technique. The increase of medium temperature from 25 °C to 40 °C increased the water contact angle from 63° to 93° for flat surfaces. However when the substrate has grooves separated by 6 micrometer from each other and is coated with PNIPAAm the contact angle for room temperature and 40 °C is 0° and 150°, respectively. The combined effect of the chemistry and topography is obviously proven by this study. Another study published by Qiang et al. [86] reported that very similar surface energy results can be obtained using PNIPAAm brush grafted on anodic aluminum oxide membranes by ATRP method. The scientists showed that the water contact angle on nanostructured PNIPAAm brushes increases from 40° to 160° by changing the temperature from 25 °C to 40 °C. The large hysteresis at room temperature and high temperature is dependent on the pore size of the membranes. As the pore size of AAO templates is larger the hysteresis is also found to be bigger (Figure 6). Alf et al. [87] employed chemical vapor deposition and deposited poly(NIPAAm-co-DEGDVE) thin films on flat silicon, nanofiber mats and multiwalled carbon nanotube (MWCNT). The resulting contact angles for low and high temperature measurements are as follows for silicon, nanofiber mats and MWCNT substrates, respectively: 60° and 90°, 0° and 125°, and 50° and 135°. Xia et al. [88] produced a dual responsive polymeric thin film from poly(N-isopropylacrylamide-co-acrylic acid) on flat and rough silicon substrates. According to the results of the study the polymeric thin film is able to respond to both temperature and pH changes in the medium. On the silicon substrate which contained arrays of micropillars the contact angles lower than 10° and higher than 150° are obtained for 20 °C and 45 °C respectively, at pH level 4.

## 2.6 Buckling as a Surface Modification Method

Especially the difficulty and high cost related to the lithography or printing techniques bring out the desire to search easier and more efficient ways of surface modification. In this regard PDMS (polydimethylsiloxane) has been extensively used for surface patterning studies. Creating wrinkles, which appears as the alternating ordered surface structures mostly in sinusoidal shape, has made PDMS one of the most studied materials as substrates for surface modification methods. The formation of wrinkles, the buckling up process, can be observed in daily life on human skin or on a fruit losing water and this phenomenon can be replicated to obtain wrinkled structure on PDMS

surface. The mechanism of the wrinkle formation is simulated as a thin strong layer on a thick soft foundation [89] (Figure 7). The generated compressive force in between top and bottom layers is denoted as [90]:

$$F = E_s \left[ \left( \frac{\pi}{\lambda} \right)^2 \frac{wh^3}{3(1-\nu_s^2)} + \frac{\lambda}{\pi} \frac{E_f w}{4(1-\nu_f^2)E_s} \right] \quad (1)$$

where  $w$ ,  $h$  and  $\lambda$  are the width, thickness of the strong layer and wavelength of the sinusoidal shape, respectively.  $E_s$  and  $E_f$  are the elastic modulus of the foundation and skin layers. When the compressive force between these layers exceeds a critical value,  $F_c$ , the wrinkling occurs:

$(dF/d\lambda)=0$ . The wavelength of the wrinkle is [91];

$$\lambda_c = 2\pi h \left[ \frac{\bar{E}_f}{3\bar{E}_s} \right]^{1/3} \quad (2)$$

$$\text{where } \bar{E}_f = \frac{E_f}{1-\nu_f^2} \text{ and } \bar{E}_s = \frac{E_s}{1-\nu_s^2}$$

The amplitude of wrinkle is formulated as [92]:

$$A = h \sqrt{\frac{\varepsilon_{pre}}{\varepsilon_c} - 1} \quad (3)$$

The wrinkle formation occurs when a compressive stress exceeds a critical one. The mechanism can be described in terms of strain also. When a strain is over a critical level  $\varepsilon_c$ , wrinkles appear and critical strain is found as [93];

$$\varepsilon_c = 0.25 \left( 3 \frac{\bar{E}_s}{\bar{E}_f} \right)^{2/3} \quad (4)$$

When the formulations are analyzed it is observed that the wrinkle wavelength is dependent on the mechanical properties of the materials and the thickness of the film. Degree of strain does not affect the wrinkle wavelength, but amplitude of the wrinkles increases by square root of the initial strain. However one has to keep in mind that these formulations are applicable under these conditions: low strain, substrate being much thicker than the film, film being much stronger than the substrate [94]. New modifications become essential when the mentioned conditions are not obeyed.

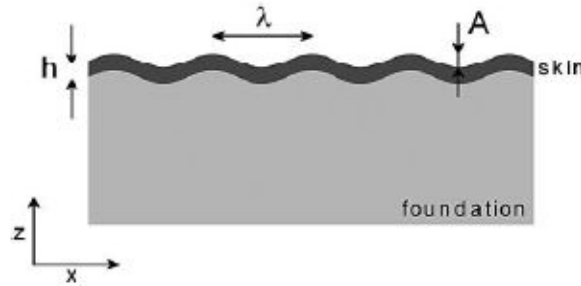


Figure 7: Schematic representing the wrinkles forming due to a thin rigid film on an elastic foundation [95].

The wrinkling studies have been mostly performed using PDMS substrates as the elastic foundations. PDMS is viscoelastic silicon based organic polymer. The biocompatibility, nontoxicity and high elasticity regarding PDMS makes it very useful for a wide range of applications. The ease of procedure to synthesize PDMS with different viscoelastic levels and therefore mechanical strengths is another advantage to employ PDMS especially for surface modification techniques.

Milestone studies regarding the surface modification of PDMS have been initiated by Bowden and the coworkers. Basically two different approaches have been presented in their works. First one is the oxygen plasma treatment to a heated and thereby thermally expanded PDMS [96]. When the samples were cooled to room temperature wrinkles of random and sinusoidal shape are obtained. The idea behind the wrinkle formation is the transformation of the top PDMS part into a hard silica-like layer. The methyl groups of PDMS can readily be replaced by the OH groups and  $O^-$  ions and this part of PDMS is strengthened. During the cooling and shrinking the compressive stress between the top silica like layer and bottom untouched soft PDMS substrate leads to formation of the wrinkles. The system mechanically releases the extra stress by creating a wavy surface structure.

They also showed that the wavelength of the wrinkles is not dependent on the magnitude of the compressive stress. Genzer and coworkers brought a very useful method to arrange the orientation of the wrinkles. In their experimental setup PDMS samples were strained to several lengths and treated by oxygen plasma. The orientation

of the forming wrinkles was perpendicular to the direction of the initial stress, and this method in literature is called uniaxial wrinkle formation [97].

Another type of the study proposed by Bowden was the coating of PDMS substrates with metals by evaporation techniques [98]. Evaporated metals were covered on PDMS substrates at high temperatures and subsequent cooling process creates a compressive stress between metal top layer and bottom PDMS layer upon shrinking. Wrinkles of randomly oriented and separated with a certain distance were observed on PDMS surfaces. Another study performed by Chen [99] revealed that herringbone-type surface structures are also possible. PDMS substrates were pre patterned by a circular depression. Evaporation of gold on heated PDMS and subsequent cooling created a unique type of wrinkling, called herringbone. Huck and colleagues proposed [100] a totally novel approach for PDMS studies. PDMS surface has been patterned by UV treatment using a mask. Some parts of the surface were illuminated and chemically altered after this process. Later on same PDMS sample was heated-gold coated-cooled and a complex wrinkle structure is obtained. This study leads to combining the lithography technique and wrinkle formation method, and created a totally new mechanism.

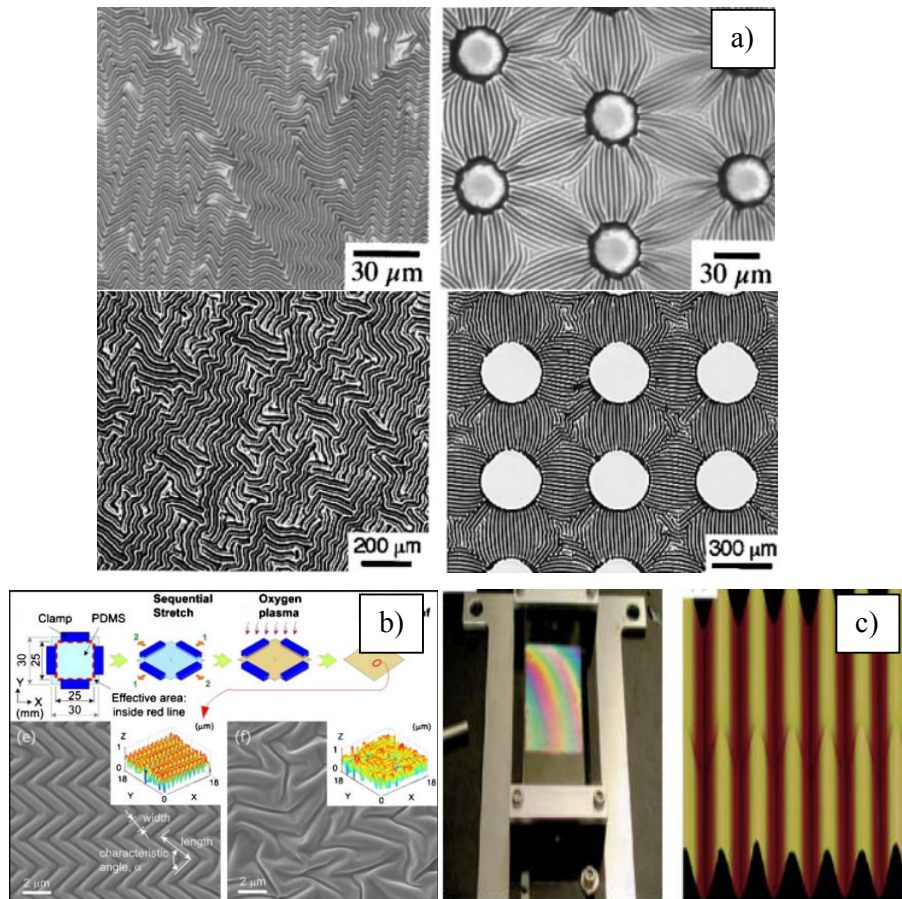


Figure 8: Different types of surface patterns obtained by a) plasma oxidation of heated PDMS sheets [101], b) zigzag pattern formation through biaxial stretch and release mechanism [102] and c) a simple strain set up and uniaxial wrinkle formation [103].

Combining the idea of pre-strain and film coverage a new method was proposed by Harrison and Stafford [104]. First approach presented by them was to place a polymeric thin layer on PDMS. Polyethylene (PE) film was synthesized by spin coating. The films were transferred to PDMS surfaces and, the composite structure was compressed in order to generate compressive stress between PDMS and PE. Later on this method has been improved in the way that PE thin films were transferred to pre-strained PDMS samples. The resulting structure was the uniaxially oriented wrinkles. Later on many researches around the world followed this procedure and polymeric films have been successfully coated on PDMS substrates. The resulting surfaces take advantage of the

polymer chemistry as well as the morphological modification that is achieved by one or the combination of the methods presented so far.

$$\bar{E}_f = 3\bar{E}_s \left[ \frac{\lambda}{2\pi h} \right]^3 \quad (5)$$

Rearranging equation 2 elastic modulus of the film can be calculated using the rest of the parameters (Equation 5). In literature this is called strain-induced elastic buckling instability for mechanical measurement, or SIEBIMM. The preliminary studies have been conducted by the deposition of polystyrene (PS) thin films on PDMS samples [105]. The wavelength of the wrinkles calculated and incorporated in the formula to find the PS elastic modulus. The results have been in good agreement with the values determined by other techniques. Also other groups calculated the elastic modulus of polyelectrolyte multilayer (PEM) using the same technique [106]. Lee et al. [107] employed SIEBIMM method to calculate the elastic modulus of poly(3-hexylthiophene) which is widely used as an active semiconductor material in organic field effect transistors. Keeping in mind that it is costly and difficult to fabricate bulk quantity of such materials this method becomes also useful for the materials used in semiconductor industry. Therefore the wrinkle formation on PDMS surfaces can be efficiently used for determining the elastic modulus values of thin films. Since the mechanical properties of thin films are hard to calculate using massive conventional tensile tests SIEBIMM offers a very simple, inexpensive and relatively fast method for thin film elastic modulus calculations. Besides SIEBIMM studies, wrinkles can be considered as useful for shapeable conductive materials [108] or anti-biofouling systems which is basically the topic of next section.

## 2.7 Anti-Fouling Studies

Fouling could be a major problem damaging the properties of the systems like filtration membranes located in seawater. At some cases controlled attachment of microorganisms might be required. Therefore the understanding of the microorganism-substrate interaction may provide useful tools to prevent fouling or tune the number of adsorbed species [109]. A bacteria or protein approaching a substrate first try to create physical bonds. That may provide a temporary and reversible attachment. The bacterial adsorption in this step is done by the basic physical forces: Brownian motion,

electrostatic interaction, Van de Waals forces. After a certain distance between the bacteria and surface both are negatively charged so that cells are immobilized (physisorption). Later on microorganisms use either their nanofibers or exocellular polymeric enzymes to irreversibly adhere to the surface. In this step the critical energy barrier required for irreversible adhesion is exceeded (chemisorption). In this step a monolayer biofilm formation is observed. Finally the presence of a monolayer biofilm on a surface attracts more microorganisms leading to colonization.

There are three basic strategies to prevent fouling: physical, mechanical and chemical [110]. All those processes are attributed to the different steps of the colonization. Physical defense systems are basically surface modification methods to prevent first the microorganisms adhering to surfaces. Mechanical strategies basically try to detach the adsorbed species. Finally chemical methods include removing the biofilm by chemical processes such as extreme pH levels or toxics.

There are many parameters to be considered in anti-bio fouling processes. Most of the times all the parameters must be accounted in order to prevent the biofilm formation. These basic parameters are the surface energy, surface wettability, surface topography, heterogeneous chemistry (i.e. HEMA-PFA copolymer system), the charge, approaching angle of organism and length of the organism. Once pioneer bacteria or microorganisms attach to the surface further bacteria adhesion is easily activated which leads to biofilm formation at the end. Therefore the smartest strategy for preventing biofilm is to physically stop the attachment at the early steps. That may require a chemically and topographically modified surface in order to have low-fouling properties. In this regard introduction of a surface morphology may hinder bacteria attachment at the first step. Mismatch of the lengths scales of surface patterns and bacteria or the unfavorable sites created on the surface morphology are the keys of this treatment.

One of the milestone studies regarding surface modification to deter fouling is the replication of the shark skin. Naturally shark skin consists of diamond like micrometer scale patterns which create an excellent antifouling surface. Shumacher et al. [111] replicated these patterns using PDMS substrates. Features of same height and width but different lengths have been produced (Figure 9). They continued the experiment by analyzing the attachment of ulva spore, a kind of sea plant. The results suggest that the initial fouling has been stopped 3 times more efficiently than a flat PDMS surface.

Nanogradient forces created at the top of each feature have created a repulsive force for the approaching species and the attachment has been drastically prevented.

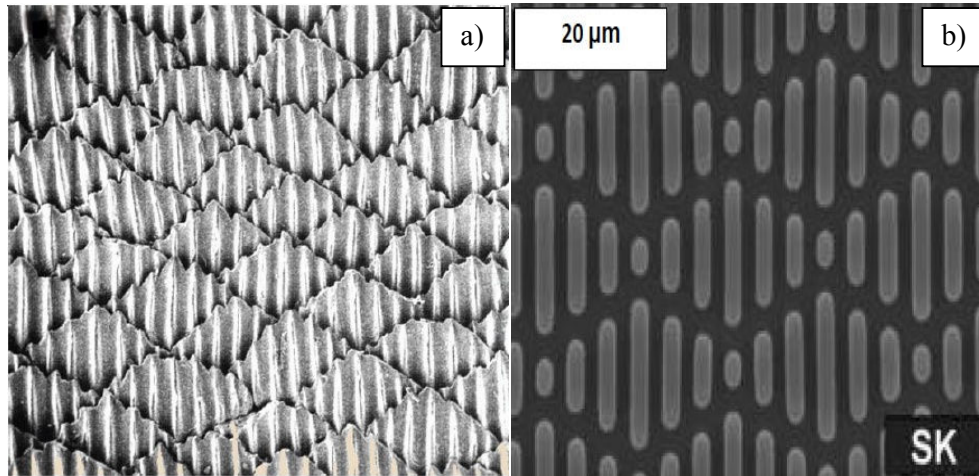


Figure 9: Surface patterns on a) a shark's skin and b) PDMS (replicated) [112].

Efimenko et al. [113] created uniaxially oriented wrinkles on PDMS. Wrinkled and smooth PDMS samples were inserted in sea water and kept there for one month. Attachment of the sea microorganism were analyzed and according to the results wrinkled PDMS surface showed a much better anti-fouling property. However this study also provided the observation of the species in the valleys of the wrinkled PDMS sample. Therefore the wrinkled PDMS cannot be told to be completely anti-biofouler.

The main scope of this thesis is the investigation of the smart polymers. A stimuli responsive polymer, such as PNIPAAm, might be seen as the proper choice for antifouling systems. The initial bacterial or protein adsorption step, which is reversible, is the rate limiting step for fouling process. [114]. Therefore the initial and most important step of fouling depends on the hydrophilicity-hydrophobicity of the surface [115] as well as the surface morphology. The distinct character of PNIPAAm, the hydrophilic to hydrophobic transition, may provide the creation of smart antifouling system. In this engineering architecture temperature changes the surface energy of the polymer and therefore any possible interaction of microorganism with the polymer can be altered. Alf et al. [116] deposited crosslinked PNIPAAm thin films on silicon wafers. The interactions of the polymeric surfaces with bovine serum albumin (BSA) at different temperatures have been analyzed by QCM-D. The data showed that the

attachment of the protein in the solution was increased when temperature rose above LCST. The hydrophobic BSA created a protein film on the polymer surface above LCST since the hydrophobic-hydrophobic interaction between the polymer and proteins were improved. Eun et al. [117] deposited PNIPAAm thin film on gold surface and investigated the interaction between BSA immobilized AFM tip and PNIPAAm thin film. Below LCST almost no interaction was observed while a clear interaction force ( $\sim 0.5$  nN) appeared between the protein and the polymer. Cunliffe et al. [118] prepared PNIPAAm films grafted on amine-functionalized glass substrates. The adsorption of cytochrome c (Cyt C) protein, Salmonella typhimurium gram negative and Bacillus cereus gram positive pathogen bacteria have been analyzed. All microorganisms have attached to PNIPAAm surfaces more when medium temperature was above LCST. They have shown that attachment of proteins and bacteria can be mediated with temperature changes. Ista et al. [119] showed that Staphylococcus epidermidis bacteria would prefer to adsorb to PNIPAA surface when temperature is below LCST unlike the ones presented so far in this thesis.

Therefore based on these consequences it becomes essential to create a smart polymeric surface which is also topographically modified. The wrinkled PNIPAAm surfaces can be considered as a promising candidate for the controlled attachment of living organisms. To test the viability of wrinkled PNIPAAm surfaces escherichia coli k12 (e. Coli) bacteria, which is a gram negative and hydrophilic organism, is selected. Having elliptic shape e-coli bacteria create many ways of chemical attachment tools using several fimbria such as Curli or AIDA. [120]. Therefore that makes these bacteria as one of the most widely observed microorganisms in daily life.

## **2.8 Initiated Chemical Vapor Deposition (iCVD)**

Chemical vapor deposition (CVD) techniques play a crucial role in thin film deposition methods. Thin films of polymers regarding many applications related to biomedical implants, microelectrical and mechanical system devices and membrane separations can be successfully coated by CVD methods. Especially the semiconducting devices which require high chemical purities and preserved electrical properties are better fabricated by CVD rather than liquid methods such as spin coating. Basically CVD systems can be divided into two categories depending on the polymerization type: those based on free

radical polymerization and step growth polymerization. Plasma enhanced CVD, initiated CVD and photo initiated CVD basically work on free radical polymerization principle [121]. Molecular layer deposition (MLD), vapor deposition polymerization (VDP) and oxidative CVD are those in which the step growth polymerization is the primary reaction kind [122].

CVD methods, in common, operate with the reaction of the gas phase molecules. Being all-dry process CVD methods take advantage of that over other solution polymerization techniques. The conformality, maintenance of the thickness over a substrate, can be considerably improved for the samples synthesized by CVD [123]. This way substrates of complex geometries are likely to be deposited with high conformality which is a difficult problem for solution polymerization techniques [124].

Besides high conformality the retention of the functional groups is another major outcome that CVD methods provide since the energy applied through the process remains comparably low [125]. Different types of stimuli responsive polymers were extensively described previously and the fact that the functional pendant groups present in a polymer backbone are responsible for responsive nature was mentioned several times. Therefore the protection of the functional groups makes CVD methods being a correct choice for thin film deposition of responsive polymers. Many types of responsive homopolymers and copolymers with protected functional groups may be deposited as thin films for the purpose of superhydrophobicity, superhydrophilicity, biopassiveness, chemical resistance and improved swelling, and tuning the ratio of the constituent monomers for copolymers can be easily performed [133]. Moreover any side reactions or undesired contaminations are paramountly limited [126].

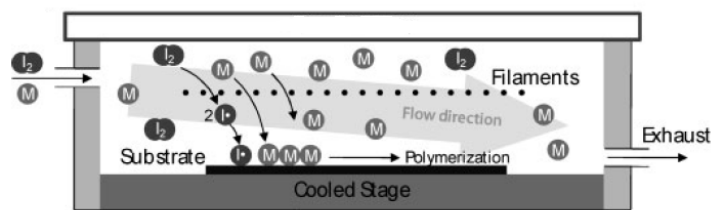


Figure 10: Schematic representing the polymerization reaction on iCVD stage [127].

Initiated chemical vapor deposition technique (iCVD) belongs to hot wire CVD family. The primary differing aspect of iCVD is the initiator molecules decomposing through hot filament wires [128]. Decomposition of initiators creates active radical molecules which meet the adsorbed monomer molecules over a temperature-controlled stage and starts the free radical polymerization (Figure 10). As described earlier iCVD relies on free radical polymerization which follows initiator, propagation and termination steps. In this regard many similarities can be detected between iCVD and free radical solution polymerization. However one of the basic differences is that iCVD method also includes adsorption and desorption of the gas phase monomers over the surface [129].

The decomposition temperature required to break initiator molecules is quite low (200 °C- 300 °C) in order to save the monomer functionality [130]. Since the overall space occupied by the wires is pretty small the heat conduction by radiation to the substrate is minimized. For iCVD systems mostly volatile initiator chemicals are chosen and therefore no extra heating is needed to form vapor pressure. The most widely used initiators are tert-butyl peroxide (TBPO), triethylamide (TEA), perfluorooctane sulfonyl fluoride (PFSF) and tert-amyl peroxide (TAPO) [131]. Moreover the increase of the initiator concentration also increases the overall reaction rate [132].

As emphasized many times iCVD is a completely gas phase process. Monomers are required to be heated to certain temperatures in order to produce vapor pressures. These vapor molecules of monomers must be adsorbed on the sample stage and experimental results suggested that adsorption step is the rate limiting step [133]. The temperature of the substrate directly affects the reaction rate; as stage temperature decreases the absorption rate of the monomers increases. Moreover the low substrate temperature associated with iCVD provides almost any kind of substrates to be deposited with polymer thin films.

Tuning the amount of monomers or ratio for more monomers can readily be done by iCVD using practical  $P_m/P_{sat}$  concept (monomer vapor pressure/saturation pressure) [134].  $P_{sat}$  is the maximum vapor pressure that a specific monomer can possess at a given temperature. Using the saturation pressure for room temperature or boiling temperature (or any two characteristic temperature) saturation pressures for a specific substrate temperature can be calculated by Clausius-Clapeyron relationship. On the

other hand  $P_m$  is directly related to the monomer flow rate and calculated by the given formula below:

$$P_m: (\text{Monomer flow rate/Total flow}) * \text{Total pressure}$$

Therefore changing the monomer flow rate or total pressure  $P_m$  becomes directly and easily controllable especially for copolymer depositions.

The ratio of  $P_m$  over  $P_{sat}$  becomes a very useful tool to determine the rate of the reaction and ratio of the reactants (i.e. A/B for AM copolymer). Comparing the  $P_m/P_{sat}$  for two different monomers the ratio of the monomers in the polymer can be roughly estimated. Besides increase of  $P_m/P_{sat}$  rises the overall reaction rate and average molecular weight despite the decreasing conformality [135]. Another useful aspect of  $P_m/P_{sat}$  is that any new monomer can be theoretically checked if it is suitable for iCVD deposition. If a new monomer establishes  $P_m/P_{sat}$  between 0.1 and 0.8 at the moderate pressure and temperature values that monomer is told to be coherent for iCVD depositions since;

Liquidification of vapor phase monomer molecules occurs when  $P_m/P_{sat}=1$  and,

Insufficient surface concentration of monomers leads to very slow or no reaction when  $P_m/P_{sat}<1$ .

Experimental observations revealed the fact that  $P_m/P_{sat}<0.8$  rather than 1 is more useful consideration. Local cold points in the system chamber are likely to appear due to Joule-Thompson effect. Therefore the upper limit of  $P_m/P_{sat}$  is better to be put below 1.

## Chapter 3

# Experimental Procedure and Characterization

### 3.1 Introduction

This chapter includes the details of the iCVD deposition of the films on silicon wafers and PDMS samples. The preparation of PDMS molds are going to be described. Moreover the characterization details regarding FTIR, water contact angle, profilometer, AFM, ellipsometer and XPS will be provided. Finally the procedure of bacteria adhesion studies will be given.

### 3.2 iCVD synthesis

The iCVD system that is used is simply a home-modified plasma vapor deposition chamber of 20 liters. The system overall includes a chamber, monomer pipeline, monomer and initiator jars, pressure controller, pump, laser system, temperature controllers for monomer jars and sample stage (Figure 11). Monomer pipelines and chamber are always heated since it prevents attachment of residue monomer vapors to the inside walls of the system. Monomer pipelines and chamber is heated to 110 °C and 50 °C, respectively. Heating is provided by cotton heating tapes (Omegalux) which are tightly surrounded by aluminum foil which functions to prevent heat loss to the environment and provide a homogeneous heat distribution. The power supplied to the heating tapes is provided by variable autotransformers (Staco Energy).

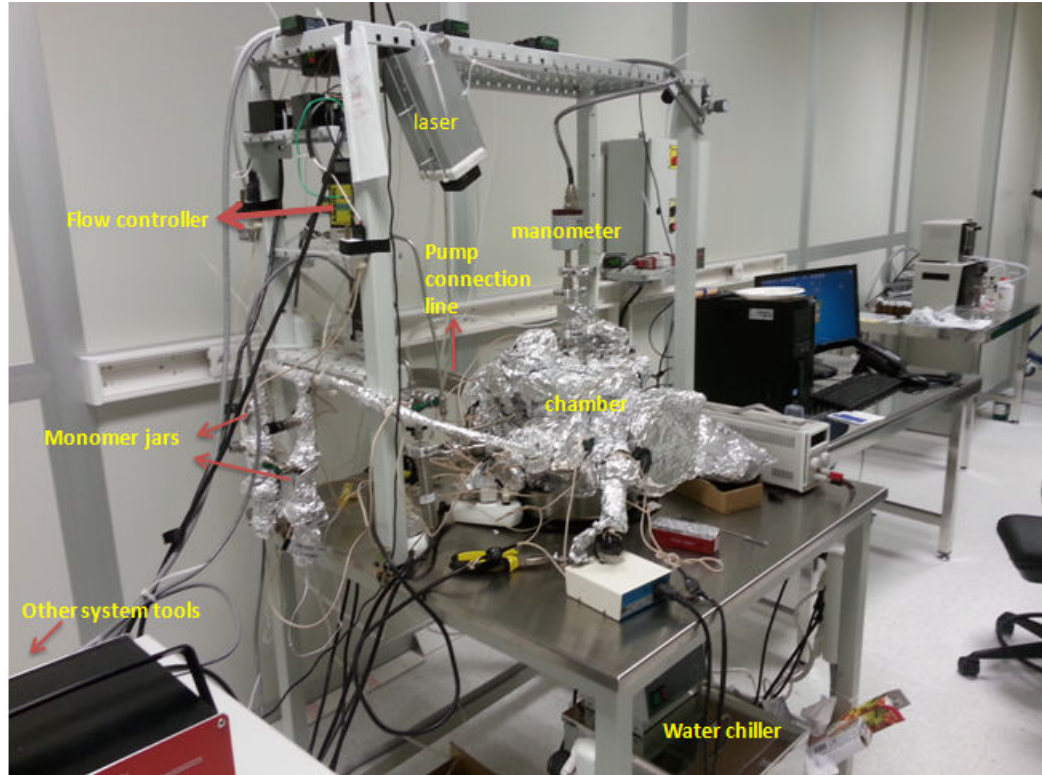


Figure 11: Total picture of iCVD system with important tools indicated.

Water chiller (LabO) controls the stage temperature where samples are located on. Basically the stage temperatures can be changed from 25 °C to 60 °C. System pressure is measured by capacitance manometer (MKS) and displayed by pressure controller (MKS 600). Pressure can be controlled by either manually (Edwards, Speedivalve) or by the butterfly valve (MKS). Filaments which are placed right above the sample stage are used for the decomposition of initiator molecules to radicals. The filament temperature is separately controlled by a power supplier (Sorensen, Ametek) which simply powers the wires. Flow rates of nitrogen and initiator are automatically controlled by mass flow meters (Aalborg). Laser system (JDSU, HeNe) is used for the in-situ observation of film thickness. However that is not a precise control over the thickness, but rather a rough estimate.

At the default position the system is always kept under low vacuum conditions. In such systems it is always probable to have some amount of air leak going through the

chamber. Leak decreases the base pressure of the iCVD chamber and may cause contaminations during the synthesis which at the end decreases the film quality. Before starting a deposition existence of leak is always checked and flow rate is determined if exists. Leak is measured by closing the pump connection and finding the pressure increase with respect to the time. The resulting leak is later subtracted from the flow rates of monomers, nitrogen and initiator.

Following procedure includes the calculation of monomer, nitrogen and initiator flow rates. Solid NIPAAm (Aldrich, 97%), liquid EGDMA (Aldrich, 98%), HEMA (Aldrich, 99%), PFA (Aldrich, 97%) are heated to 75 °C, 85 °C, 80 °C and 85 °C, respectively. Monomers are heated in order to obtain sufficient vapor pressure, and heating must start at least 1 hour before the calibration step. Another critical note to keep in mind is that monomer vapor temperatures must be always lower than the monomer pipeline temperature. Thermodynamics states that material in vapor phase adsorbs to “colder” surfaces. Therefore condensation of monomer vapor is prevented if the monomer temperature is kept lower than the pipeline temperature. The idea behind calculating flow rate of the vapor phase monomers is same as the calculation of the leak. When the system is at the base pressure each monomer valve (Swagelok) is separately opened and pressure increase with time is measured. The process is conducted individually for NIPAAm, EGDMA, HEMA, PFA, nitrogen and TBPO (Aldrich, 70%) For the standardization of samples, NIPAAm flow rate is kept constant (0.6 sccm) and EGDMA flow rate (0.01-0.1 sccm) is tuned by the turning valves. In the similar way the flow rates of HEMA (0.6-1 sccm) and PFA (0.05-0.3 sccm) are changed accordingly in order to obtain the estimated monomer ratios. The details of  $P_m/P_{sat}$  were given in the chapter 2.

Considering that iCVD is a radical polymerization method initiator amount affects the polymer chain lengths and reaction rate. Therefore TBPO flow rate is kept constant at 1 sccm to eliminate the effect of this parameter. In iCVD depositions nitrogen acts as diluter in the system. Because it does not affect the film properties nitrogen flow can be changed to tune the  $P_m/P_{sat}$  ratio of the monomers. Another parameter for the polymer synthesis is the sample stage temperature. At the earlier trials of PNIPAAm depositions different stage temperatures have been tried. Temperatures lower than 40 °C have always been problematic because it was observed that NIPAAm vapor was directly crystallized at the walls of the system. For this reason PNIPAAm depositions are

operated at 40 °C stage temperature. For poly(HEMA-co-PFA) depositions the stage temperature is fixed to 30 °C.

Having calibrated gas flow rates and heated the stage a small piece of Si wafer (Wafer World) placed right over the sample stage. Laser beam must fall on the sample and be reflected back to the detector. Because the sample stage area is big enough many samples can be deposited at the same time and with almost same film properties. After the chamber door is closed it is important to wait for the system to come to base pressure again.

Further on nitrogen and initiator are fed into the system. Monomer valves are opened in order for the vapors of the monomers to reach the system chamber. Afterwards filaments are heated gradually to 250 °C. Generally PNIPAAm thin films are deposited around 300-350 mTorr while pressure vary between 100 and 300 mTorr for HEMA-PFA copolymer deposition. After each parameter is set up the free radical polymerization reaction begins which is detected from the laser data profile. The thickness of the film and the rate of reaction can be monitored by the laser system software in-situ. Basically the system (633 nm HeNe laser source, JDC uniphase) is a laser reflection interferometer that measures the periodic interference of light waves with the growing film. In-situ observation of the synthesis allows the experimenter to interfere the system when necessary. An example of thickness profile is given at Figure 12.

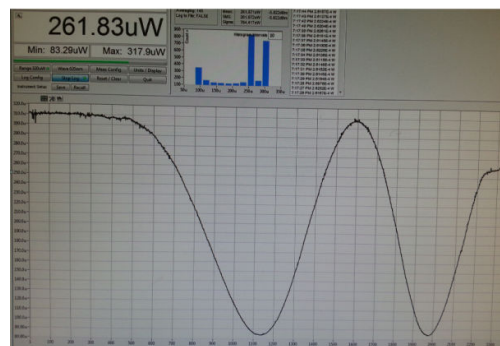


Figure 12: An example of the laser-thickness data. The estimated film thickness is approximately 370 nm and the real thickness measured by ellipsometer is 385 nm.

When the film thickness comes to the targeted value the monomers are closed first. One should wait for a few minutes for the residue monomer vapor to be sucked by the pump. Later on initiator valve is closed and a few minutes waiting time is provided since the residue initiator molecules continue to react on the stage. Filament temperature is decreased gradually and pump valve is fully opened. The system must go back to base pressure. When system arrives the base pressure nitrogen is closed as well. The polymer deposited sample can be taken out from the chamber. Examples of polymer coated wafers are provided in Figure 13.

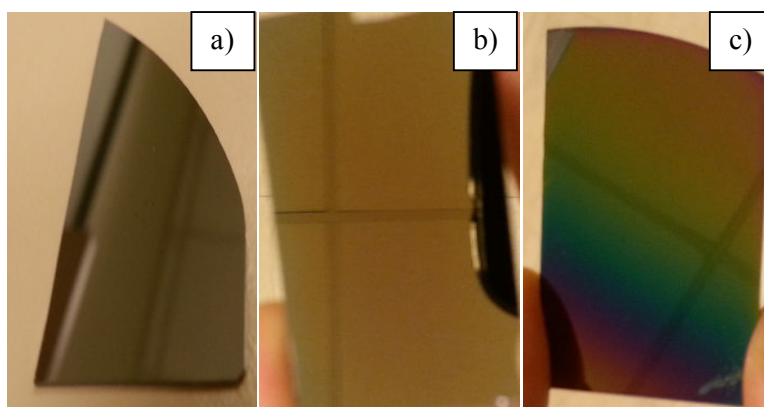


Figure 13: Pictures of a) bare Si wafer, b) conformal PNIPAAm film, and c) heterogeneous thickness over PNIPAAm film. The clear reflections on the surfaces indicate absence of condensation.

### 3.3 Synthesis of PDMS

Wrinkled polymer thin films can be produced by the deposition of the polymer thin film on strained PDMS surfaces. PDMS is synthesized from the kit (Dow Corning's Sylgard 184) which contains both agent and base chemicals. In the raw form PDMS is a highly viscous liquid. Therefore the agent, crosslinker material, has to be added into the base for structural rigidity. Different compositions of the agent and base materials will produce PDMS samples with different mechanical, optical and elastic properties. The amount of the crosslinker determines to what extent PDMS is going to be strong and elastically can be stretched.

PDMS synthesis begins with the careful adjustment of the agent-base ratio. Agent material with the defined amount is poured into a container on an electronic weighing machine. Then base chemical with the proper amount is added over crosslinker and the solution is mixed well enough. Good mixing provides uniform distribution of crosslinker which at the end affects the homogeneity of the solid PDMS. Mixing step should take at least 10 minutes. Later on 5 gr of solution is poured over a plastic petri dish (diameter: 8.7 cm). In this thesis 5 gr of solution is fixed in order to obtain same thickness for solid PDMS. Considering the size of the petri dish 5 gr of solution produces 1 mm thick samples. The final mixture in the petri dish is filled with the air bubbles which come from the mixing procedure. The solution is then put into a vacuum furnace to eliminate the forming bubbles before curing step. Solution is observed to be cleared of bubbles approximately in 30 minutes. When bubbles are completely removed the solution becomes ready for curing. PDMS mold is baked at 60 °C for 2 hours. Curing agent crosslinks the bonds of base chemical with the aid of heat. An important note here is that the curing time and temperature drastically affect the mechanical properties of PDMS [136]. Therefore curing time and temperature is kept constant in this project. Once baking step is over PDMS mold is carefully taken out from the petri dish. The overall procedure is given with the pictures in Figure 14. Sample is then cut into the smaller bars with sizes of 5 cm x 0.5 cm.

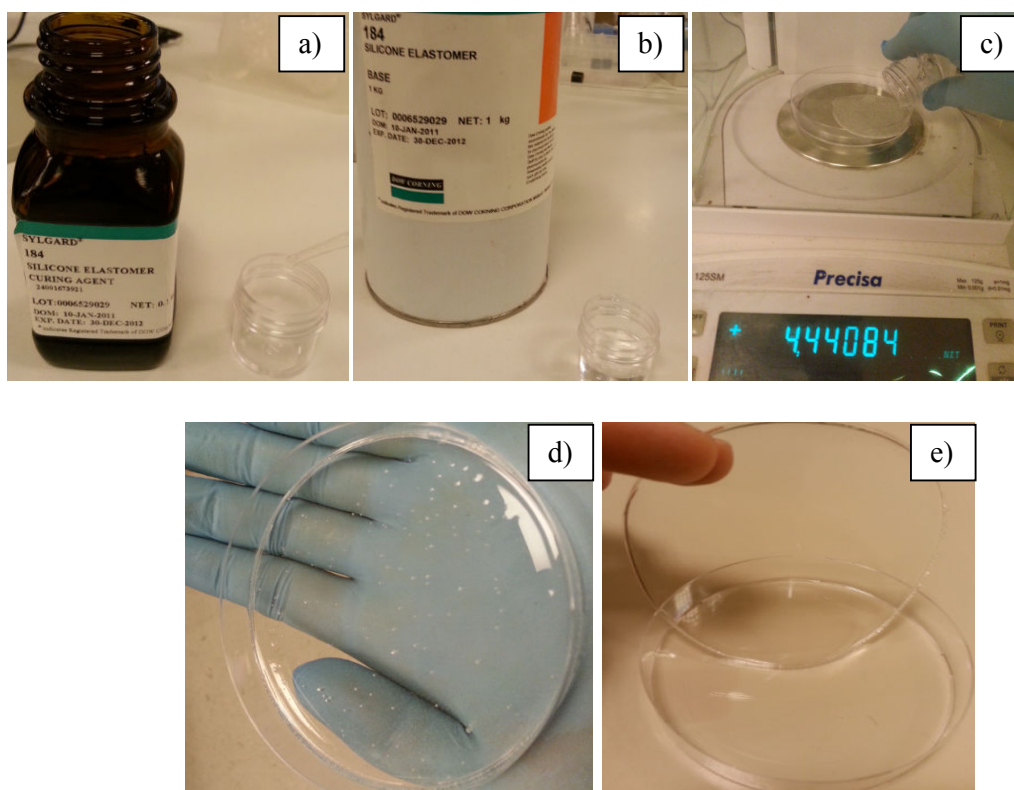


Figure 14: Pictures from the different steps of PDMS production; a) agent addition, b) base addition, c) pouring the solution over petri dish, d) bubbles in the solution and e) rigid PDMS mold after baking.

The crosslinking scheme of PDMS is depicted in Figure 15. Crosslinking of PDMS is achieved by the  $\text{Si-CH}_2\text{-CH}_2\text{-Si}$  bonding formed between the vinyl groups of the oligomer and  $\text{SiH}$  bonds of crosslinker. The bond linkage between two materials is facilitated by the platinum-based catalyst which is present in the base chemical.

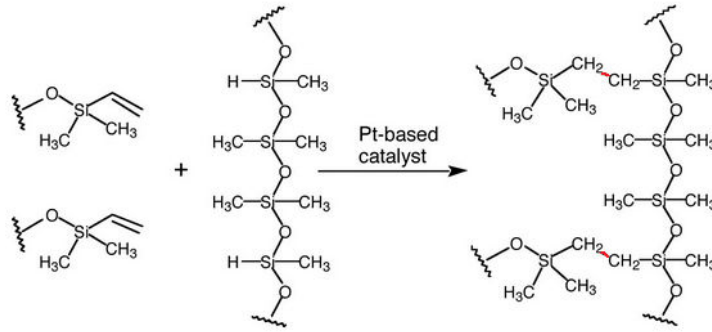


Figure 15: Crosslinking of siloxane oligomer with siloxane crosslinker to form hardened PDMS [137].

Clamps are used in order to hold the stretched PDMS bars. 2 of bars are put over big microscopy slides. 0.5 cm from each end of PDMS is being used for clamping area, which leaves 4 cm of PDMS length to be strained. An example of the procedure is depicted in Figure 16.

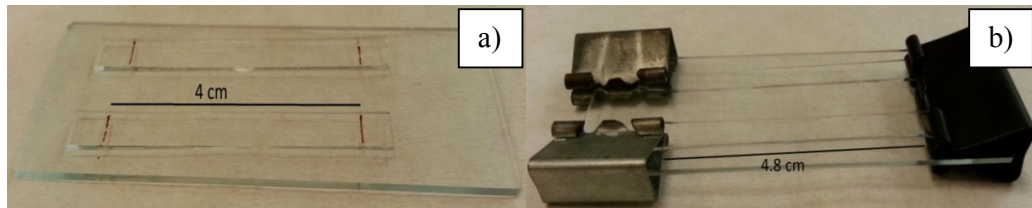


Figure 16: Preparation of PDMS bars for iCVD deposition. For 20% strain the lengths of PDMS sticks a) 4 cm (unstrained) and b) 4.8 cm.

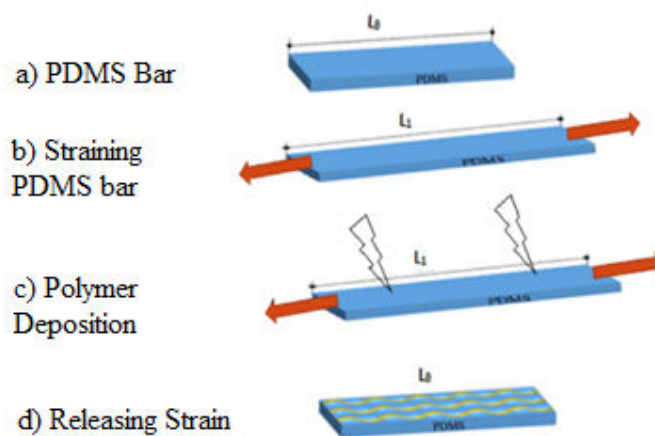


Figure 17: Schematic showing the wrinkle formation steps on PDMS bars [138].

Strained PDMS bars are carefully placed into the iCVD chamber. Since PDMS cannot reflect the laser light which is used for thickness control, a small piece of silicon wafer is placed on the area where laser light falls. The iCVD stage is large enough to put maximum 4 glass slides for simultaneous deposition of samples. The procedure of polymer deposition on PDMS is exactly same as depositing silicon wafers. Once the deposition is finished the strains over the sticks have to be removed in a controlled fashion. If releasing the strain happens too fast surface defects are likely to form over PDMS surface [139]. Therefore the release step must be held very slowly in order to prevent the possible defect formation which annihilates PDMS mechanical properties. In Figure 17 overall wrinkle formation procedure is depicted with graphics.

### 3.4 Characterization details

**FTIR Analysis:** FTIR analyses of the films are performed by FTIR (Thermo Fisher Scientific, Model NICOLET iS10). For the films deposited on silicon wafers the reference background is taken as bare (non-deposited) wafer and these spectra are subtracted from those of the deposited silicon wafers. For the films deposited on PDMS sticks the background is determined as the bare PDMS. The FTIR characterizations were carried out in normal transmission and ATR mode for Si wafer and PDMS samples, respectively. The spectra are averaged over 32 scans in  $400\text{ cm}^{-1}$  to  $4000\text{ cm}^{-1}$  with  $4\text{ cm}^{-1}$  resolution. All spectra were baseline corrected and normalized to 100 nm. The detector chamber of the machine is purged with nitrogen for 20 min before each measurement in order to eliminate the background noise since polymer films are able to give low intensity signal.

**Profilometer:** Profilometer (KLA-Tencor P-6) analyses have been performed in order to obtain the thickness, surface roughness and wrinkle wavelength information. The sample surfaces are scanned with  $2\text{ }\mu\text{m/s}$  scan rate and 2000 Hz sampling rate with tip force of 2 mg in non-contact mode. The sample information is obtained by the software analysis program (Mountain Map 6, Digital Surf). For all scans double Gaussian filters are operated in order to minimize the background noise.

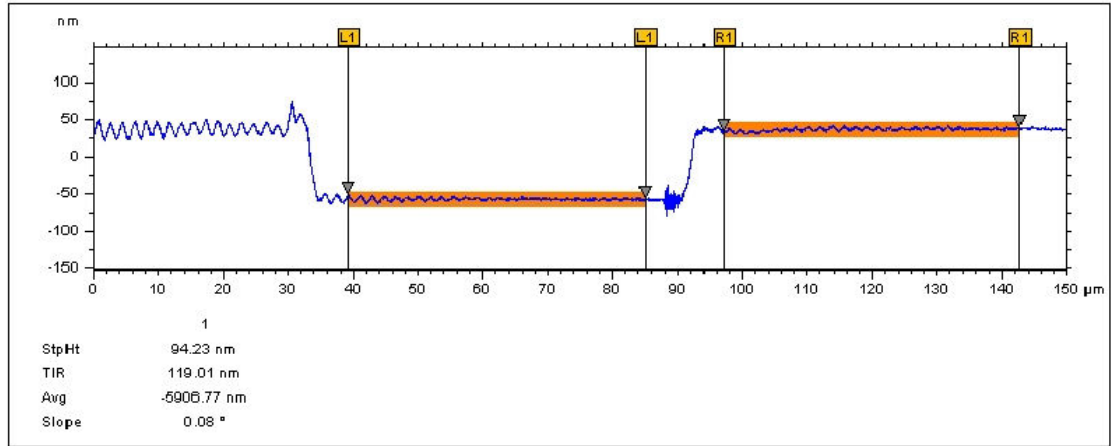


Figure 18: Calculation of the film thickness over Si wafer. The thickness for this example is 94 nm.

In order to find the film thickness a small scratch is generated on silicon wafers to remove the film locally. Since the profilometer is also equipped with an optical microscopy the scratched region is detected. A long scan passing through that region is performed. Therefore the height difference between the film region and scratched region is determined by the “step height” tool provided in the software program, and film thickness is determined.

In order to calculate the roughness of the films a clean region is determined using optical microscopy, where no visible contaminations or surface defects are present. The “rq-root mean square deviation of the raw profile” tool is selected from the “calculations” section in order to find the surface roughness. This operation basically calculates the square root of the vertical deviation of the surface scan height from the average value. Surface roughness is formulated as;

$$R_q = \sqrt{\frac{1}{n} \sum_{i=1}^n y_i^2} \quad (6)$$

Where  $R_q$ ,  $n$  and  $y_i$  are the roughness, total data point and distance of point  $i$  from the average value.

Surface scans are operated to derive statistical information from wrinkles. Different ways to find the average wavelength are possible. A long scan can be operated on

PDMS surface and the ratio of scan distance to number of wavelengths can be manually calculated to find the average wrinkle wavelength. The software of the machine provides a more scientific operation. In the “calculations” tool “plq-arithmetic wavelength average of the raw profile” can be selected to deduce the average wavelength with a standard deviation. This button basically calculates the distance between the top of the hills and averages for each subsequent wave. Filtration option might be very useful eliminate extremely small and extremely big waves to get a more accurate standard deviation.

**Contact Angle:** Water contact angle studies are performed by drop shape analysis system (KRÜSS GmbH Drop Shape Analysis System, Model DSA 10-Mk2). Double distilled water is used in order to eliminate any effect of water content. Droplets of 4  $\mu\text{L}$  are fixed for the measurements. Contact angle tests are conducted in dark room to prevent the interference of room lights to the system camera. The machine system is heated in order to perform high temperature measurements for PNIPAAm samples. The droplets are kept on PNIPAAm samples for 10 s for high temperature measurements in order to hinder the water evaporation due to heat. For low temperature measurement the waiting time is extended to 60 s for the droplets to interact better with polymeric surfaces. Dynamic advancing angles are taken at the point where the droplet size stop enlarging as more water is injected. Dynamic receding angles are taken at the point where the droplet size remains constant as water is retracted to syringe. The static and dynamic advancing angles for HEMA-PFA copolymers are conducted in the similar fashion. However a different procedure was operated for dynamic receding angles: A water droplet is placed on copolymer surface and stays there for about 30 mins. The contact angle no longer decreases and this final angle is determined the receding angle. For all measurements on PNIPAAm and HEMA-PFA final results are averaged over 3-5 droplets.

**Ellipsometer:** Ellipsometer (M-2000, J.A. Woollam) analyses are performed to find the thin film thickness, refractive indexes, surface roughness and the swelling ratios. Before each measurement a  $\text{SiO}_2$  reference sample is tested for the accuracy of the system. Besides the reflection angle and the signal intensity are checked. The data is acquired

over 3 different incident angles of  $65^{\circ}$ ,  $70^{\circ}$  and  $75^{\circ}$  between 313 and 718 nm in order to be fit to refractive index and thickness. Cauchy-Urbach isotropic model with Si with Transparent Film option was performed using modeling software (WVASE32, J.A. Woollam). The modeling fits the refractive index and thickness to the experimental data.

The swelling studies are performed with a different sample stage shown at Figure 19. The measurements are conducted with a single laser angle of  $75^{\circ}$ . The swelling measurement begins with a dynamic analysis of the samples in air medium. Afterwards double distilled water is injected to the sample cell and the dynamic analysis continues in water medium. The experimental data is divided into two parts for two different mediums. Using Cauchy-Urbach isotropic modeling the medium refractive index is individually changed for the initial air medium and remaining water medium part. These two graphs are re-combined in order to calculate the total film thickness change and see the kinetics of the process.

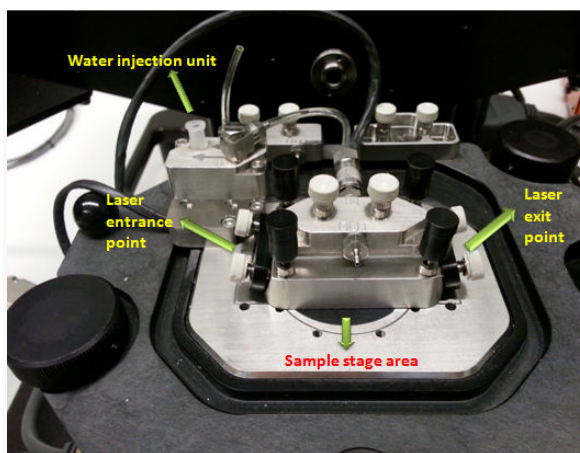


Figure 19: Ellipsometer system used for swelling experiments.

**XPS:** Depth profiling of wrinkled PNIPAAm films on PDMS substrates were analyzed by Thermo Scientific K-Alpha XPS spectroscopy with 1487 eV anode. Measurements were performed with 400  $\mu\text{m}$  spot size,  $90^{\circ}$  take-off angle and 10 nm probe depth. Samples were etched approximately with 0.2 nm/s.

**Bacterial studies:** GFP (Green Fluorescent Protein) containing GFPuv vector are injected to BL21 e-coli bacteria cells in order to visualize and calculate the number of bacteria under inverted fluorescent microscope. After inoculation at 37 °C overnight a single colony of bacteria is selected. In the LB environment a small culture of 5 ml is prepared with ampicilina and the growth of the solution takes place at 37 °C and 250 rpm. A bigger culture (200 ml) is inoculated with the small culture and the protein production is accomplished by the existence of IPTG (Isopropyl β-D-1-thiogalactopyranoside). After the induction bacteria reach the plateau phase in their growth curves which corresponds to approximately 1.25 OD. Equal amounts of the solution are poured on each sample. 1 ml double distilled water is sprayed in washing step. Olympus 1x70 Inverted Optical Microscopy is used for the analysis of the samples. The working distance, excitation distance and emission distances are 9500 μm, 450-495 nm and 510-550 nm, respectively. The pictures were taken by the software program ImageJ. The regions of 3000 x 4000 pixels are selected for the analysis.

## **Chapter 4**

# **Analysis of the Flat Thin Films**

### **4.1 Introduction**

In this chapter the polymeric thin films of PNIPAAm and poly (HEMA-co-PFA) coated on silicon substrates are going to be analyzed. Since the responsive thin films are coated on flat silicon wafers no surface morphologies are contributed to the film properties. FTIR, contact angle, ellipsometer and surface roughness results are going to be presented.

## 4.2 Flat PNIPAAm Thin Films

### 4.2.1 FTIR Discussion

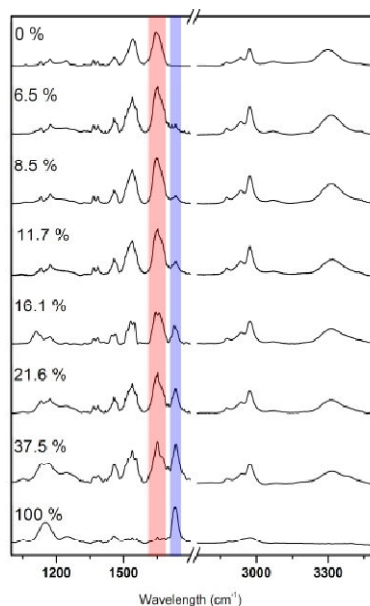


Figure 20: FTIR spectra for PNIPAAm films of different EGDMA proportions.

Figure 20 shows the FTIR spectra of PNIPAAm films with varying EGDMA ratios. The band seen around  $3330\text{ cm}^{-1}$  is associated with the secondary N-H stretching. Besides the existence of amide C-N-H bending (amide II) at  $1530\text{ cm}^{-1}$  and C=O stretching (amide I band) at  $1654\text{ cm}^{-1}$  shows the incorporation of NIPAAm monomer into the film [140]. Other important peaks regarding PNIPAAm are the doublet isopropyl band ( $1388\text{ cm}^{-1}$  and  $1370\text{ cm}^{-1}$ ),  $\text{C}(\text{CH}_3)_2$  symmetric deformation band at  $1440\text{ cm}^{-1}$  and asymmetric stretching vibrations of methyl groups ( $3000\text{ cm}^{-1}$ ) [141].

C=O stretching band of EGDMA is visible at  $1730\text{ cm}^{-1}$ . The amide I band is located at  $1645\text{ cm}^{-1}$  for pure PNIPAAm film. The shift of this peak to  $1654\text{ cm}^{-1}$  indicates the copolymerization of NIPAAm and EGDMA rather than mixture of the homopolymers. That shift of amide I band to higher wave numbers occurs due to the EGDMA which is more electronegative than NIPAAm [142].

Using FTIR it is also possible to obtain the crosslinker ratio in a film. For that purpose the bands corresponding to the C=O stretching are chosen. NIPAAm and EGDMA produces C=O stretching peaks at  $1645\text{--}1655\text{ cm}^{-1}$  and  $1730\text{ cm}^{-1}$ , respectively. According to the Beer-Lambert model, the absorbance of a band is proportional to the

concentration of the bands, therefore to amount of the chemical if the band oscillation power is same for each band. For this reason the ratio of the areas under C=O stretching bands give the relative amounts of NIPAAm and EGDMA molecules. Before finding the ratios the spectrums are Gaussian fitted. Since each EGDMA molecule includes 2 group of C=O the area of C=O stretching band for EGDMA is divided by 2:

$$\frac{[\text{EGDMA}]}{[\text{NIPAAm}]} = \frac{A_{\text{C=O(EGDMA)}/2}}{A_{\text{C=O(NIPAAm)}}} \quad (7)$$

The concentration of each film is also shown in Figure 20.

#### 4.2.2 Surface Topography Analysis

Surface roughness of the films is analyzed for different EGDMA ratios. In order to eliminate any possible effect of the thickness PNIPAAm films of equal thicknesses (200 nm) are investigated. The measurements are conducted at room temperature and for 200  $\mu\text{m}$  surface distances. Each data is provided as the average of 3 surfaces scans. An example of surface scan graph (amplitude vs scan distance) is provided at Figure 21.

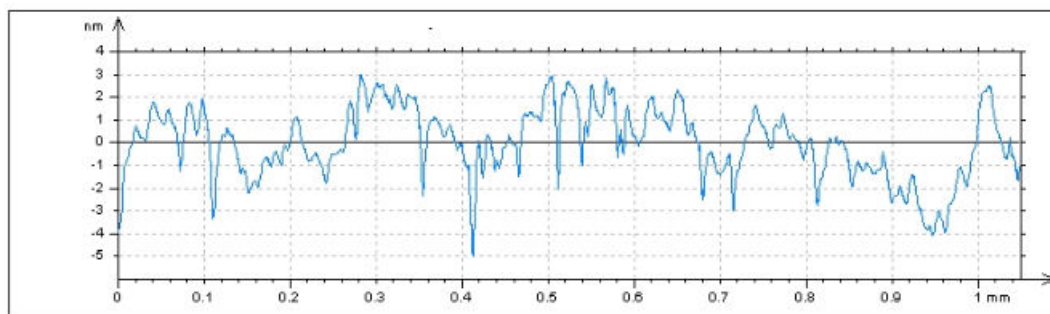


Figure 21: An example of the surface scan on a representative PNIPAAm film.

According to the Table 2 no direct effect of EGDMA ratio over the surface roughness is observed. The overall size of a single EGDMA molecule is obviously bigger than that of NIPAAm (see Figure 3). Bigger molecules tend to create more rough surfaces since the 2D assembling of the molecules is not as compact as of smaller molecules. Therefore it was expected that as the EGDMA ratio would increase the corresponding surface roughness would have gone up as well. However the results show that there is no clear relationship between the surface roughness and EGDMA amount of the film. Nevertheless surface roughness values vary between 1-5 nm. The claim that iCVD can produce smooth thin films is proven to be correct.

Table 2: Relationship between the surface roughness and EGDMA ratio for PNIPAAm films.

EGDMA Ratio (%)	0	6.5	8.5	11.7	16.1	21.6	37.5	100
Average Roughness (nm)	4.8±1	4.3±0.4	2.6±1.1	2.6±0.2	3.14±0.7	3,9±0.5	2.71±0.3	1.77±1

### 4.2.3 Contact Angle Studies

Contact angle measurements at room (22 °C) and high temperatures (50 °C) are performed in order to investigate the thermoresponsive character of PNIPAAm films (remember  $LCST_{PNIPAAm}$ : 32 °C). Both static and dynamic contact angles are measured. Effect of EGDMA ratio over the contact angles is investigated.

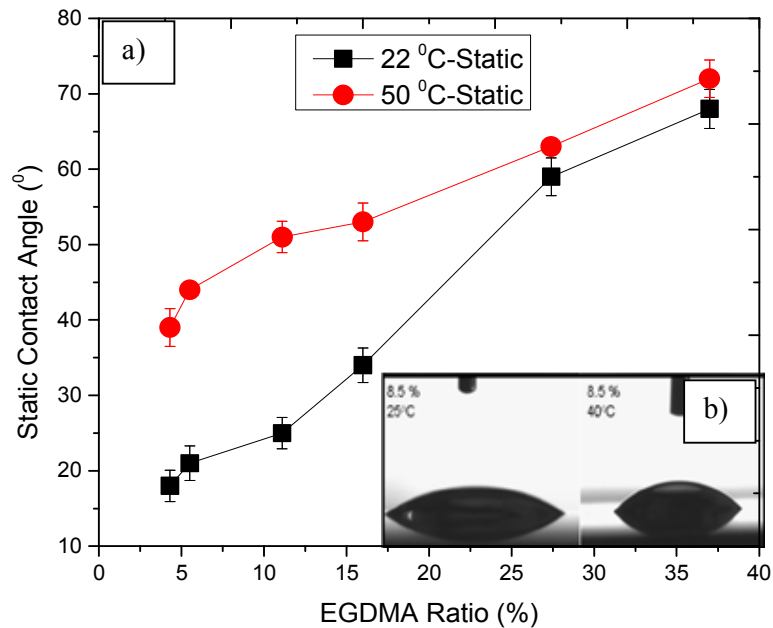


Figure 22: Static contact angle results for PNIPAAm films of various EGDMA ratios (a). Also a representative illustration for the contact angle change by temperature is provided (b).

Previously it was reported that the surface roughness of PNIPAAm thin films was very low. Therefore the contact angle differences result from the chemistry effect rather than the topographical variations. As shown at the Figure 22, the contact angle for highly crosslinked films are relatively higher than those of low crosslinked films, and the difference between the angles at 22 °C and 50 °C is pretty small. Such high contact angle values result from the hydrophobic nature of EGDMA. Also the crosslinker molecules decrease the temperature responsive activity of PNIPAAm molecules.

As the EGDMA ratio in a film decreases overall contact angles decrease as well. However the difference between low temperature and high temperature contact angles increase for low crosslinked films. Overall contact angle decreases because of the lower EGDMA concentration. The larger gap between 22 °C and 50 °C measurements can be explained with the responsive nature of PNIPAAm. As figured out before PNIPAAm faces a coil to globule transition after passing LCST. Hydrated molecules in the coil state transforms to dehydrate-collapsed globule state where the polymer molecules no longer make hydrogen bond with water.

For the transition to occur readily PNIPAAm molecules and chains must be saved from any sort of obstacle. The crosslinker EGDMA hinders the PNIPAAm molecule motion, and therefore degree of reversible volumetric phase transition is lowered. Therefore it is no surprise that as the EGDMA ratio decreases the PNIPAAm shows a better hydrophilic-hydrophobic angle difference. For very low crosslinked films hydrophilic angle goes down to very low angles, but hydrophobic angle is not high enough too. It is concluded that PNIPAAm films having 15-20% EGDMA ratio show the best temperature response.

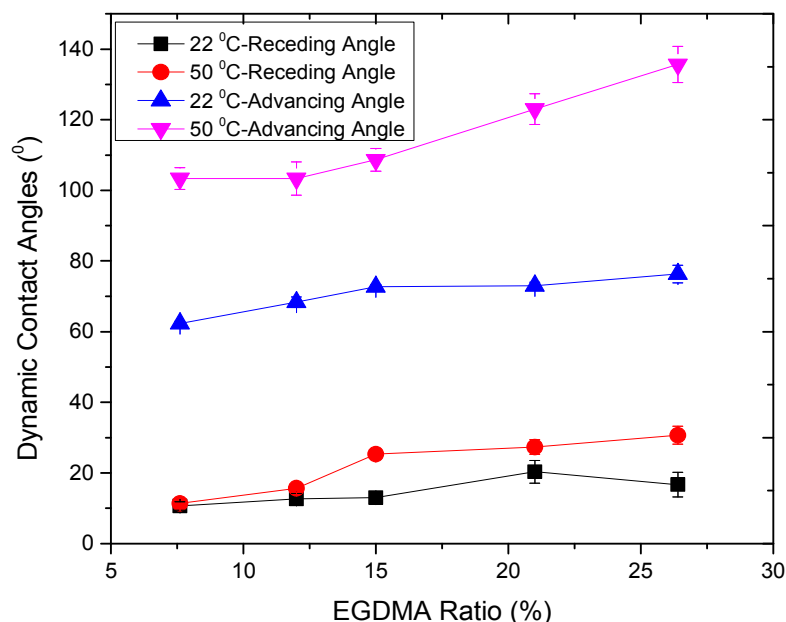


Figure 23: Dynamical contact angle results of PNIPAAm films of various EGDMA ratios.

Dynamic contact angle studies for PNIPAAm films of varying EGDMA ratios are presented in Figure 23. Advancing and receding angles are captured both at room temperature and 50 °C. Firstly; the hysteresis, the difference between the advancing and receding angles, for each temperature increases with increasing EGDMA ratio. Secondly, in contrast to static contact angle results the low and high temperature advancing angles did not come closer after a certain EGDMA ratio. Rather the difference between the low and high temperature angles increased with EGDMA ratio for advancing analysis. That can be understood from the nature of the dynamic angle studies. Since the dynamic contact angles are taken while the droplets are in motion no enough time is given for the films to be equilibrated with water. The surfaces of the films still show high temperature response, even at high crosslinking levels, since the equilibrium molecular arrangement of PNIPAAm and PEGDMA chains are disturbed with the droplet motion. That gives chance to PNIPAAm films to respond to temperature even if they are highly crosslinked. Another important result of this study is that the films show really high hydrophobic advancing angles at high temperature

region as well as showing a good response to temperature. The conclusion can be given as that EGDMA acts positively to show highly hydrophobic behavior.

Despite the advancing angle measurements the difference between receding angles for 2 different temperatures changed very little. The template response is not very clearly observed by receding angle studies. Because the water is swollen by PNIPAAm films during the angle measurements it becomes very difficult to detect the real receding angle (remember that receding angle is taken at the point where angle begins changing while the droplet is taken back to syringe).

### **4.3 Flat HEMA-PFA Thin Films**

Previously the characterization results of temperature responsive PNIPAAm were presented. Another candidate to be used as anti-fouler smart polymer can be produced by copolymerization of HEMA and PFA monomers. Basically HEMA shows hydrophilic nature while PFA is one of the well known hydrophobic monomers. Copolymerization of these two gives amphiphilic type of new polymer especially when they are synthesized in certain ratios. For the samples to be analyzed the thicknesses are kept constant as 200 nm.

The PFA percentages in the copolymers are measured by ellipsometer analysis. Following the procedure described in chapter 3 the refractive indexes of the films at 632 nm are found. The refractive indexes for pure PHEMA and pure PFA are found to be as 1.512 [143] and 1.36, respectively. Having calculated the refractive indexes of the copolymers the PFA percentages in the copolymers are simply calculated through linear interpolation using the refractive indexes of PFA and PHEMA. Each measurement is conducted 3 times. In the following section the results of the copolymers with 7%, 10%, 13%, 20% and 47% PFA ratios are going to be presented.

#### **4.3.1 FTIR results**

Each spectrum is baseline corrected and normalized to 100 nm thickness.

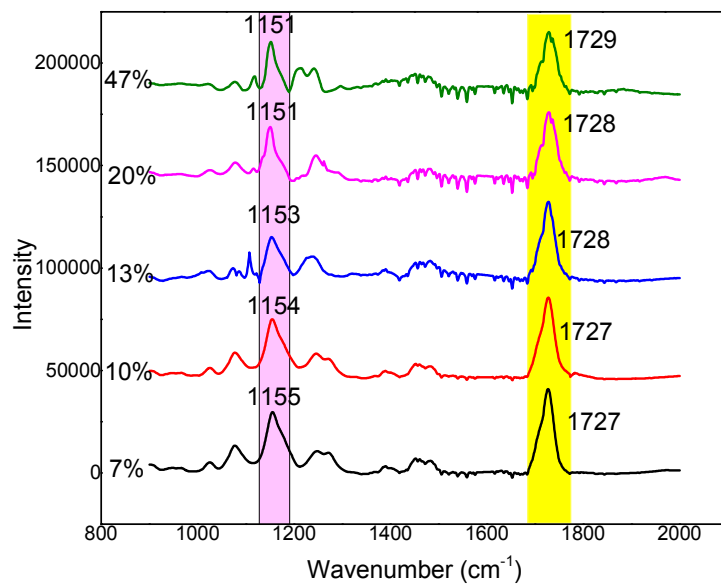


Figure 24: FTIR spectra of poly(HEMA-co-PFA) with varying PFA ratios.

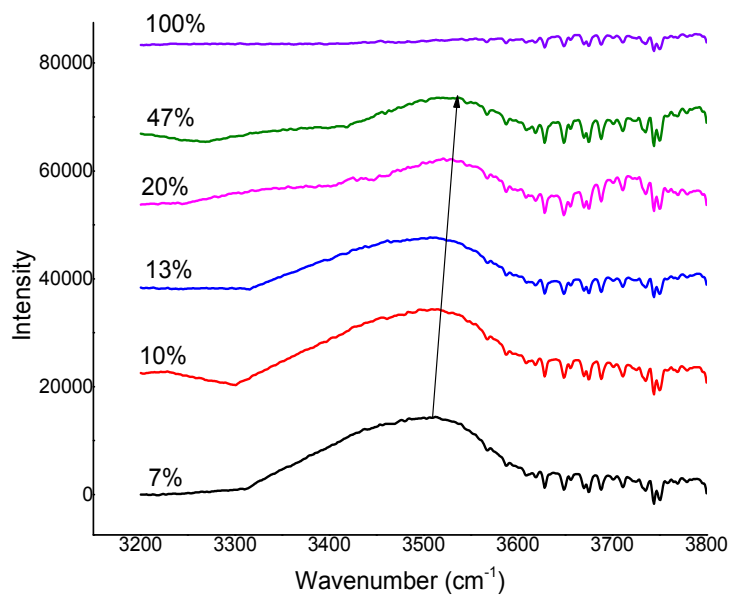


Figure 25: Positions of the bands associated with the O-H stretching frequency of PHEMA as PFA ratio is changed.

In Figure 24 the FTIR spectrum of the copolymers are depicted with increasing PFA ratios. The basic bands associated with PHEMA are O-H stretching ( $3700-3050\text{ cm}^{-1}$ ), C-H stretching ( $3050-2700\text{ cm}^{-1}$ ), C=O stretching ( $1750-1690\text{ cm}^{-1}$ ), C-H bending ( $1500-1350\text{ cm}^{-1}$ ) [144]. Existence of the peaks around  $3500\text{ cm}^{-1}$  and  $1720\text{ cm}^{-1}$  shows that the hydroxyl and carbonyl groups are preserved. The peak located at  $1150\text{ cm}^{-1}$  rises from the  $\text{CF}_2\text{-CF}_3$  stretching of the fluorinated carbon chain in PFA backbone. The bands at  $1205\text{ cm}^{-1}$  and  $1239\text{ cm}^{-1}$  are produced from the symmetric and asymmetric stretching frequencies of fluorinated carbon chain [145]. These findings prove that both HEMA and PFA exist in the copolymer. However the more important issue is the copolymerization of the monomers instead of monomer blends. The frequency of carbonyl increases ( $1727-1729\text{ cm}^{-1}$ ) by increasing amount of PFA, and that band is located at  $1741\text{ cm}^{-1}$  for pure PPFA [146]. That shift occurs due to the fact that PFA is a more electronegative molecule than HEMA. Therefore the electronic environmental change of the carbonyl group leads to wavenumber shifts to higher values. The  $\text{CF}_2\text{-CF}_3$  stretching frequency related to PFA shifts from  $1155\text{ cm}^{-1}$  to  $1151\text{ cm}^{-1}$  with increasing PFA ratios.

Also the carbonyl band appears as one single band instead of two splits; each split coming from HEMA and PFA. Figure 25 gives the band intensity related to hydroxyl group. The peak intensity of hydroxyl group decreases for increasing PFA percentages simply because PFA does not include OH group. Also the position of the peak shifts from  $3550\text{ cm}^{-1}$  to higher positions when the PFA percentage is increased.

### 4.3.2 Surface Roughness

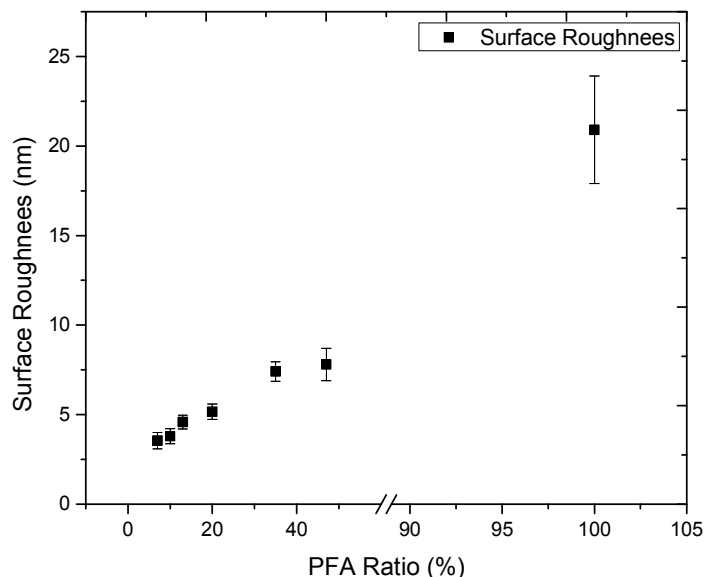


Figure 26: Surface roughness results of the copolymer thin films.

Surface roughness values of the copolymers for different PFA percentages are presented in Figure 26. The measurements are conducted by ellipsometer using Cauchy-Urbain isotropic modeling. Each data is provided as the average of 3 measurements. For varying PFA ratios the surface roughness values are found to be between 3-8 nm. Thinking that the film thicknesses are 200 nm almost flat surfaces of thin films are produced by iCVD likewise PNIPAAm thin films. The surface roughness values are found to be increasing with PFA ratio. Chemically PFA is a bigger molecule due to the long fluorinated carbon chain. This long chemical structure creates difficulty for 3-D assembly of the polymeric chains. The molecular configuration becomes more chaotic and disordered when the PFA ratio increase in the copolymer.

### 4.3.3 Contact angle studies

The nature of the copolymers can be better understood by the contact angle results. Hypothetically the hydroxyl groups of HEMA go outward in water medium why the fluorinated carbon chain of PFA dominates the surface structure in air medium. To

understand this behavior static and dynamic contact angle studies are performed. Each data is provided as the average 3 different measurements.

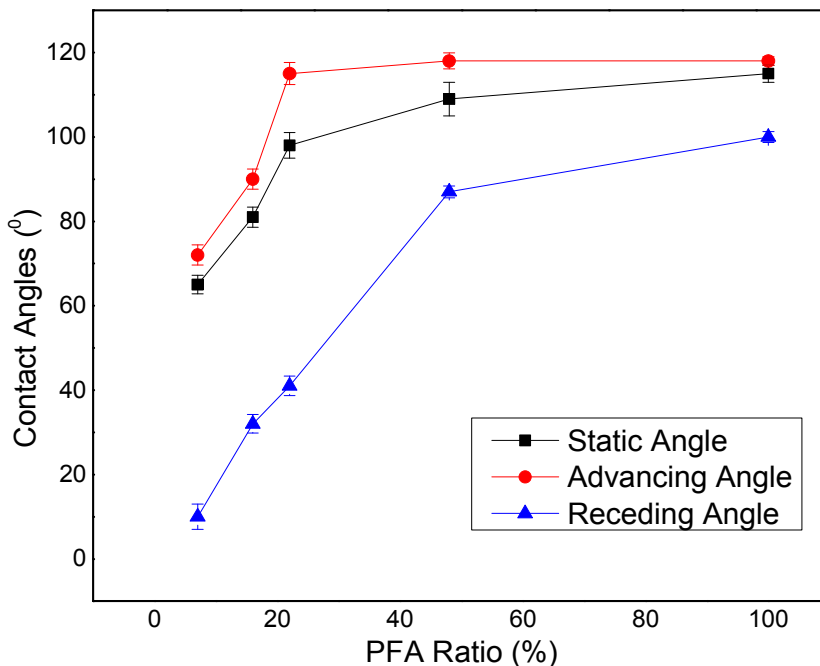


Figure 27: Contact angle results of the copolymers.

Since PHEMA is mechanically weak the static contact angles are determined right after droplets are put on the films. The results show that the static contact angles rise with the increase of PFA percentage. Firstly the increase behavior tends to be linear. After 30-40% PFA the angles appear as saturated, and addition of more PFA into the copolymer does not drastically increase the angles. The results reveal that PFA as hydrophobic monomer may form highly hydrophobic copolymer surfaces. The surface energy of the copolymer can be easily tuned by the ratio of PFA.

The dynamic advancing angles are taken by usual procedure. However a different way is proposed for the determination of the dynamic receding angles. The common procedure to obtain receding angles is problematic since the angles continuously decrease as the droplet volume lessens. Therefore the droplets are poured over the copolymer surfaces and at least 30 min of waiting time is provided. This suggested way also provides the observation of the copolymers in water medium. Remembering that

static angles are taken right after the fall of the droplets the behavior of the surfaces in dry medium can be deduced in this way since the surface of the copolymers are populate with the PFA's fluorinated carbon chains. When droplets stay for 30 min on the surfaces the enough time for the interaction of the surface with water is given [147]. Therefore the equilibrium angels simply denote the tendency of the copolymers in water medium. Receding contact angles are found to be lower than the static contact angles of the corresponding films for each PFA ratio: high surface energy in water medium and low surface energy in dry medium. Also the difference between the static and receding angels decreases with increasing ratio of PFA which proves that the surfaces become more hydrophobic.

#### 4.3.4 Swelling properties

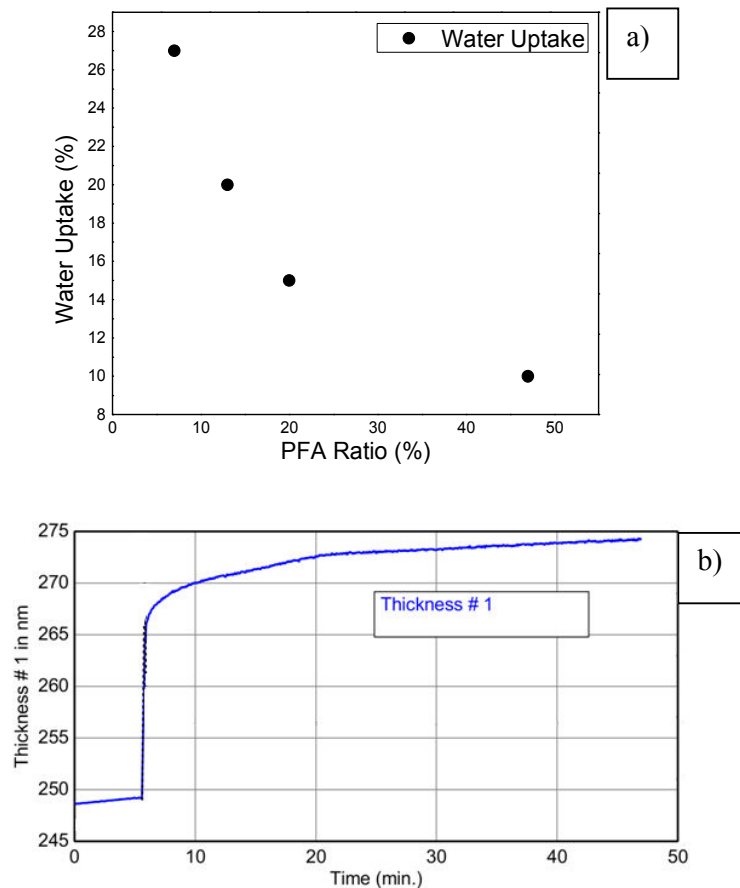


Figure 28: Swelling degrees of the copolymers for different PFA proportions (a) and the dynamical thickness change for a representative sample having 47% PFA (b).

As previously reported PHEMA is able to swell and deswell according to the medium. Since PFA increases the hydrophobic interactions in the films the swelling properties are directly affected by the PFA ratio. To test the effect of PFA the films of same thicknesses ( $235 \pm 10$  nm) and different PFA ratios are used for this experimental setup. The water temperature is  $25$  °C.

In the Figure 28-a, the water uptake results of the films are presented. The water uptake ratio is calculated as;

$$\text{water uptake} = \frac{t_w - t_d}{t_d} * 100 \quad (8)$$

where  $t_w$  and  $t_d$  are the thickness of the films in water and dry medium, respectively.

When the PFA ratio in the copolymer is low the swelling ratio rises closer to 30%. At the 50% PFA amount the water uptake is found to be nearly 10%. Clearly PFA is able to lower the swelling capacity of PHEMA due to the hydrophobic groups present at PFA's backbone.

## Chapter 5

# Wrinkled PNIPAAm and HEMA-PFA Films

### 5.1 Introduction

In this chapter the numerical and topographical studies related to wrinkled PNIPAAm and poly(HEMA-co-PFA) surfaces are given. Different ways of wrinkle formation are going to be presented. Also the temperature response of wrinkled PNIPAAm films is going to be investigated.

### 5.2 Control Experiments: Understanding the Reason of Wrinkle Formation

It is known that there are several methods to form wrinkles on PDMS surfaces. Thermal effects, stretching, bending, oxygen plasma and different type of factors (even humidity) can play a role in buckling. For the initial studies, PDMS bars are placed into iCVD chamber and the deposition conditions are reproduced without the monomer flow. To investigate the effects of deposition conditions on the wrinkling formation PDMS bars of different strengths are put into the iCVD system. Both stretched (10% strain: 10S) and nonstretched bars are used. Standard experimental conditions are used: The system pressure, stage temperature and filament temperature are fixed to 300 mTorr, 40 °C and 250 °C, respectively. The samples are kept in the system for about 20 minutes which is an average deposition time. The samples are then analyzed with optical microscopy for any possible topographical change over the surfaces.

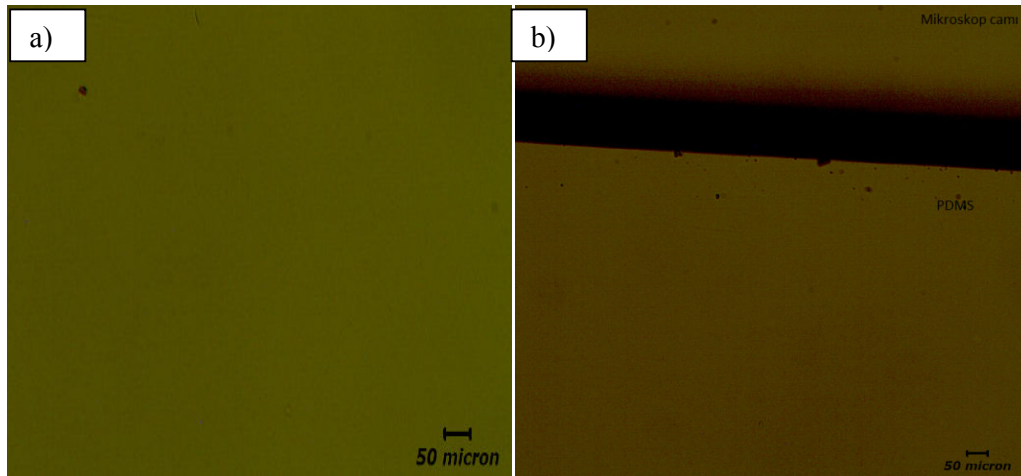


Figure 29: Optical microscopy images of the PDMS sticks after iCVD treatment. No monomer vapor is fed during the treatment. The surfaces of 2.5% crosslinked PDMS surfaces with the strains a) 10% and b) 0%.

Optical microscopy analysis showed no evidence of wrinkle formation over PDMS surfaces. In Figure 29-a and b both 10S and 0S strained 2.5% crosslinked PDMS sticks are shown with no pattern formation on top of the samples. The same experiments are repeated for 5% and 10% crosslinked PDMS bars, and likewise no wrinkle formation is observed. The black dots at the pictures (Figure 29) are the surface defects, and intentionally selected to show that images are on focus. As a concluding remark nitrogen flow, pressure, heat or any combinations of these are not responsible for wrinkle formation when they are alone. Therefore the wrinkled patterns which will be reported in the following sections result from the polymer deposition. Henricks and colleagues [148] tested two different sample sets: first only heated PDMS molds and then both heated and oxygen plasma operated samples. They also observed no wrinkle formation on the heated PDMS samples. Wrinkles were formed over the second sample set which suggests that both oxygen plasma and heat are responsible for buckling. This conclusion is also proven by the results given by Figure 29.

## 5.3 Wrinkling Patterns on PNIPAAm Films

### 5.3.1 Uniaxial Wrinkling

Before the depositions the elastic modulus of the bare PDMS molds are measured by AFM nanoindentation method. The details of the method are going to be given in the following sections. The results of elastic modulus study for varying PDMS strengths presented in Table 3.

Table 3: Reduced elastic modulus of PDMS molds.

PDMS Crosslinking Ratio (%)	Reduced Elastic Modulus (MPa)	Stdv
2.5	0.099	0.03
5	0.25	0.01
10	0.67	0.02
20	0.7	0.01

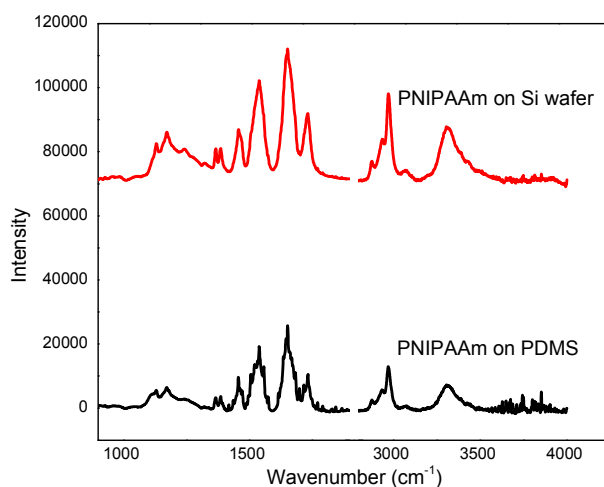


Figure 30: IR spectrum of PNIPAAm films (15%) on Si substrate and PDMS substrate.

As the wrinkles can only form with polymer deposition, stretched-polymer coated PDMS bars are analyzed. The stretching procedure was mentioned in chapter 3. However since the uniaxial wrinkle formation is well formulated and understood in low strain boundaries, 5-20% strains are experimented in this project. Before the optical

microscopy investigation IR spectra of the films are analyzed (Figure 30). The characteristic IR absorption bands of PNIPAAm can be observed on PDMS substrates confirming that PNIPAAm could successfully be deposited on PDMS surfaces. The optical microscopy images for uniaxial buckling patterns are presented in Figure 31.

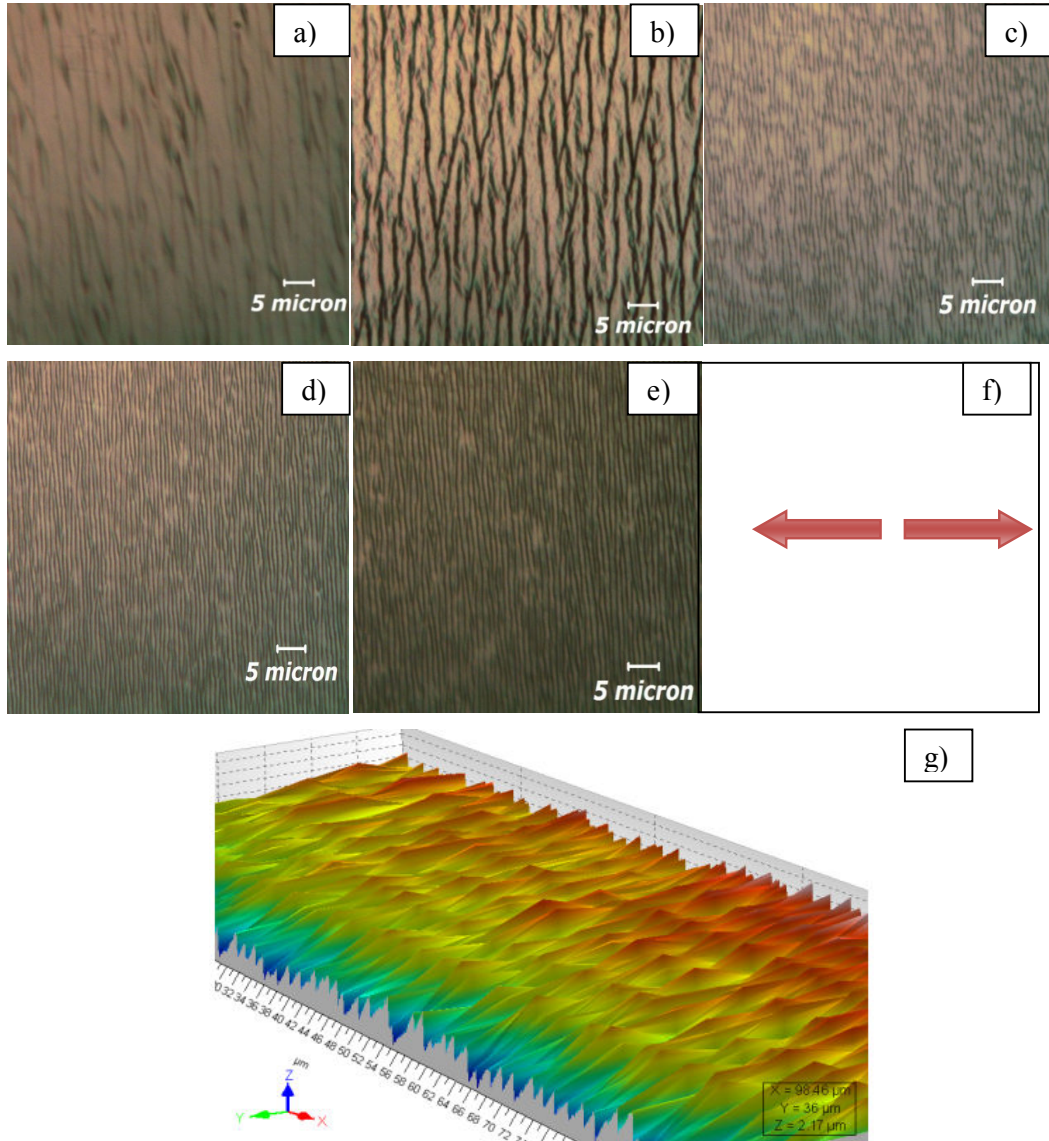


Figure 31: Optical microscopy images of uniaxially wrinkled PNIPAAm surfaces. (Film thickness: 130 nm, Film EGDMA ratio: 20%). The crosslink ratios for PDMS samples are a) 2.5%, b) 5%, c) 10%, d) 20% and e) 30%, and i) a representative 3-D image of uniaxial wrinkling.

As shown in Figure 31 wrinkles appear on PDMS samples with different crosslink ratios (2.5-30%). As the crosslinking of PDMS increases the average distance between two black alternating layers (which is simply wavelength) decreases which is consistent with the formula 2. Also the wrinkles become more ordered in the vertical axis. The physical mechanism behind wrinkle formation is the stress that forms between top and bottom layers of the dual system (film+substrate). By coating the stretched PDMS bars with PNIPAAm and releasing the stain afterwards the polymer thin film layer is put into the compression force. Two competing forces, bending force of stiff film layer and stretching force of relatively softer substrate, create a wavy surface structure with an optimum wavelength. Increasing the crosslink ratio of the substrate increases the elastic modulus (and the spring constant). Therefore the stretching force of the bottom layer is increased for highly crosslinked PDMS bars, which explains the wavelength reduction and better arrangement of the wrinkles. The wavelength change with respect to increasing PDMS strength is depicted in Figure 32.

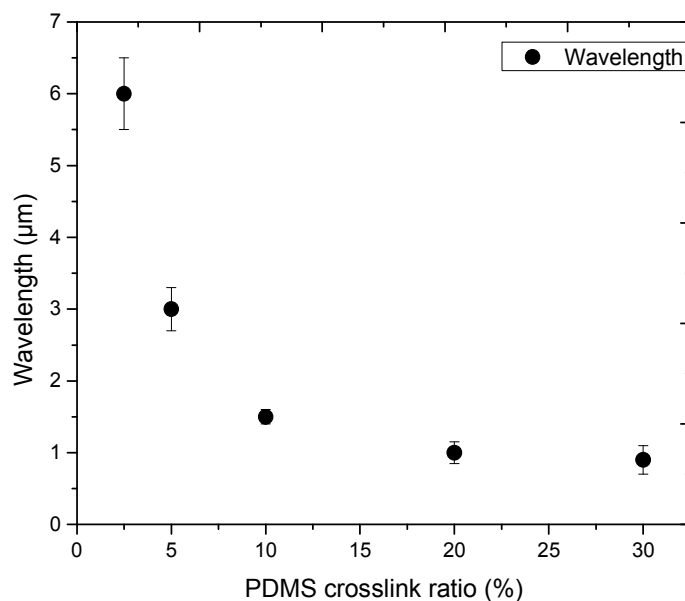


Figure 32: Wavelength of the uniaxial wrinkles with respect to changing PDMS crosslink ratios. For each film; thickness is 130 nm and EGDMA ratio is 20%.

Figure 33 shows the wavelength with respect to varying film EGDMA ratio. As the EGDMA ratio in the film increases the average wavelength also increases as well, which is related to the film elastic modulus discussion. The elastic modulus of PNIPAAm films,  $E_f$ , increases with increasing level of crosslinking in the film (see Figure 34) which is consistent with formula 2.

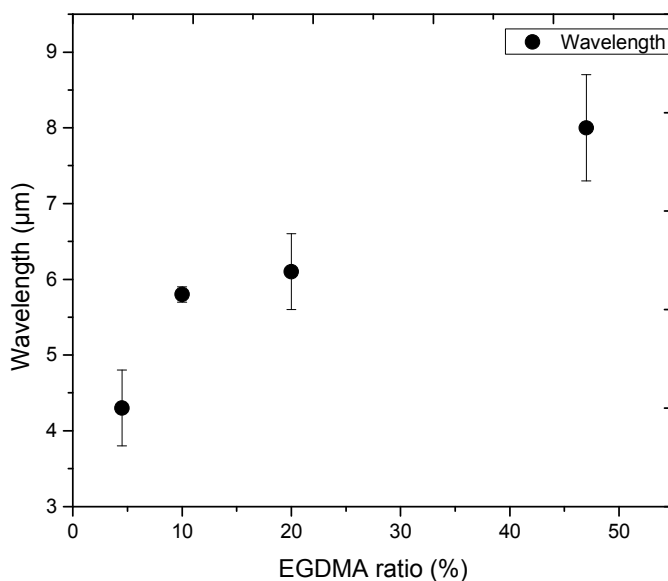


Figure 33: Wavelength of the uniaxial wrinkles with respect to changing film crosslink ratios. For each film; thickness 130 nm and PDMS crosslinking 2.5 %.

### 5.3.1.1 Elastic Modulus Calculations on PNIPAAm Thin Films

Measuring the elastic modulus of PNIPAAm is a difficult task because of the nature of thin films. One of the most efficient ways is to use AFM nanoindentation technique. PNIPAAm thin films of several EGDMA ratios are deposited on silicon wafers and elastic modulus analysis is performed by MultiMode™ AFM. Peak force quantitative nano-mechanics (QNM) mode is selected since it gives quantitative information about small scale materials. With this method it is possible to obtain information on adhesion, modulus, deformation and so on. Prior to elastic modulus calculation of the thin films, the system requires calibration regarding the cantilever parameters. These parameters (spring constant, tip radius and deflection sensitivity) are being used during the

modeling for elastic modulus. After the calibrations are done a small piece of silicon wafer with PNIPAAm film on is scanned with the defined scan size and scan area. During the scanning many force curves are obtained from the different points. These force curves are saved in the proper format to be used in nano scope analysis software. Force curves are converted into force versus separation curves and necessary modifications are operated (baseline correction, deformation sensitivity correction, tip radius correction and so on). Hertzian fit modeling is applied in order to find elastic modulus of the films from the force vs separation curves.

The resulting reduced Young modulus data is given in Figure 34.

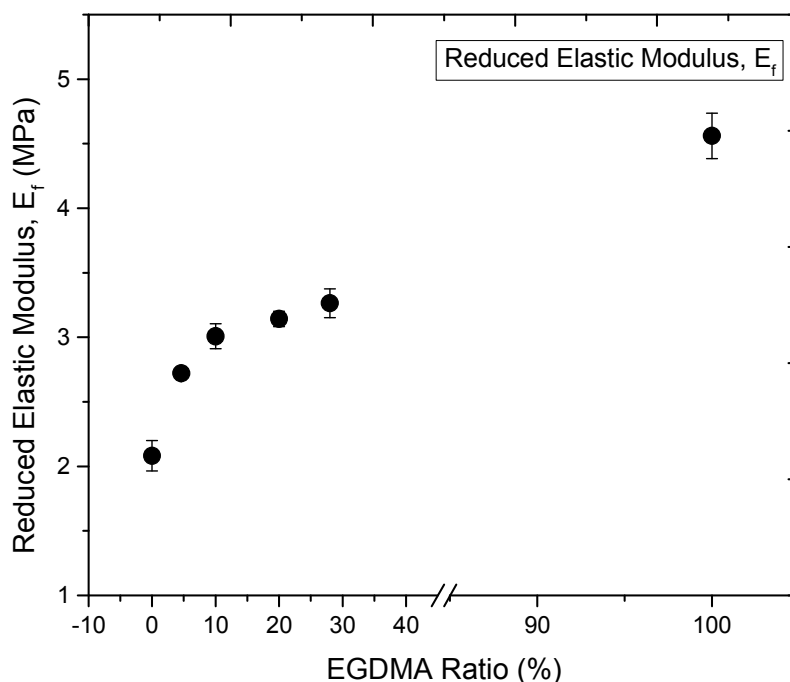


Figure 34: Elastic modulus values of PNIPAAm films calculated by AFM nanoindentation method. The films thickness for each sample is 130 nm.

As seen in the Figure 34 the PNIPAAm elastic modulus increases with EGDMA ratio. The values vary between 2 and 3.4 MPa while pure EGDMA has an elastic modulus of 4.5 MPa. This result suggests that EGDMA increases the strength of the film. Besides the fact that EGDMA, due to the hydrophobic nature, tunes the thermoresponsive capacity of PNIPAAm, it also improves the strength of the film. It was already known

that EGDMA provides the molecular integrity for PNIPAAm chains and a strong resistance to water. PNIPAAm films of low crosslinking degree (<5%) dissolve in water while films with higher EGDMA ratios (>10%) are strong enough to prevent film dissolution which is due to the crosslinking function of EGDMA. Adjusting the EGDMA ratio in the film makes it possible to change the film elastic modulus and this becomes another tool that an experimenter can use to play with wavelength value of wrinkles (Figure 33).

### 5.3.1.2 Calculating the elastic modulus of PNIPAAm thin films by Strain Induced Elastic Buckling Instability for Mechanical Measurements (SIEBIMM) method

The details of this method were given in chapter 2. In brief the idea was finding the film elastic modulus from the substrate elastic modulus, film thickness and wavelength using formula 4. Any material which is under investigation is deposited on stretched PDMS samples and the wavelengths of the wrinkles are calculated. Same procedure is followed for wrinkled PNIPAAm thin films as well. PNIPAAm thin films of varying thicknesses and EGDMA ratios are deposited on 2.5% crosslinked PDMS bars and the forming wrinkle wavelengths are calculated by profilometer. Then wavelength, substrate elastic modulus ( $E_{s,2.5\%} = 0,099$  MPa) and thickness data are used to find film elastic modulus. The comparison chart is given at Table 4.

Table 4: Comparison chart including the elastic modulus values calculated by SIEBIMM method and measured by AFM nanoindentation technique.

EGDMA Ratio (%)	Measured value (MPa)	Calculated value (MPa) (by SIEBIMM)
4.5	2.7±0.08	3.5
10	3.14±0.1	3.3
20	3.25±0.22	4.5
100	4.5±0.3	6.2

Table 4 compares the elastic modulus values calculated by SIEBMM and measured by AFM nanoindentation. For each EGDMA ratio the calculated and measured elastic modulus values are close enough to each other. However apparently it is misleading to confirm that the numbers are completely matching. Wavelength, substrate elastic

modulus and film thickness data are separately measured and each contains some degree of standard deviations. Adding the possible mistake for measurements, the difference between film elastic modulus values in Table 4 becomes slightly reasonable. Also, one should remember that formula that is used for calculated values is formula 2. For this formula to be completely valid the strain levels must be lower than 5%. Keeping in mind that the applied strain for PDMS bars was 20% formula 2 might be modified in the way that calculated values come closer to measured values.

### 5.3.2 Random Wrinkling Patterns on PNIPAAm Films

Earlier the wrinkle patterns forming on uniaxially stretched PDMS were given. Uniaxial stretching determines the type of the pattern because it aligns the direction of the compressive stress and reduces to one single axis. PDMS bars with no initial strain (0S) are placed in iCVD chamber and coated with PNIPAAm. The resulting optical microscopy images are presented in Figure 35.

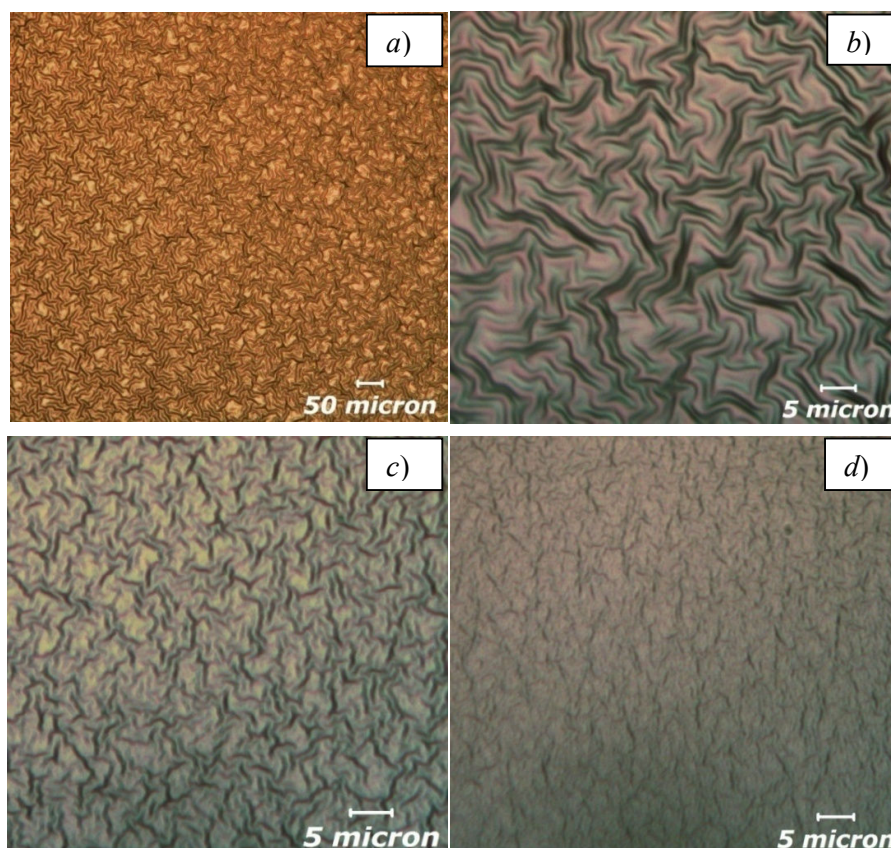


Figure 35: Optical microscopy images of the random wrinkling patterns observed on PNIPAAm surfaces (Film thickness 130 nm and EGDMA ratio 20%). The PDMS crosslinking ratios; a) 2.5% (20x), b) 2.5 % (100x), c) 5% (100x) and d) 20% (100x).

When PDMS sticks are not strained from neither end but coated with PNIPAAm, wrinkles with a specific distance but not a preferred direction form on PDMS surface. The buckling pattern becomes even clearer for PDMS sticks of low crosslink degree (2.5%). Whitesides and colleagues [149] whose studies of PDMS wrinkles have been milestones, observed the same phenomena during the e-beam evaporation of metals over PDMS. In their research PDMS samples with no strain encounters thermal expansion by heat coming from the experimental setup. Thermally expanding PDMS samples are simultaneously coated with several types of metals. When the samples are then taken to room temperature disordered wrinkle formation was observed (see chapter 2.6). A heat-induced strain forms on the PDMS samples after thermal expansion. As the thermal expansion coefficient of the substrate (PDMS) ( $3 \times 10^{-4} \text{ } ^\circ\text{C}^{-1}$ ) [150] is much larger than the metal, the top film layer encounters a compressive force after the samples are brought to room temperature. However since heat-induced strain does not have a preferred direction, instead symmetric in x-y plane, the compressive stresses that push the top layer becomes also symmetric and produce randomly oriented but almost equally spaced wrinkles. It is thought that the surface patterns that are presented in Figure 35 also form by the same way. The heat that causes the thermal expansion originates from the hot filaments and heated stage. In Figure 35 the wrinkle pattern for 20% crosslinked PDMS is not as clear as those forming over 2.5% crosslinked surface. That is related to the thermal expansion coefficient of PDMS samples of different crosslink levels. Physically it is known that thermal expansion coefficient is oppositely related to elastic modulus of the sample. As the linear thermal expansion coefficient for 20% crosslinked sample decreases the forming heat-induced strain is going to be lower. Remembering that amplitude of the wrinkles is enhanced by amount of strain, the wrinkle amplitude for 20% crosslinked PDMS is decreased compared to other samples. The wavelength of the random wrinkles with respect to the PDMS crosslinking ratio is provided in Figure 36.

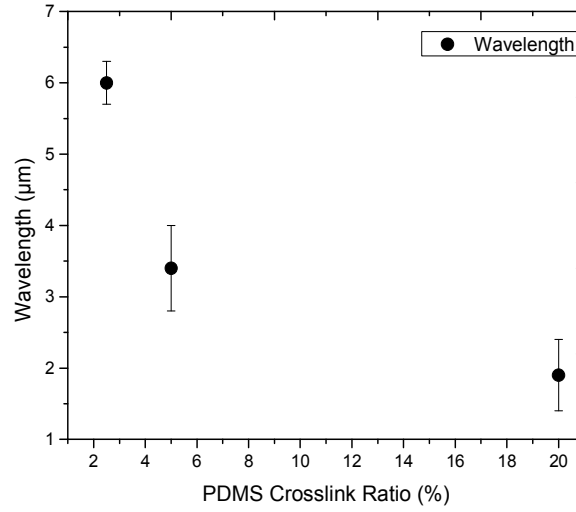


Figure 36: Wavelength data for randomly wrinkled PNIPAAm surfaces with respect to varying PDMS crosslinking ratio. The films thickness for each sample is 130 nm.

The formation of the wrinkles depends on the principle that the compressive stress must exceed a critical level. Hendricks et al described the formulations for the random wrinkles resulting from the thermal expansion mismatch. The compressive stress is [151];

$$\sigma = \frac{E_f(\alpha_s - \alpha_f)}{(1 - \nu_f)} \Delta T \quad (9)$$

where  $E_f$ ,  $\alpha_f$ ,  $\alpha_s$ ,  $\nu_f$  and  $\Delta T$  are the film elastic modulus, film thermal expansion coefficient, substrate thermal expansion coefficient, film Poisson's ratio and temperature change.

The compressive force required for the wrinkle formation is;

$$\sigma_c = \sqrt[3]{\frac{9 E_f E_s^2}{64 (1 - \nu_s^2)^2 (1 - \nu_f^2)}} \quad (10)$$

where  $E_s$ , and  $\nu_s$  are the substrate elastic modulus and substrate Poisson's ratio.

For a 20% crosslinked PNIPAAm film on 2.5% crosslinked PDMS stick the forming compressive stress is 0,270 MPa for a typical deposition ( $\Delta T = T_{\text{deposition}} - T_{\text{RT}} = 105 \text{ } ^\circ\text{C} - 25 \text{ } ^\circ\text{C}$  and assuming  $\nu_f = 0.5$ ).

The critical compression stress required for wrinkle formation in the defined systems is found as 0.210 MPa. Therefore the heat induced stress is bigger than the critical stress

required for the wrinkle formation. For this composite system the critical wrinkle formation temperature is calculated as 87 °C.

For some applications formation of these random wrinkles would not be desired. Whereas it is challenging to prevent these heat-induced wrinkles there is a limited knowledge in the literature. It is observed that implementation of silica nanoparticles in between the top and bottom layers highly eliminate the wrinkle formation [152]. The hypothesis given is that silica nanoparticles somehow prevent the compressive stresses which finally reduce the number and amplitude of the wrinkles. The hypothesis given still requires a better explanation and more experiments to be conducted. Although formation of these random wrinkles due to the heating effect was unpredicted and out of the desire, it is possible to turn it to advantage for different applications.

#### **5.3.2.1 Random Wrinkling Patterns of PNIPAAm Under Varying Deposition Temperatures**

It was previously reported that on OS PDMS bars random type of surface topography formed with PNIPAAm deposition. It seems a relevant study to see effect of the temperature on buckling. In order to understand this effect PDMS samples are deposited under several filament temperatures. The sample temperature is affected by both stage heat through conduction and hot filament wires through convection. At the first glance changing the stage temperature looks more logical than altering filament temperature since samples are directly in touch with stage. However one should remember that 40 °C stage temperature is an optimum one for PNIPAAm depositions. Therefore changing filament temperature is preferred for this study. The decomposition temperature of initiator molecules into radicals is around 180 °C. Besides, the monomers used in this project chemically degenerate after 320 °C. Therefore filament temperature is switched to 210 °C, 250 °C and 300 °C and experiments are conducted at these different temperatures. The corresponding temperatures that PDMS surfaces feel are 100 °C, 113 °C and 120 °C, respectively.

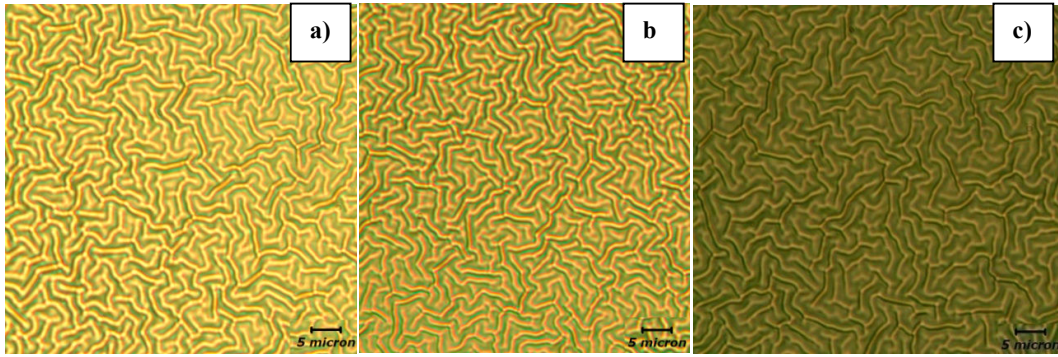


Figure 37: Surface wrinkling patterns at different deposition temperatures; a) 100 °C, b) 113 °C and c) 120 °C.

In Figure 37 optical microscopy images are presented for randomly buckled PNIPAAm surfaces which are deposited on 2.5% crosslinked PDMS bars under 3 different filament temperatures. For all temperature levels the random wrinkles are observed. Knowing that the critical temperature for wrinkling is 87 °C the results are consistent with the discussion. There is no pronounced difference between 3 images in terms of wrinkle pattern type. The wavelengths are  $1.65 \pm 0.3 \mu\text{m}$ ,  $1.7 \pm 0.3 \mu\text{m}$  and  $1.6 \pm 0.7 \mu\text{m}$ , respectively. Considering the standard deviations as well there is no clear distinction or trend with respect to temperature. The fact that random surface structure is formed for all 3 temperatures suggests that the critical wrinkle formation temperature ( $T_c$ ) is lower than 105 °C. Same experiments are repeated for 5%, 10% and 20% crosslinked PDMS sticks and same results are obtained. Temperature difference is linearly correlated with strain ( $\epsilon = \Delta T * \alpha$ ). However strain is not one of the parameters affecting wrinkle wavelength. Therefore it is consistent with the formulations that no difference is observed among the images of Figure 37. As long as the critical strain necessary for wrinkle formation is satisfied the amount of strain does not affect wavelength quantities. In the studies where PDMS samples are heated and simultaneously oxygen plasma treated the wavelengths are found to be independent of the temperature [153].

### 5.3.2.2 Symmetrical Wrinkle Pattern Formation on PNIPAAm surfaces and further studies

Interesting wrinkle patterns are observed on 2.5% crosslinked and 0% (0S) strained PDMS surfaces which are coated with PNIPAAm.

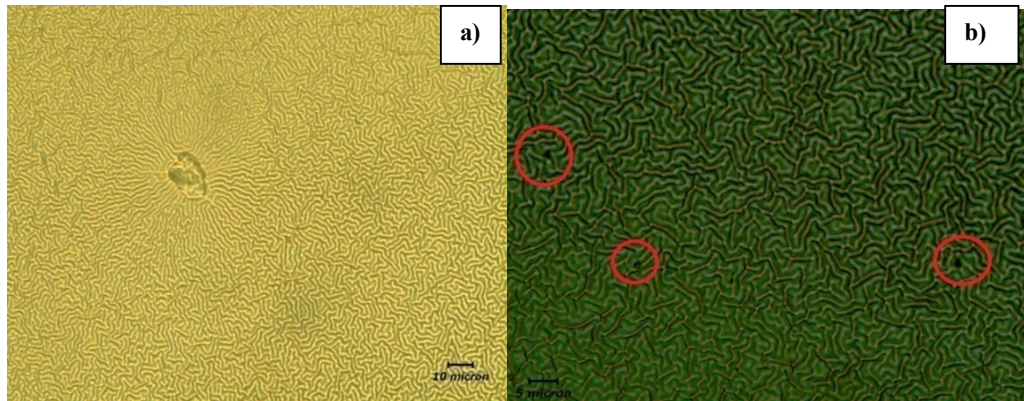


Figure 38: Effects of the surface defects on wrinkle distribution; a) disturbance of the wrinkles and b) no effect of the defects.

In Figure 38-a a spherulite-like wrinkle pattern is observed in a random wrinkle matrix. Apparently the center structure is a surface defect or some kind of contamination that came during iCVD deposition. Wrinkles arise from this center in a sunshine fashion and maintain this formation to some extent. The center structure produces a circular and local stress field which also shapes the orientation of the wrinkles present at the region. This unexpected observation gives the idea that OS PDMS substrates deposited with thin films can be easily altered topographically. In literature there are many researches regarding the surface modification of PDMS using lithographic techniques [154, 155, 156]. Using lithographic masks it is possible obtain complex wrinkle patterns by oxygen plasma treatment. The present studies are mostly performed with oxygen plasma treatment. On the other hand the thin film studies over PDMS substrates are generally on e-beam evaporation of metals. At this point iCVD method can be very useful in order to combine many advantages. Specific polymers for different applications can be deposited which cannot be achieved by oxygen plasma treatment. At the same time the surface topography can be modified in the desired fashion because of the thermal effect provided by iCVD. Remembering that mechanical treatments such as uniaxial stretching only makes certain wrinkle alignments, iCVD system and lithographic methods can be combined. Although the heating effect was told to be out of desire, these phenomena can be used in the way that it can be utilized to form different wrinkle patterns.

In a study published by Illson et al. [157] the surface patterns emerging around the circular columns which are placed with certain distances and heights are presented. If the column diameter is much smaller than the wavelength the wrinkle pattern is still

random. However when the column diameter is bigger than wavelength wrinkles appear to be spreading out from the column centers. As the column diameter increases more the wrinkle orientation becomes even more directional; from column to column. The optical microscopy images given in Figure 38 support this observation. In Figure 38-a where the defect diameter ( $10\ \mu\text{m}$ ) is bigger than wavelength ( $2.5\ \mu\text{m}$ ) spherulite-type pattern is observed whereas if the defect (Figure 38-b) diameter ( $<0.5\ \mu\text{m}$ ) is less than wavelength random wrinkle pattern is not affected by the existence of the defect. Besides, a topographically modified PDMS mold is being coated with PNIPAAm with no initial strain (Figure 39). The wrinkles are found to be directed from column to column. These results are promising that modified PDMS molds can be coated with any kind of polymer to create certain surface morphologies.

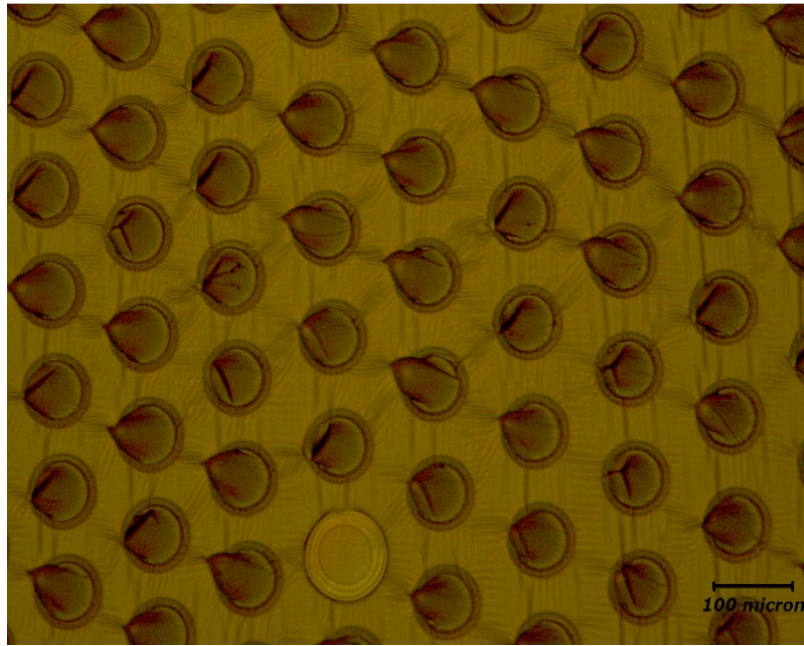


Figure 39: Column to column wrinkling pattern of PNIPAAm on a surface modified PMDS mold.

## 5.4 Wrinkling Patterns on HEMA-PFA Thin Films

### 5.4.1 Elastic Modulus Calculations of HEMA-PFA Copolymers

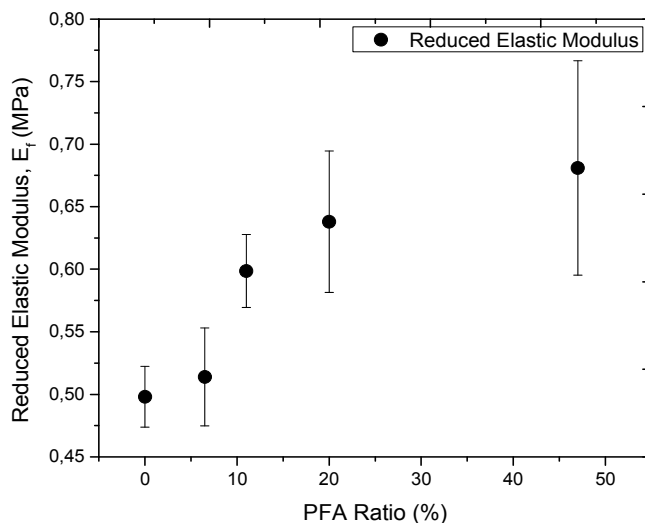


Figure 40: Reduced elastic modulus values of HEMA-PFA copolymers with varying PFA ratios.

Previously elastic modulus calculations of PNIPAAm thin films were reported. Same study is conducted for poly(HEMA-co-PFA) copolymers. Again the calculations are performed by AFM nanoindentation technique. The copolymers are deposited with varying PFA ratios and at constant thickness of 200 nm. The thin film elastic modulus of the copolymer increases with increasing PFA ratio. The elastic modulus values vary between 0.5-0.7 MPa, which are apparently much lower than PNIPAAm's values. PFA being a hydrophobic monomer changes the swelling properties of the copolymer as presented by contact angle and swelling studies. Besides PFA also affects the strength of the nanomaterial. Therefore wavelengths of wrinkled copolymer can be changed by tuning PFA ratio as well as thickness and substrate strength.

### 5.4.2 Elastic Modulus Calculations by SIEBIMM Method

SIEBIMM study is also performed for HEMA-PFA copolymers and elastic modulus values are compared.

Table 5: Comparison chart including the elastic modulus values calculated by SIEBIMM method and measured by AFM nanoindentation technique.

Thickness (nm)	PFA ratio (%)	Average wavelength ( $\mu\text{m}$ )	Stdv of average wavelength ( $\mu\text{m}$ )	Calculated $E_f$ (MPa)	Measured $E_f$ by AFM (MPa)
610	4	4.9	1.4	0.325	0.51
628	15	9.4	0.2	0.400	0.54
605	27	9.2	0.8	0.402	0.64
580	45	14.3	3.2	0.473	0.69

The elastic modulus values calculated by SIEBIMM seem to be increasing with PFA ratio. If one would compare this table to Table 4 a closer match between calculated and measured elastic modulus values is observed. Approximately 0.2 MPa difference is observed for each sample. The films are coated on 2.5% crosslinked PDMS substrates which have approximately 0.1 MPa elastic modulus with reasonably high standard deviations. 2.5% crosslinked PDMS is very sticky and difficult to analyze by AFM study. Therefore an error would have come from the elastic modulus calculation of 2.5% crosslinked PDMS which might leads to 0.2 MPa difference between the values in the Table 5. Nevertheless the close matching between the elastic modulus values found by SIEBIMM and AFM nanoindentation method seems promising.

#### 5.4.3 Uniaxial Wrinkling of HEMA-PFA Copolymers

HEMA-PFA copolymers were coated on flat silicon wafers, and experimental results (contact angle, surface roughness and swelling properties) were presented in chapter 4. This time amphiphilic copolymers are coated on stretched PDMS bars and uniaxial wrinkles are obtained. The thin films of the copolymers are topographically modified just like the work performed for PNIPAAm.

No wrinkle formation is observed for 7.5%, 10%, 20% and 30% crosslinked PDMS sticks. Considering that the elastic modulus of these PDMS samples are larger than the copolymer elastic modulus it remains valid to not to observe buckling pattern. In order to form wrinkles on soft PDMS substrates the films must be stiffer than the bottom layer. This rule is not satisfied with 7.5%, 10% 20% and 30% crosslinked PDMS

substrates. Therefore the experiments are conducted on 2.5% crosslinked PDMS bars. The elastic modulus of this PDMS is found to be 0.099 MPa. Copolymers are coated in different PFA ratios on stretched PDMS sticks and strains are removed after the depositions. For all experiment setups wrinkle formation is observed.

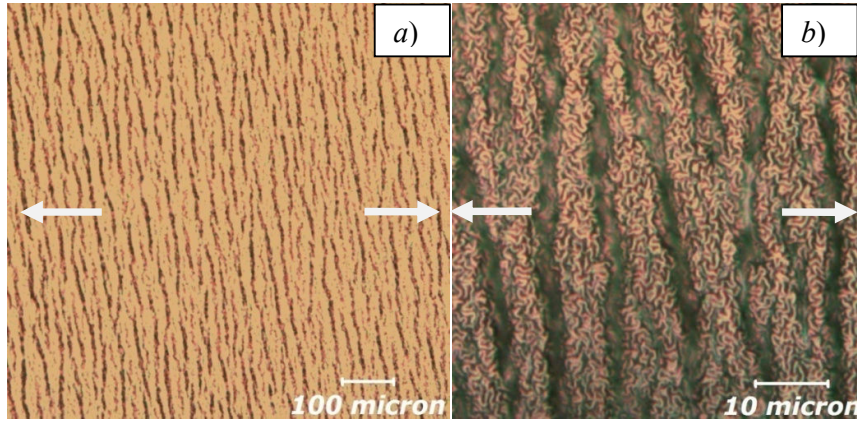


Figure 41: Optical microscopy images of wrinkled copolymers coated on 2.5% crosslinked PDMS sticks. (Film thickness: 200 nm, PFA ratio: 14%, and strain: 5%). a) 20x magnification and b) 100x magnification. White arrows show the direction of strain.

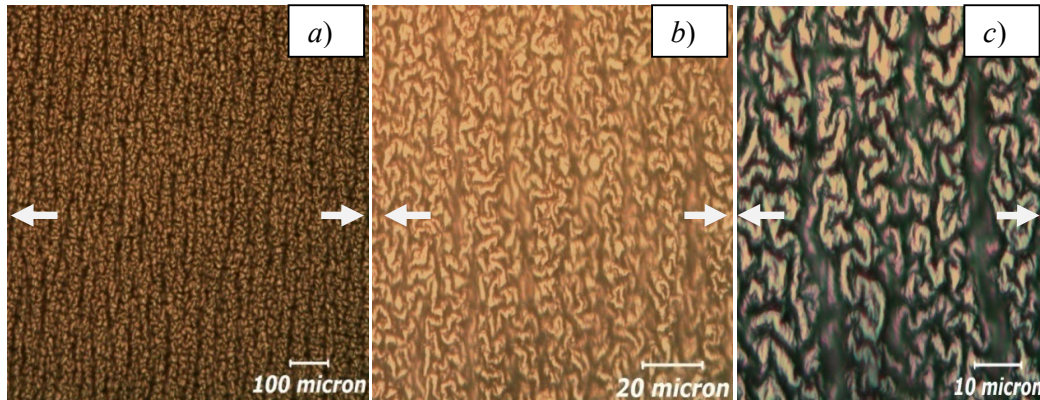


Figure 42: Optical microscopy images of wrinkled copolymers deposited on 2.5% crosslinked PDMS sticks. (Film thickness: 1500 nm, PFA ratio: 15%, and strain: 10%). a) 20x magnification, b) 50x magnification and c) 100x magnification. White arrows show the direction of strain.

In Figure 41 and 42 optical microscopy images from different samples are presented. The first realization is that the surface wrinkle pattern is different than that is formed by PNIPAAm deposition. In PNIPAAm's case the forming wrinkles were denser and

better aligned in  $y$  direction. When it comes to HEMA-PFA copolymer worm-shaped structures appears to be distributed along big vertical primary wrinkles. The wormy type of wrinkles does not have any preferred direction, and their wrinkle wavelength ( $4\ \mu\text{m}$ ) is smaller than primary uniaxial wrinkles ( $10\ \mu\text{m}$ ). Two different wrinkle formation mechanisms, mechanical stretching and heat-induced, are in competition in Figure 41 and 42. One would say that both factors are contributing to the surface wrinkle structure: mechanical stretching effect creating the bigger wrinkles and heating effect forming little wormy wrinkles. Remembering the Figure 31 PNIPAAm depositions on uniaxially stretched-2.5% crosslinked PDMS bars create only primary vertical wrinkles, and random type of buckling is not observed. The difference between two phenomena is related to the elastic modulus of PNIPAAm and HEMA-PFA copolymer. Since HEMA-PFA copolymer has a low elastic modulus the effect of mechanical stretching cannot become the dominating factor and heat-induced wrinkle formation mechanism is also active.

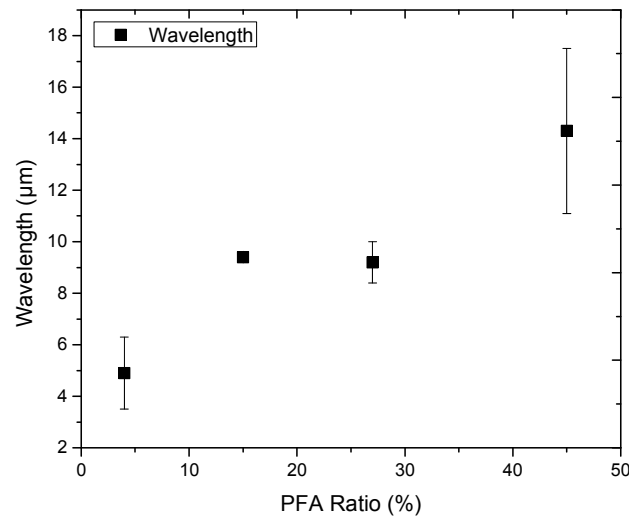


Figure 43: Wavelength data for wrinkled copolymer films with respect the varying PFA ratio. Film thickness is 300 nm for each sample.

Figure 43 provides the average wavelength of the copolymer wrinkles. As stated before (Figure 40) the elastic modulus of the copolymer increases with increasing proportion of PFA. Therefore the results provided with Figure 43 are consistent with formula 2 saying that  $E_f$  increases the average wavelength.

## 5.5 Temperature Response of Uniaxially Wrinkled PNIPAAm Films

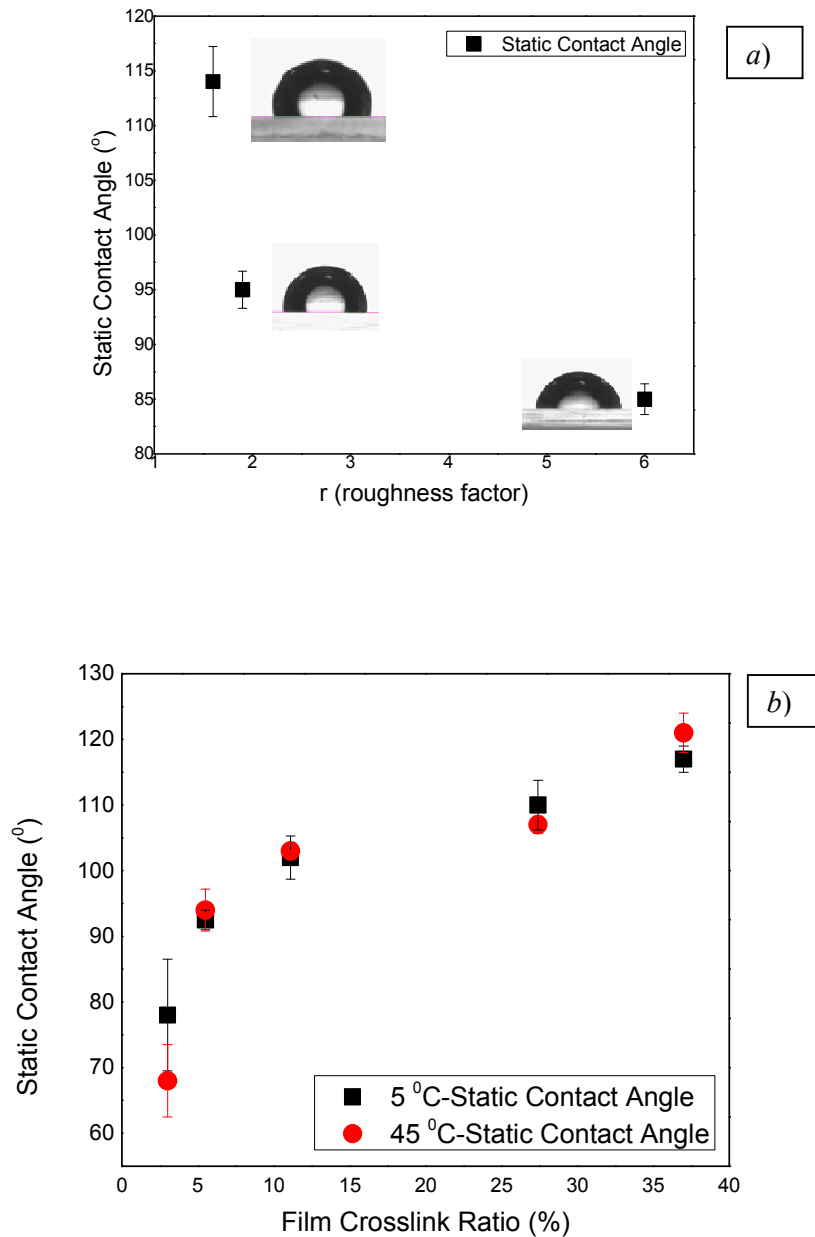


Figure 44: Contact angle results on uniaxially wrinkled PNIPAAm films; a) topographical effect and b) effect of film EGDMA ratio.

Figure 44-a gives the contact angle results on uniaxially wrinkled PNIPAAm thin films of same film composition (15%) and thickness (200 nm). The only varying parameter is the roughness factor (true area / projected area). The measurements are conducted at room temperature. According to the results the contact angle decreases with the

increasing roughness factor. As the surface becomes rougher the droplets are getting wetted over the surface. Remembering that PNIPAAm is in hydrophilic regime at room temperature increased roughness factor increases the hydrophilicity of the wrinkled surfaces. The results can be explained by Cassie-Baxter model;

$\text{Cos } \theta^* = r_f f \text{Cos } \theta + f - 1$  where  $\theta^*$ ,  $\theta$ ,  $f$  and  $r_f$  are apparent contact angle, contact angle on flat surface, fraction of wet solid area and roughness factor.

15% crosslinked PNIPAAm flat surface gives contact angle of  $40^\circ$ . Using  $f$  values of 0.26, 0.37 and 0.2 for increasing  $r$  factors (1.6, 1.9 and 6) apparent contact angles are measured as  $114^\circ$ ,  $95^\circ$  and  $85^\circ$ , respectively. These results show that topography certainly affects the water contact angle on wrinkled PNIPAAm films.

Figure 44-b gives the static contact angle results on uniaxially wrinkled PNIPAAm films (200 nm thickness) of different EGDMA ratios, for both  $5^\circ\text{C}$  and  $45^\circ\text{C}$ . Increasing EGDMA ratio in the film increases the overall contact angles. This result is consistent with data provided at Figure 22 (contact angles on flat PNIPAAm films). Besides compared to Figure 22 overall contact angles increase with the topographical modification.

However, no change is observed between  $5^\circ\text{C}$  and  $45^\circ\text{C}$  angles for any sample. No transition from being hydrophilic to hydrophobic is observed as it did for flat PNIPAAm films (see Figure 22). Wrinkled PNIPAAm thin films remain unreactive to temperature change. The expectation was superhydrophilic PNIPAAm surface at low temperatures and superhydrophobic PNIPAAm surface at high temperatures. It is known that surface modifications mostly increase the wetting over the hydrophilic surfaces while they decrease the wetting over hydrophobic surfaces. In order to find the reasoning behind response problem several studies are performed.

Firstly it is suspected that wrinkled PNIPAAm thin films experience a topographical or chemical damage during the high temperature contact angle measurements due to the hot water droplets. Water droplets of  $25^\circ\text{C}$  and  $40^\circ\text{C}$  are put on the wrinkled PNIPAAm surfaces. After 5 min optical microscope and FTIR analysis are done on those regions in order to investigate any possible effect of high temperature and water contact.

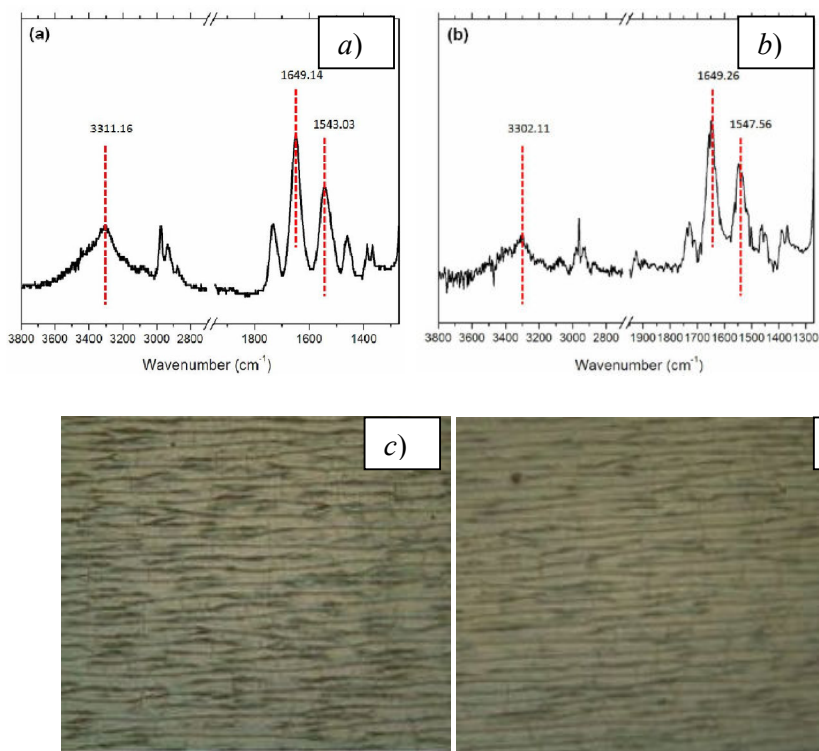


Figure 45: Hot water treatment on wrinkled PNIPAAm films. FTIR spectra of a) control sample and b) treated sample; optical microscopy images of c) control sample and d) treated sample.

Figure 45 provides the optical microscopy and FTIR analysis of the control sample (25 °C- water) and the treated sample (40 °C-water). FTIR spectra show that the characteristics PNIPAAm bands are preserved on both samples and completely matching with those on Si wafer (See Figure 20). Optical microscopy analysis revealed that no significant surface topography change is observed. The wrinkle direction and wavelengths are found to be stable. Optical microscope image of the treated sample looks less bright than that of control sample. That probably results from the film thickness loss which causes the reduced light intensity on the image.

Although the macroscopic analysis studies showed no evidence of chemical or topographical change it is suspected that elemental level changes might be occurring at the film + substrate system. Especially formation of an interface between the film and substrate could be the reason behind the non-response of wrinkled PNIPAAm to temperature. Atomic diffusions from film to substrate might spoil the film chemistry and therefore thermoresponsive properties. In order to investigate that uniaxially wrinkled PNIPAAm films of 120 nm thickness are studied by XPS. Depth etching study

is performed for control sample (25 °C) and treated sample (70 °C). A remainder here is that although the sample is heated to 70 °C for 30 min the XPS measurement on both films are conducted at room temperature. As reference atom nitrogen (N) is chosen since PDMS does not include it but PNIPAAm does. The samples are etched from the film side and nitrogen atomic percentage through the etched depth is presented in Figure 46.

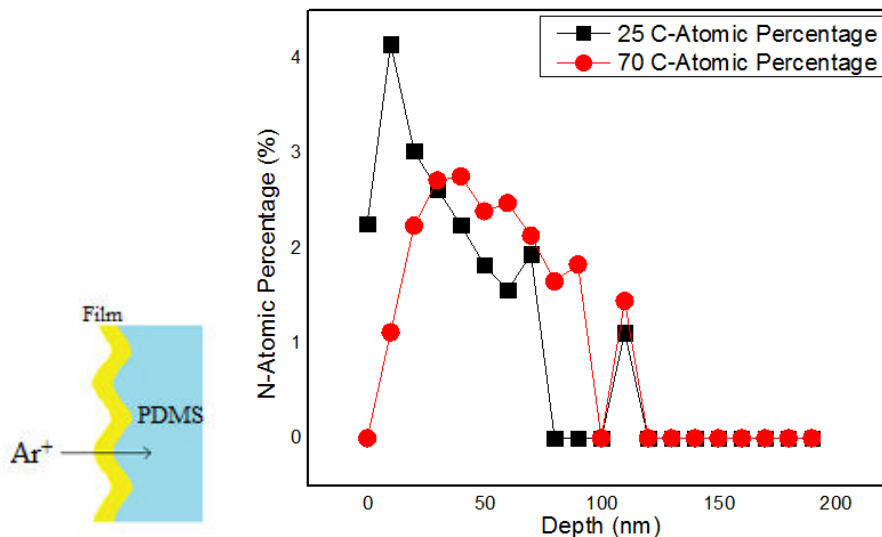


Figure 46: Elemental nitrogen percentage profile detected by XPS depth etching.

The results show that nitrogen atom is no more present after 110 nm thickness. It is useful to remember that the film thickness of PDMS sample is determined according to the Si samples which are simultaneously coated. The measured thickness on Si wafer is 120 nm. Considering that PDMS and Si wafer adsorbs different amount of monomer during deposition the thickness deviation remains reasonable. Therefore the depth at which nitrogen atom is last observed approximately matches with the film thickness. Also the fact that no nitrogen is present after 110 nm proves that N atom does not diffuse to PDMS during the heat treatment. Therefore one could say that there is no interface formation between the two layers or no change in the polymer chemistry.

In order to observe the thermoresponsiveness of PNIPAAm swelling experiments are performed on 20% crosslinked-wrinkled PNIPAAm films. 0.032 gr of water is put on several samples and stay there for 30 min. For control samples (water and sample temperature: 5 °C) the water droplets are removed and amount of swollen water is

measured after 20 min considering the response time of PNIPAAm. For treated samples (water and film temperature: 40 °C) the measurement are done right after the droplets are removed to prevent water evaporation. The idea behind this experiment is to see the fraction of water swelling at room temperature (in hydrophilic regime) and high temperature (in hydrophobic regime). The results are presented in Table 6. The swelling fraction is calculated as;

Swelling fraction: Swollen water weight / Initial total water weight.

Table 6: Swelling fractions for uniaxially wrinkled PNIPAAm films.

R factor	5 °C swelling fraction	40 °C swelling fraction
0	0.003	0
1	0.0090	0.0001
3.1	0.037	0
3.4	0.012	0

According to the results in Table 6 the wrinkled PNIPAAm films are able to swell at 5 °C which proves PNIPAAm chains show hydrophilic behavior. On the other hand when temperature is raised above LCST no water uptake is observed. This result suggests that PNIPAAm chains show hydrophobic behavior at high temperature. No direct relationship is observed between the roughness factor and water uptake.

Swelling studies confirm that wrinkled PNIPAAm thin films are in fact showing response to temperature. The wrinkled films show hydrophilic and hydrophobic behavior at 5 °C and 40 °C, respectively. Also bacterial adhesion studies which will be presented in the next chapter show that wrinkled PNIPAAm films show temperature response. We showed that there is no change in the polymer chemistry and topography after the samples are exposed high temperatures. In this regard contact angle results seem contradicting the swelling and bacterial adhesion studies. One might highlights the XPS results and emphasizes the deviations at the nitrogen concentration through the depth profile. It is observed that nitrogen concentration is low and the film surface might be populated by EGDMA at the early depths. Therefore this composition variation along the thickness (high concentration near the top surface) might have

prevented PNIPAAm chain from responding to temperature. However considering Figure 22 this assumption becomes invalid since the flat PNIPAAm films which are simultaneously coated with wrinkled PNIPAAm films showed temperature response. As a reason to the problem with the contact angles results one might put forward that the wrinkling structure prevents PNIPAAm chains from conformational changes by temperature. However swelling experiments showed that the surface energy can be changed by temperature. Also considering the size of polymeric chains (nm) and wrinkle wavelengths ( $\mu\text{m}$ ) this reasoning remains invalid.

Therefore it is believed that the problem with the contact angle results is not the unreactive chains but a possible methodological mistake. Although no satisfactory answer is found yet repetition of the experiments with a drop shape analyzer having automatic temperature controller may provide a solution.

## Chapter 6

# Bacterial Adhesion Studies

### 6.1 Introduction

In this chapter bacteria adsorption studies regarding different samples of PNIPAAm surfaces are going to be presented. The effect of polymer chemistry and surface morphology are going to be discussed.

### 6.2 Comparing Bare Si wafer and Flat PNIPAAm Films

The first step of the work is the imaging of the e-coli (average length: 10  $\mu\text{m}$  and average width: 3  $\mu\text{m}$ ) cells on standard glass microscope slides in order to verify their size and GFP expression.

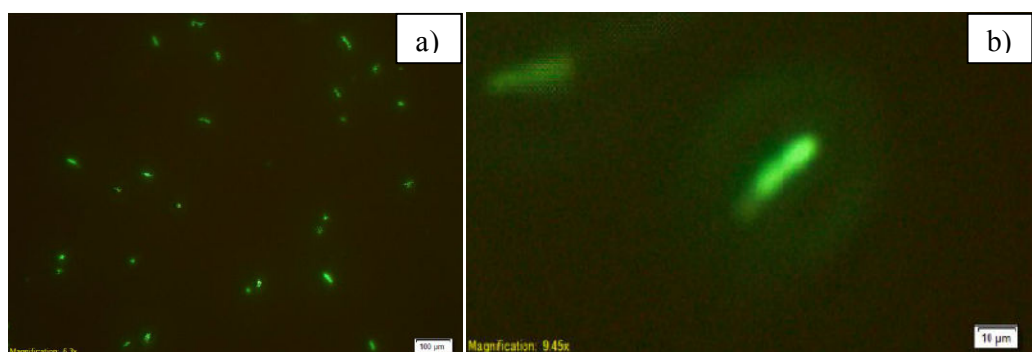


Figure 47: Imaging of bacteria on microscope glass slides at 2 different magnifications; a) 927.9 x 698.8  $\mu\text{m}^2$  scanning area and b) 155.5 x 84.6  $\mu\text{m}^2$  scanning area.

Figure 47-a and b show the visualization of the bacteria at two different magnifications. The images suggest that GFP expression is enough to detect one single bacterium. The appearance of the bacterium in Figure 47-b is out of focus because of the bacterium motion.

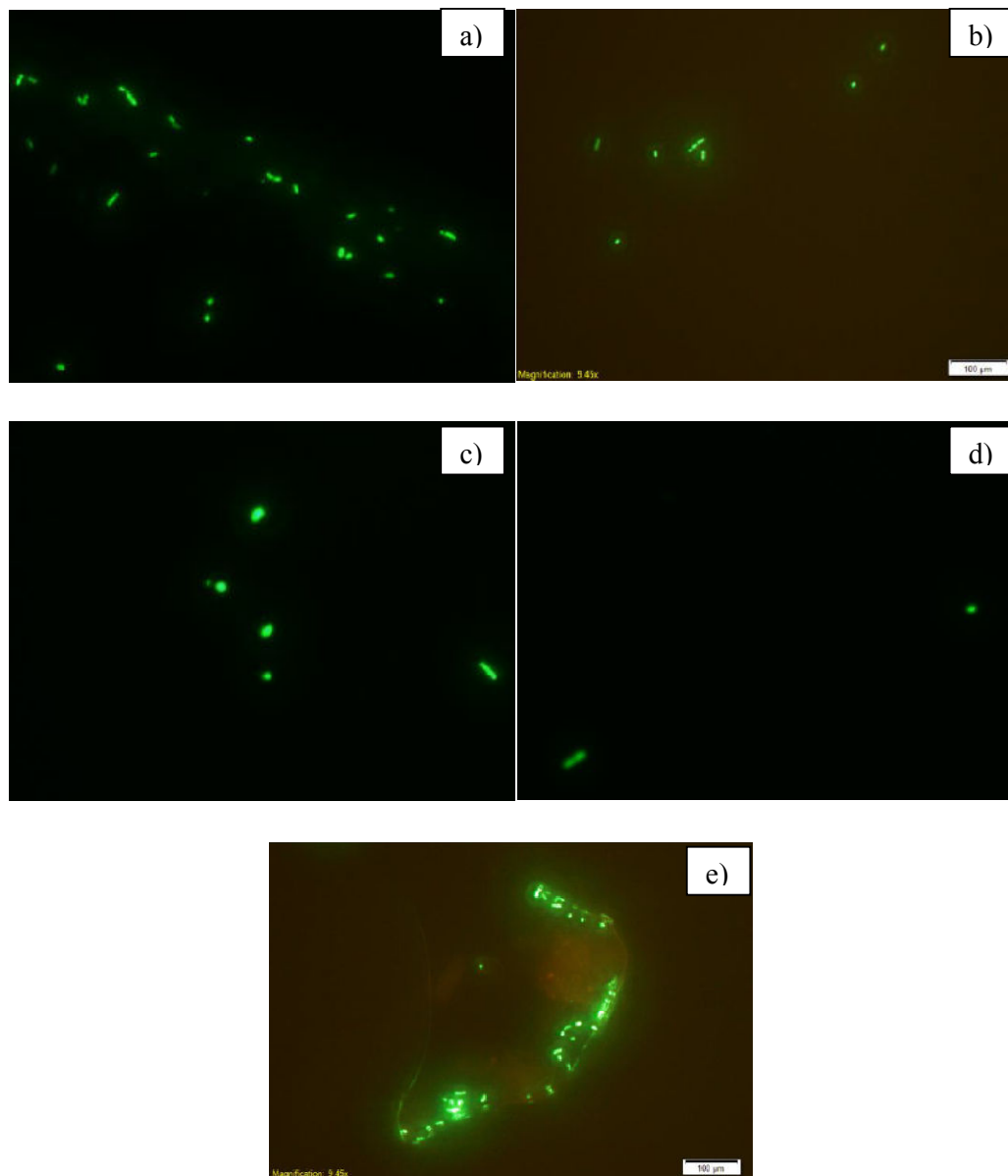


Figure 48: Inverted fluorescent microscope images of the surfaces. Washed by NaCl for 1 min a) bare Si wafer and b) 15% crosslinked PNIPAAm flat film; washed by NaCl for 5 min c) bare Si wafer and d) 15% crosslinked PNIPAAm flat film; and e) bacteria accumulation around defects. All measurements are conducted at room temperature.

Figure 48 briefly summarizes the effects of the washing time and the polymer coating on wafers. Figure 48-a and b belongs to the samples which are washed by NaCl for 1 min: Bare Si wafer and flat PNIPAAm thin film, respectively. The visualization of the bacteria on bare wafer (Figure 48-a) is less bright than those which are visualized on glass side. Probably the dark colored Si wafer absorbs more light compared to glass slides. Apparently there is a huge difference between two images. The flat PNIPAAm thin film coating on Si wafer leads to less number of bacteria adsorbed on the surface. Therefore PNIPAAm shows an improved anti-biofouling effect compared to bare Si wafer at room temperature. The same study is repeated by increasing washing time: 5 min. This time on both bare wafer and PNIPAAm coated surfaces less number of bacteria are detected (Figure 48-c and d) compared to Figure 48-a and b. Therefore washing time drastically affects the amount of the bacteria attached to the surfaces. At Figure 48-e accumulation of bacteria around surface defects on PNIPAAm thin film is presented. Compared to the other images the concentration of the green light, the density of the bacteria, is highly increased in the defected region. The physical barriers (sample edges, defects, contamination, valleys and so on) increase the accumulation of the bacteria since they hinder the motion of the bacteria providing a good shelter to survive and grow. Therefore for the anti-biofouling systems all possible surface inhomogeneities must be eliminated unless they are intentionally introduced. The orange-yellowish color on some of the images comes from the HCl which is being used in washing step, and not related to the surface deficits. Therefore for the further studies ethanol solution instead of HCl is preferred.

### 6.3 Effect of PNIPAAm Chemical Composition on Bacteria Attachment

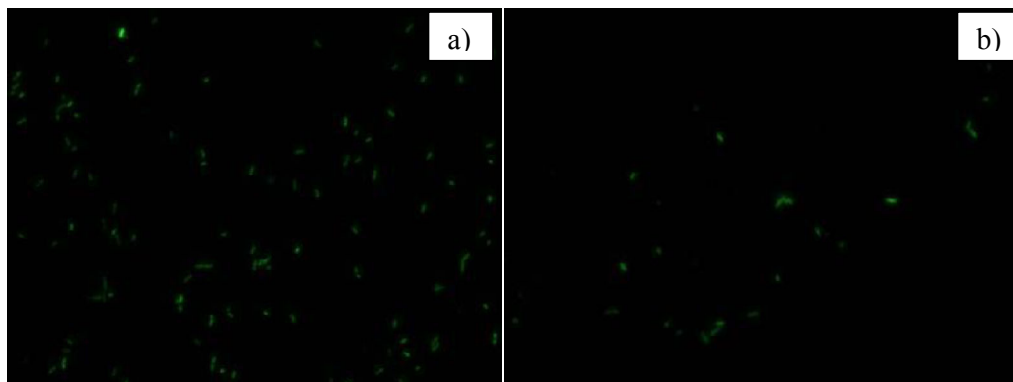


Figure 49: Inverted fluorescent microscope images of flat PNIPAAm surfaces; a) 5% crosslinking and b) 20% crosslinking. All measurements are conducted at room temperature. Thickness of each film is around 200 nm.

After the control group experiments the crosslinking effect on bacteria attachment is studied. Figure 49 gives the visualization of the e-coli bacteria on 5% crosslinked (Figure 49-a) and 20% crosslinked (Figure 49-b) PNIPAAm surfaces, at room temperature. Obviously low crosslinked polymeric film adsorbs more bacteria than the high crosslinked film. That is directly related to the chemical nature of the films. As more EGDMA is incorporated into the film, the hydrophilic nature of the PNIPAAm at room temperature is reduced. The film becomes more hydrophobic which favors the hydrophobic-hydrophobic interactions. Therefore hydrophilic e-coli bacteria chemically encounter an unfavorable place on the highly crosslinked film where the surface energy is comparably low. In the studies it is found that least number of bacteria is adsorbed on 28% crosslinked flat PNIPAAm films.

## 6.4 Comparing Flat PNIPAAm Film and Uniaxially Wrinkled PNIPAAm Films

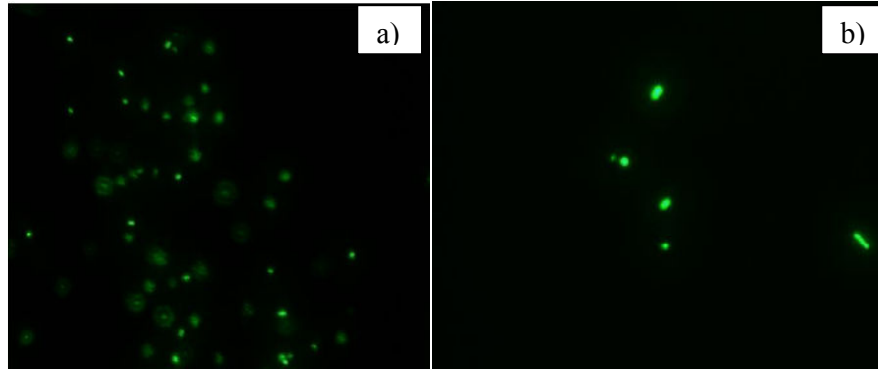


Figure 50: Inverted fluorescent microscope images of a) 10% crosslinked flat PNIPAAm film and b) wrinkled ( $\sim 5 \mu\text{m}$  wavelength) PNIPAAm thin film (10% crosslinked). All measurements are performed at room temperature. Thickness of each film is around 200 nm.

Figure 50 compares the bacterial attachment density on a flat PNIPAAm surface and a wrinkled PNIPAAm thin film. For each sample 4 images are taken from different places over the samples. Bacteria are counted by naked eye and the final number is given as the average of 4 different images. Based on the images there are less number of e-coli bacteria adsorbed on the wrinkled PNIPAAm film ( $\sim 6$  bacteria /  $12 \times 10^6$  pixels<sup>2</sup>) compared to the those on flat PNIPAAm surface ( $\sim 55$  bacteria /  $12 \times 10^6$  pixels<sup>2</sup>). This consequence directly results from the surface topography effect since the chemical compositions of the film are the same. The periodic roughness introduced to the surface creates mismatch between the surface topographical and bacterial dimensions. Therefore the attachment of the bacteria becomes difficult due to the spatial restrictions. Geometrically a single bacterium tend to place in between the wrinkles (valleys) (bacteria A, D and E at Figure 53-a) instead of rougher positions such as wrinkle tops (bacterium C at Figure 53-a) or with a direction perpendicular to the wrinkle orientation (bacterium B at Figure 53-a). Since e-coli bacteria are hydrophilic any bacterium encountering a hydrophilic surface tends to maximize the hydrophilic-hydrophilic interactions which can be simply achieved by larger interaction area.

The orientations of the attached bacteria on wrinkled polymer films are expected to be aligned according to uniaxial wrinkling direction. However that expectation is not observed clearly. Random adhesion of bacteria with no specific orientation is commonly observed at different places of the same sample. That truly results from the fact that uniaxial wrinkling orientation is not perfect such that the pattern includes inhomogeneities. Non-uniform distribution of the wrinkles (deviations in wrinkle wavelength and direction) may offer more available spaces for elliptical e-coli bacteria. Moreover the dimensions of the bacteria in this work have some degree of standard deviation. Therefore it is believed that the attachment of the bacteria only in between the wrinkles can be better observed with more regular bacteria culture and uniformly wrinkled samples.

### **6.5 Investigation of the Bacteria Behavior on Uniaxially Wrinkled PNIPAAm Surfaces**

The effect of polymer composition and wavelength of the uniaxial wrinkles on bacteria attachment is studied. The sample parameters are listed in Table 7.

Table 7: List of the sample parameters to be studied in this section.

Name	Waiting Time	Washing	Film Thickness (nm)	EGDMA Ratio (%)	Wavelength ( $\mu\text{m}$ )
Control_20 (20% Bare PDMS)	3 hours	150 mM NaCl, 1 ml			
Control_5 (5% Bare PDMS)	3 hours	150 mM NaCl, 1 ml			
Set1_20 (20% PDMS, uniaxial wrinkling)	3 hours	150 mM NaCl, 1 ml	130	10	0,8
Set1_5 (5% PDMS, uniaxial wrinkling)	3 hours	150 mM NaCl, 1 ml	130	10	1,6
Set2_20 (20% PDMS, uniaxial wrinkling)	3 hours	150 mM NaCl, 1 ml	130	23	1,25
Set2_5 (5% PDMS, uniaxial wrinkling)	3 hours	150 mM NaCl, 1 ml	130	23	1,9
Set3_20 (20% PDMS, uniaxial wrinkling)	3 hours	150 mM NaCl, 1 ml	130	28	1,2
Set3_5 (5% PDMS, uniaxial wrinkling)	3 hours	150 mM NaCl, 1 ml	130	28	2,6

PDMS bars are uniaxially stretched (20% strain) and coated with PNIPAAm films. Basically 3 different sets (set 1, set 2 and set3) of samples are investigated. The basic difference between each set is the EGDMA ratio: 10 %, 23% and 28%. Apart from that 2 different substrates of PDMS are used for each set: 5 % crosslinked and 20 % crosslinked. The use of different substrates for each set is to create wrinkles of different wavelengths. Therefore in this experimental setup both chemical and topographical effects are analyzed. The average bacteria number is given after the 4 different pictures on each sample.

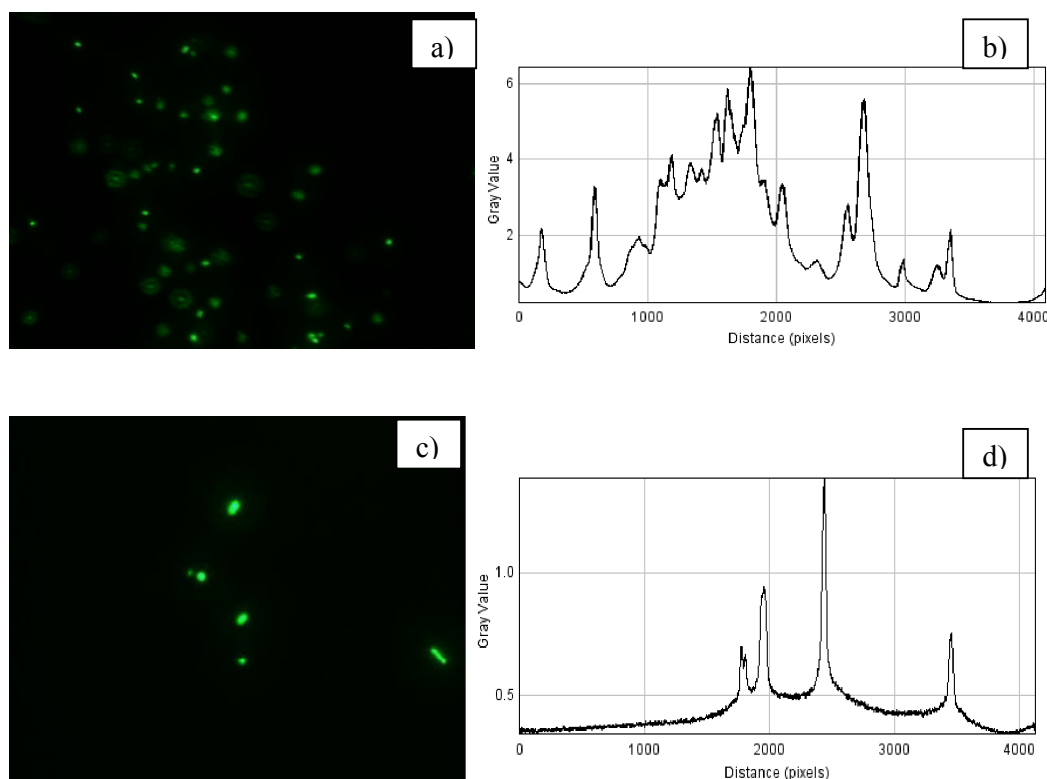


Figure 51: Images of bacterial attachment of the surfaces of a) 5% crosslinked bare PDMS, c) uniaxially wrinkled PNIPAAm thin films (10% crosslinked) on 20% crosslinked PDMS, the corresponding the light intensity graphs b) for a and d) for c. Each peak on light intensity graphs represents a single bacterium. All measurements are conducted at room temperature.

Higher number of the bacteria is observed on the control group: bare PDMS bars (no polymeric coating). Compared to the wrinkled PNIPAAm surfaces bare PDMS sticks are found to be highly fouled. Also bacteria are found to be adhered more to 5% crosslinked bare PDMS compared to 20% crosslinked one. This result suggests that bacteria prefer to attach to the softer PDMS surfaces unless a surface treatment or thin film deposition is operated. The light intensity graphs provided at Figure 51 –b and d measure the intensity of the light over the selected areas on the microscope images. Width of the peaks basically refers to the bacterium dimension and the intensity corresponds to the GFP expression. Each bacterium is found to be creating a peak width of 25-30 pixels at the background profile. Therefore number of the peaks with certain widths on background profile gives the number of the bacteria on the selected image. In this regard the graphs presented at Figure 51-b and d gives consistent data with the images presented at Figure 51-a and c.

The results overall suggest that as the crosslinking ratio of the film increases the number of attached bacteria decreases. 28% crosslinked wrinkled PNIPAAm surfaces has very little or no bacteria attachment on their surfaces (0.75 bacteria at the area of  $232.0 \times 174.7 \mu\text{m}$ ). The average number of the bacteria on 10% crosslinked and 23 % crosslinked surfaces are found to be 6 and 2.5 bacteria at the area of  $232.0 \times 174.7 \mu\text{m}$ . These results are consistent with the ones presented at Figure 49. The highly crosslinked PNIPAAm surfaces show more resistance against the adhesion of the hydrophilic bacteria because of the decreased surface energy. Although PNIPAAm is still in the hydrophilic regime at room temperature the crosslinking degree lowers the surface energy which affects the surface interactions with the incoming species.

In this study no effect of the wavelength on fouling is detected. For each sample set no difference is observed between the films which are deposited on 5% and 20% crosslinked PDMS samples (see Table 7 for wavelength differences). This can be explained from the mismatch between the bacterial dimensions and wrinkle sizes. The maximum wrinkle wavelength used in this experimental setup is  $2.6 \mu\text{m}$  which is far smaller than the bacterial size. For the better analysis of the wavelength effect it is better to synthesize the wrinkled surfaces which have longer wavelengths than  $10 \mu\text{m}$ , which is the average length of e-coli.

## 6.6 Investigation of the Bacteria Behavior on Randomly Wrinkled PNIPAAm Surfaces

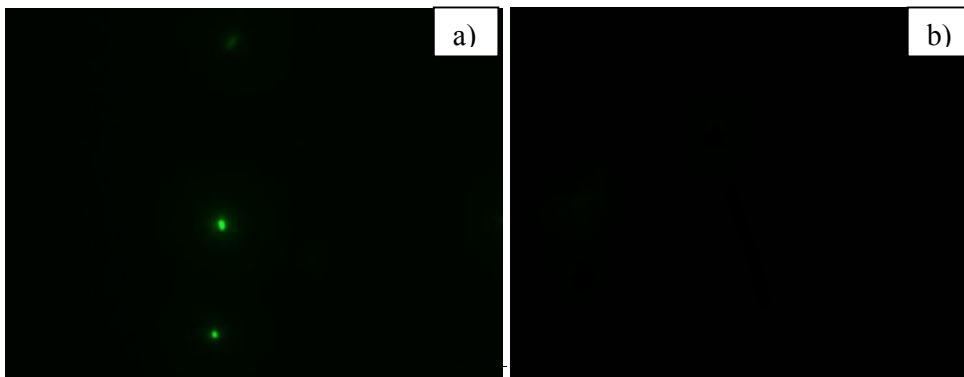


Figure 52: Images of the bacterial attachment on randomly wrinkled PNIPAAm thin film of a) 10 % crosslinking and b) 28% crosslinking. All measurements are performed at room temperature.

In the previous section the bacterial attachment behavior on the uniaxially buckled PNIPAAm thin films with varying EGDMA ratios were given. The same experiments are repeated for the randomly buckled PNIPAAm thin films. The experimental parameters (film crosslinking ratio and PDMS crosslink ratio) are the same for the samples to be analyzed in this session. The wavelengths of the samples are very similar to the corresponding uniaxially wrinkled samples. Therefore the primary difference between the samples of previous section and here is the wrinkling pattern.

The results reveal that the number of the bacteria attached to the randomly wrinkled PNIPAAm surfaces is much lower compared to the uniaxially wrinkled film; for each sample set. The random wrinkling created an enormous resistance to the bacterial attachment and the number of the bacteria are observed to be almost 0. Although the uniaxially forming wrinkles showed better resistance compared to bare PDMS bars and flat PNIPAAm thin films the bacterial attachment could not be completely eliminated. Because of the periodic configuration of the wrinkles the valleys still provide shelters for bacteria and those bacteria may not be swept away upon washing. However when the wrinkling pattern is transformed to randomly oriented type, even with the same wavelength, there is no place or gap that a bacterium of  $10\ \mu\text{m}$  is geometrically able to find. In order to understand the spatial restriction one can see Figure 53-b. As discussed in Chapter 6.4 the bacteria-surface interaction can be improved with larger contact area. A single bacterium of  $10 \times 3\ \mu\text{m}$  dimensions can barely find a position that maximizes the contact area, and therefore the bacteria which suffer from the limited physical and chemical adhesion can be readily removed at washing step.

Figure 52 presents the images of the randomly buckled PNIPAAm thin films of different EGDMA ratios. On the film of higher crosslinking (Figure 52-b) no bacterial attachment is observed. Like the results gathered for uniaxially wrinkled PNIPAAm thin films, crosslinking ratio of the film decreases the number of the attached e-coli bacteria for randomly buckled ones as well since the decreased hydrophilicity of the surface complicates the physical and chemical interaction of the bacteria. Therefore it can be concluded that randomly wrinkled PNIPAAm surfaces might create completely anti-biofouling surfaces against e-coli bacteria.

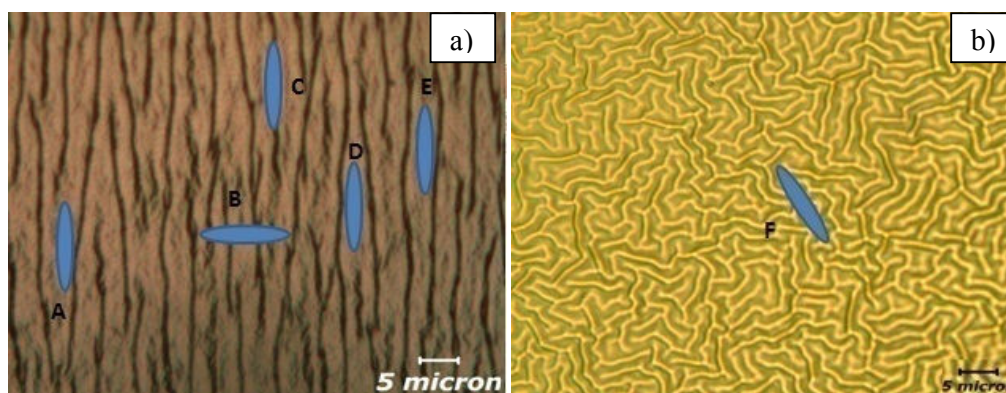


Figure 53: Schematic showing the geometrical considerations regarding bacterial adhesion on a) uniaxially wrinkled and b) randomly wrinkled surfaces.

### 6.7 Effect of the Temperature on the Bacterial Attachment Behavior of Wrinkled PNIPAAm Films

One of the basic goals of this thesis is to show the temperature response of the PNIPAAm thin films. The thermoresponsive property of wrinkled PNIPAAm thin films is used for the bacteria attachment studies. Two different experimental setups are used: Attachment of the bacteria at room temperature and attachment behavior of the bacteria when temperature is raised above LCST to 37 °C. For the sake of ease each procedure is denoted as RT (room temperature) and RTTHT (room temperature to high temperature). Three different uniaxially wrinkled PNIPAAm films (crosslinking 15%) of varying wavelengths are investigated for each setup: 2.7, 1.5 and 0.9  $\mu\text{m}$ . Each film has the thickness of 130 nm. The bacteria cultures are kept on the samples for 3 hours and later washed by 1 ml distilled water.

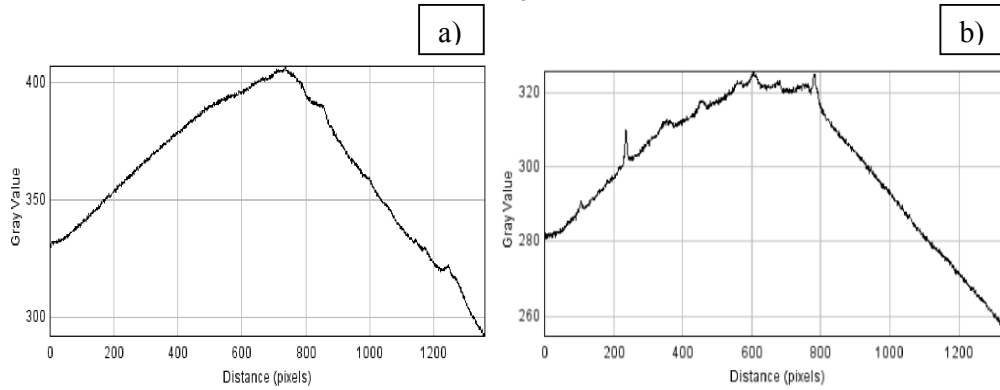


Figure 54: Light intensity graphs for bacterial attachment on the surfaces of a) RTTHT sample (0.9  $\mu\text{m}$  wavelength), b) RT sample (0.9  $\mu\text{m}$  wavelength). Film thickness and EGDMA ratio for each film is 130 nm and 15%, respectively.

According to the results more bacteria are attached to RT samples compared to RTTHT samples. Since PNIPAAm thin films show coil-to-globule transition through LCST, changing the surface energy, the behavior of the surfaces at different temperatures are expected to be different as well. PNIPAAm thin film goes from hydrophilic regime to hydrophobic regime around LCST upon temperature increase. For RTTHT samples the bacteria attached to hydrophilic PNIPAAm thin films are affected by the temperature increase and some of the bacteria are detached when the surface becomes hydrophobic. The change of the surface-bacteria interaction causes the detachment of some for RTTHT samples. Therefore PNIPAAm thin films are proven to be responding to the temperature changes.

In contrast to the results presented so far the wavelength of the wrinkles affect the number of bacteria attached. For RTTHT samples least number of bacteria is observed on the one having 0.9  $\mu\text{m}$  wavelength. Although the surface topography does not affect the number of bacteria for RT samples the decrease in the wavelength (increase of the roughness coefficient: real area/ projected area) improves the thermoresponsive properties of the film. The reason behind that might be the easier transformation of the PNIPAAm chains when the wavelength is small. However this conclusion requires more bacterial adhesion studies and especially the investigation of the molecular level changes that polymeric chains of a wrinkled thin film undergoes around LCST.

## Chapter 7

### Conclusion

Within the scope of this thesis, initiated chemical vapor deposition method (iCVD) has been successfully employed in order to form intelligent nano-scale polymeric materials. iCVD method is shown to be able to form conformal thin polymeric films on different types of substrates.

This work basically targeted to indicate how polymeric properties change/improve with surface modifications. For this purpose two polymer systems, poly(N-isopropylacrylamide) and poly(hydroxyethylmethacrylate-co-perfluorodecylacrylate), are deposited on flat Si wafers and stretched PDMS molds in order to modify the surface morphology. The properties of the flat and surface modified polymers with respect to varying copolymer compositions are analyzed by several surface characterization techniques. The results related to flat form of the films suggest that the responsive properties of PNIPAAm and PHEMA based polymeric thin films can be tuned by the introduction of the crosslinker and a hydrophobic monomer, respectively. The contact angle studies reveal that PNIPAAm based polymeric thin films can respond differently under varying temperatures. PHEMA based polymeric thin films, on the other hand, exhibited totally different surface properties in dry and water mediums.

The polymeric thin films are deposited on stretched PDMS molds in order to transform the surface structure in such way that uniformly distributed, periodic and sinusoidally shaped surface topography can be achieved. Based on this method, so called uniaxial wrinkling, the surface topographies of the films are shown to be dependent on the mechanical properties of the system; polymeric thin film elastic modulus, PDMS substrate elastic modulus and film thickness. The optimum wavelengths of the buckled

structures are found to be varying by these parameters. Moreover the surface morphology studies indicate that the type of the wrinkling pattern is significantly affected by the film elastic modulus. As PNIPAAm thin films have bigger elastic modulus values than HEMA-PFA copolymer the resulting uniaxial wrinkling pattern of PNIPAAm is found to be better aligned and nicely distributed compared to that of HEMA-PFA. During the studies the heat sources in iCVD system are observed to be causing to random wrinkling patterns on polymeric thin films. Contact angle studies on PNIPAAm films show that no difference was observed between the angles of low and high temperature regimes. It is believed that this observation results from methodological mistakes during contact angle studies since swelling studies prove that wrinkled PNIPAAm films respond to temperature change.

As the last work packet both flat and surface modified PNIPAAm films were investigated for the attachment studies of e-coli bacteria. Introduction of uniaxial or random wrinkling pattern to polymer surfaces improve the anti-biofouling properties. The number of the bacteria adsorbing to the wrinkled surfaces is much less than those attaching to flat surfaces. Besides the effects of film composition and wrinkle wavelength are analyzed for each case. Finally and most importantly the temperature effect on fouling is analyzed. It is shown that some of the bacteria adhering to wrinkled PNIPAAm surfaces at room temperature could be detached upon temperature increase above LCST. The mechanism is a direct result of the surface energy transition that comes up with temperature change. Therefore it is concluded that wrinkled PNIPAAm surfaces can be utilized as controlled anti-biofoulers.

## Bibliography

- [1] J. Hu, H. Meng, G. Li, and S. Ibekwe. A review of stimuli-responsive polymers for smart textile applications. *Smart Materials and Structures*, 21(5): 2012.
- [2, 3, 4, 16] S. Eun and S. M. Hudson. Stimuli-responsive polymers and their bioconjugates. *Progress in Polymer Science*, 29: 1173-1222, 2004.
- [5] F. Liu and M. W. Urban. Recent advances and challenges in designing stimuli-responsive polymers. *Progress in Polymer Science*. 35(1-2): 3-23, 2010.
- [6] V. Carelli, S. Coltelli, G. DiColo, E. Nannipieri, and M. F. Serafini. Silicone microspheres for pH-controlled gastrointestinal drug delivery. *International Journal of Pharmaceutics*, 179(1): 73-83, 1999.
- [7] L. Chu, R. Xie, and X. Ju. Stimuli responsive membranes: Smart tools for controllable mass-transfer and separation processes. *Chinese Journal of Chemical Engineering*, 19(6): 891-903, 2011.
- [8] J. Z. Hilt, A. K. Gupta, R. Bashir, and N. A. Peppas. A microsensor based on a microcantilever patterned with an environmentally sensitive hydrogel. *BioMEMS and Bionanotechnology*, 2002.
- [9] N. S. Satarkar, W. Zhang, R. E. Eitel, and J. Z. Hilt. Magnetic hydrogel nanocomposites as remote controlled microfluidic valves. *Lab on a Chip*, 9: 1773-1779, 2009.

- [10] K. Kwon and T. Matsuda. Photo-iniferter-based thermoresponsive block copolymers composed of poly(ethylene glycol) and poly(N-isopropylacrylamide) and chondrocyte immobilization. *Biomaterials*, 27(7): 986-995, 2006.
- [11] J. R. Morones-Ramirez. Environmentally responsive polymeric intelligent materials: the ideal components of non-mechanical valves that control flow in microfluidic systems. *Brazilian Journal of Chemical Engineering*, 27(1): 1-14, 2010.
- [12] D. Jovic, A. Tourette, P. Glampedaki, and M. M. C. G. Warmoeskerken. Application of temperature and pH responsive microhydrogels for functional finishing of cotton fabric. *Materials Technology*, 24(1): 14-23, 2009.
- [13] S. R. Tonge and B. J. Tighe. Responsive hydrophobically associating polymers: a review of structure and properties. *Advanced Drug Delivery Reviews*, 53(1): 109-122, 2001.
- [14] H. Almedia, M. Helena, and P. Lobao. Temperature and pH stimuli responsive polymers and their applications in controlled and self-regulated drug delivery. *Journal of Applied Pharmaceutical Science*, 2(06): 01-10, 2012.
- [15] S. T. Grainer and M. E. H. El-Sayed. Stimuli-sensitive particles for drug delivery. *biologically-responsive hybrid biomaterials: a reference for material scientists and bioengineers*. World Scientific Publishing Co. Pte. Ltd., Danvers (2010) 171-189.
- [17] M. Okubo, H. Ahmad, and T. Suzuki. Synthesis of temperature-sensitive micron-sized monodispersed composite polymer particles and its application as a carrier for biomolecules. *Colloid Polymer Science*, 276(6): 470-475, 1998.
- [18] V. Balamuralidhara, T. M. Pramodkumar, N. Srujana, M. P. Venkatesh, N. Vishal Gupta, K. L. Krishna and H. V. Gangadharappa. pH Sensitive drug delivery systems: A review. *American Journal of Drug Discovery and Development*, 1(1): 34-48, 2011.
- [19] E. Bellomo, M. D. Wyrsta, L. Pakstis, D. J. Pochan, and T. J. Deming. Stimuli responsive polypeptide vesicles by conformation-specific assembly. *Nature Materials*, 3: 244-248, 2004.
- [20] X. Yu, Z. Wang, Y. Jiang, and X. Zhang. Reversible pH-responsive surfaces: from superhydrophobicity to superhydrophilicity. *Advanced Materials*, 17: 1293-1295, 2005.

- [21] R. Huang, Z. Mah, M. Malta, L. K. Kostanski, C. D. M. Filipe, and R. Ghosh. Chromatographic separation of proteins using hydrophobic membrane shielded with an environment-responsive hydrogel. *Journal of Membrane Science*, 345(1-2): 177-182, 2009.
- [22] A. Kumar, A. Srivastava, I. Galaev, and B. Mattiasson. Smart polymers: Physical forms and bioengineering applications. *Progress in Polymer Science*, 32: 1205-1237, 2007.
- [23] M. A. Ward and T. K. Georgiou. Thermoresponsive polymers for biomedical applications. *Polymers*, 3(3): 1215-1242, 2011.
- [24] E. Mah and R. Ghosh. Thermo-responsive hydrogels for stimuli-responsive membranes. *Processes*, 1(3): 238-262, 2013.
- [25] S. S. Pennadam, K. Firman, C. Alexander and D. Gorecki. Protein-polymer nanomachines. Towards synthetic control of biological processes. *Journal of Nanobiotechnology*, 2(8): 2004.
- [26, 35] C. Bradley, N. Jalili, S. K. Liqiang, R. Förch, J. S. Gutmann, and R. Berger. Response characteristics of thermoresponsive polymers using nanomechanical cantilever sensors. *Macromolecular Chemistry and Physics*, 210(16): 1339-1345, 2009.
- [27, 28, 29, 38] R. Liu, M. Fraylich, and R. Saunders. Thermoresponsive copolymers: from fundamental studies to applications. *Colloid and Polymer Science*, 287(6): 627-643, 2009.
- [30, 44] H. G. Schild. Poly(N-isopropylacrylamide): experiment, theory and application. *Progress in Polymer Science*, 17(2): 163-249, 1992.
- [31] T. Maeda, K. Yamamoto, and T. Aoyagi. Importance of bound water in hydration-dehydration behavior of hydroxylated poly(N-isopropylacrylamide). *Journal of Colloid and Interface Science*, 302(2): 467-474, 2006.
- [32] J. M. Song, F. M. Winnik, and J. L. Brash. Synthesis and solution properties of fluorescently labeled amphiphilic (N-alkylacrylamide) oligomers. *Macromolecules*, 31(1): 109-115, 1998.

- [33, 39] L. M. Geever, D. M. Devine, M. J. D. Nugent, J. E. Kennedy, J. G. Lyons, A. Hanley, and C. L. Higginbotham. Lower critical solution temperature control and swelling behavior of physically crosslinked thermosensitive copolymers based on N-isopropylacrylamide. *European Polymer Journal*, 42(10): 2540-2548, 2006.
- [34] X. Ma, X. Zhao, S. Zheng, and X. Tang. Different deswelling behavior of temperature-sensitive microgels of poly(N-isopropylacrylamide) crosslinked by polyethyleneglycol dimethacrylates. *Journal of Colloid Interface Science*, 276(1): 53-59, 2004.
- [36] O. Tagit, N. Tomczak, and G. J. Vansco. Probing the morphology and nanoscale mechanics of single poly(N-isopropylacrylamide) microgels across the lower-critical-solution temperature by atomic force microscopy. *Small*, 4(1): 119-126, 2008.
- [37] K. N. Plunkett, X. Zhu, J. S. Moore, and D. E. Leckband. PNIPAM chain collapse depends on the molecular weight and grafting density. *Langmuir*, 22(9): 4259-4266, 2006.
- [40] X. Ma, J. Xi, X. Huang, X. Zhao, and X. Tang. Novel hydrophobically modified temperature-sensitive microgels with tunable volume-phase transition temperature. *Materials Letters*, 58(27-28): 3400-3404, 2004.
- [41] T. Patel, G. Ghosh, S. Yusa, and P. Bahadur. Solution behavior of poly(N-Isopropylacrylamide) in water: Effect of additives. *Journal of Dispersion Science and Technology*, 32(8): 1111-1118, 2011.
- [42, 43] X. Z. Zhang, X. D. Xu, S. X. Cheng, and R. X. Zhuo. Strategies to improve the response rate of thermosensitive PNIPAAm hydrogels. *Soft Matter*, 4(3): 385-391, 2008.
- [45] D. J. Beebe, J. S. Moore, J. M. Bauer, Q. Yu, R. H. Liu, C. Devadoss, and B. H. Jo. Functional hydrogel structures for autonomous flow control inside microfluidic channels. *Nature*, 404: 588-590, 2000.
- [46] X. Z. Zhang and R. X. Zhuo. A novel method to prepare a fast responsive, thermosensitive poly(N-isopropylacrylamide) hydrogel. *Macromolecular Rapid Communications*, 20(4): 229-231, 1999.

- [47] Y. Kaneko, S. Nakamura, K. Sakai, T. Aoyagi, Y. Sakurai, and T. Okano. Rapid deswelling response of poly(N-isopropylacrylamide) hydrogels by the formation of water release channels using poly(ethylene oxide) graft chains. *Macromolecules* 31(18): 6099-6105, 1998.
- [48] M. E. Alf, A. Hatton, and K. K. Gleason. Novel N-isopropylacrylamide based polymer architecture for faster LCST transition kinetics. *Polymer*, 52(20): 4429-4434, 2011.
- [49, 87] M. E. Alf, P. D. Godfrin, T. A. Hatton, and K. K. Gleason. Sharp hydrophilicity switching and conformality on nanostructured surfaces prepared via initiated chemical vapor deposition (iCVD) of a novel thermally responsive copolymer. *Macromolecular Rapid Communications*, 32(24): 2166-2172, 2010.
- [50] E. C. Cho, Y. D. Kim, and K. Cho. Thermally responsive poly(N-isopropylacrylamide) monolayer on gold: synthesis, surface characterization, and protein interaction/adsorption studies. *Polymer*, 45(10): 3195-3204, 2004.
- [51] I. Hirata, M. Okazaki, and H. Iwata. Simple method for preparation of ultra-thin poly(N-isopropylacrylamide) hydrogel layers and characterization of their thermo-responsive properties. *Polymer*, 45(16): 5569-5578, 2004.
- [52] R. K. Bose and K. K. S. Lau. Initiated chemical vapor deposition of poly(2-hydroxyethyl methacrylate) hydrogels. *Thin Solis Films*, 519(14): 4415-4417, 2011.
- [53] S. H. Baxamusa, L. Montero, J. M. Dubach, H. A. Clark, S. Borros, and K. K. Gleason. Protection of sensors for biological applications by photoinitiated chemical vapor deposition of hydrogel thin films. *Biomacromolecules*, 9(10): 2857-2862, 2008.
- [54, 56] K. Chan and K. K. Gleason. Initiated chemical vapor deposition of linear and cross-linked poly(2-hydroxyethyl methacrylate) for use as thin-film hydrogels. *Langmuir*, 21(19): 8930-8939, 2005.
- [55, 121] A. Asatekin, M. C. Barr, S. H. Baxamusa, K. K. S. Lau, W. Tenhaeff, J. Xu, and K. K. Gleason. Designing polymer surfaces via vapor deposition. *Materials Today*, 13(5): 26-33, 2010.

- [57] B. J. McMahon, C. A. Pfluger, B. Sun, K. S. Ziemer, D. D. Burkey, and R. L. Carrier. Photoinitiated chemical vapor deposition of cytocompatible poly(2-hydroxyethyl methacrylate) films. *Journal of Biomedical Materials Research*, 2013.
- [58] G. O. Ince, G. Demirel, K. K. Gleason, and M. C. Demirel. Highly swellable free-standing hydrogel nanotube forests. *Soft Matter*, 6(8): 1635-1639, 2010.
- [59] L. Montero, S. H. Baxamusa, S. Borros, K. K. Gleason. Thin hydrogel films with nanoconfined surface reactivity by photoinitiated chemical vapor deposition. *Chemistry of Materials*, 21(2): 399-403, 2009.
- [60] B. Ahmad, S. Bashir, S. Nisa, and M. B. Huglin. Chemically crosslinked N-Vinyl-2-Pyrrolidone/2-Hydroxyethyl Methacrylate (VP/HEMA) copolymer for the controlled release of cyclic oligopeptide. *Turkish Journal of Chemistry*: 279-285, 2004.
- [61] Y. Wei and Y. Chen. Surface modification of PMMA IOLs by the immobilization of hydroxyethyl methacrylate for improving the biocompatibility. Retrieved 2013 from <http://www.ispc-conference.org/ispcproc/ispc20/43.pdf>
- [62] S. Kang, M. Kim, S. Park, and C. Joo. Comparison of clinical results between heparin surface modified hydrophilic acrylic and hydrophobic acrylic intraocular lens. *European Journal of Ophthalmology*, 18(3): 377-383, 2008.
- [63] T. Okano, S. Nishiyama, I. Shinohara, Y. Sakurai, K. Kataoka, and T. Tsuruta. Effect of hydrophilic and hydrophobic microdomains on mode of interaction between block polymer and blood platelets. *Journal of Biomedical Materials Research*, 15(3): 393-402, 1981.
- [64] M. Shimada, M. Miyahara, H. Tahara, I. Shinohara, T. Okano, K. Kataoka, and Y. Sakurai. Synthesis of 2-Hydroxyethyl Methacrylate-Dimethylsiloxane Block Copolymers and their ability to suppress blood platelet aggregation. *Polymer Journal*, 15(9): 649-656, 1983.
- [65] L. Ravenstein, W. Ming, R. D. Grampel, R. Linde, G. With, T. Loontjens, P. C. Thüne, and J. W. Niemantsverdriet. *Macromolecules*, 37(2): 408-413, 2004.

- [66, 67, 145, 147] S. H. Baxamusa and K. K. Gleason. Random copolymer films with molecular-scale compositional heterogeneities that interfere with protein adsorption. *Advanced Functional Materials*, 19: 3489-3496, 2009.
- [68] F. Xia, Y. Zhu, L. Feng, and L. Jiang. Smart responsive surfaces switching reversibly between super-hydrophobicity and super-hydrophilicity. *Soft Matter*, 5: 275-281, 2009.
- [69] A. Solga, Z. Cerman, B. F. Striffler, M. Spaeth, and W. Barthlott. The dream of staying clean: Lotus and biomimetic surfaces. *Bioinspiration & biomimetics*, 2(4): 126-134, 2007.
- [70] J. Shiu, C. Kuo, P. Chen, and C. Y. Mou. Fabrication of tunable superhydrophobic surfaces by nanosphere lithography. *Chemistry of Materials*, 16(4): 561-564, 2004.
- [71] X. Lu, C. Zhang, and Y. Han. Low-density polyethylene superhydrophobic surface by control of its crystallization behavior. *Macromolecules Rapid Communications*, 25(18): 1606-1610, 2004.
- [72] V. A. Gahesh, H. K. Raut, A. S. Nair, S. Ramakrishna. A review on self-cleaning coatings. *Journal of Materials Chemistry*, 21: 16304-16322, 2011.
- [73] M. Qu, B. Zhang, S. Song, L. Chen, J. Zhang, and X. Cao. Fabrication of superhydrophobic surfaces on engineering materials by a solution-immersion process. *Advanced Functional Materials*, 17(4): 593-596, 2007.
- [74] E. Martines, K. Seunarine, H. Morgan, N. Gadegaard, C. D. W. Wilkinson, and M. O. Riehle. Superhydrophobicity and superhydrophilicity of regular nanopatterns. *Nano Letters*, 5(10): 2097-2103, 2005.
- [75] K. Taeshima, H. Sugimura, Y. Inoue, O. Takai, and A. Takano. Transparent ultra water-repellent poly(ethylene terephthalate) substrates fabricated by oxygen plasma treatment and subsequent hydrophobic coating. *Applied Surface Science*, 244(1-4): 619-622, 2005.
- [76] Z. Yoshimitsu, A. Nakajima, T. Watanabe, and K. Hashimoto. Effects of surface structure on the hydrophobicity and sliding behavior of water droplets. *Langmuir*, 18: 5818-5822, 2002.

- [77] D. Öner and T. J. McCarthy. Ultrahydrophobic surfaces. Effects of topography length scales on wettability. *Langmuir*, 16: 7777-7782, 2000.
- [78] M. Gupta and K. K. Gleason. Surface modification of high aspect ratio structures with fluoropolymer coatings using chemical vapor deposition. *Thin Solid Films*, 517(12): 3547-3550, 2009.
- [79] K. E. Karakitsou and X. E. Verykios. Effects of altermultivalent cation doping of titania on its performance as a photocatalyst for water cleavage. *The Journal of Physical Chemistry*, 97(6): 1184-1189, 1993.
- [80] A. Lepre, N. Elliott, S. Bhopal, I. P. Parkin and S. A. O'Neill. Characterization of the photocatalyst Pilkington Active (TM): a reference film photocatalyst. *Journal of Photochemistry and Photobiology A-Chemistry*, 160(3): 213-224, 2003.
- [81] S. Balamurugan, S. Mendez, S. S. Balamurugan, M. J. O'Briee, and G. P. Lopez. Thermal response of poly(N-isopropylacrylamide) brushes probed by surface plasmon resonance. *Langmuir*, 19(7): 2545-2549, 2003.
- [82] P. C. Rieke, J. Liu, G. E. Fryxell, J. S. Young, M. H. Engelhard, and K. L. Alford. Surfaces with reversible hydrophilic/hydrophobic characteristics on cross-linked poly(N-isopropylacrylamide) hydrogels. *Langmuir*, 16(21): 8016-8023, 2000.
- [83] P. S. Curti, M. R. Moura, W. Veiga, E. Radovanovic, A. F. Rubira, and E. C. Muniz. Characterization of PNIPAAm photografted on PET and PS surfaces. *Applied Surface Science*, 245(1-4): 223-233, 2005.
- [84] P. A. Tamirisa, J. Koskinen, and D. W. Hess. Plasma polymerized hydrogel thin films. *Thin Solid Films*, 515(4): 2618-2624, 2006.
- [85] T. Sun, G. Wang, L. Feng, B. Liu, Y. Ma, L. Jiang, and D. Zhu. Reversible switching between superhydrophilicity and superhydrophobicity. *Angewandte Chemie International Edition*, 43: 357-360, 2004.
- [86] Q. Fu, G. V. R. Rao, S. B. Basame, D. J. Keller, K. Artyushkova, J. E. Fulghum, and G. P. Lopez. Reversible control of free energy and topography of nanostructured surfaces. *Journal of American Chemical Society*, 126(29): 8904-8905, 2004.

- [88] F. Xia, L. Feng, S. Wang, T. Sun, W. Song, W. Jiang, and L. Jiang. Dual-responsive surfaces that switch between superhydrophilicity and superhydrophobicity. *Advanced Materials*, 18(4): 432-436, 2006.
- [89, 90, 91, 95, 101, 108] J. Genzer and J. Groenewold. Soft matter with hard skin: From skin wrinkles to templating and material characterization. *Soft Matter*, 4(2): 310-323, 2006.
- [92, 93, 107] D. Y. Khang, J. A. Rogers, and H. H. Lee. Mechanical buckling: Mechanics, metrology, and stretchable electronics. *Advanced Functional Materials*, 19(10): 1526-1536, 2009.
- [94, 102] A. Schweikart and A. Fery. Controlled wrinkling as a novel method for the fabrication of patterned surfaces. *Advances in Polymer Science*, 165(3-4): 249-263, 2009.
- [96, 97] N. Bowden, W.T.S. Huck, K. E. Paul, and G. M. Whitesides. The controlled formation of ordered, sinusoidal structures by plasma oxidation of an elastomeric polymer. *Applied Physics Letters*, 75: 2557, 1999.
- [100] W. T. S. Huck, N. Bowden, P. Onck, T. Pardoen, J. W. Hutchinson, and G. W. Whitesides. Ordering of spontaneously formed buckles on planar surfaces. *Langmuir*, 16(7): 3497-3501, 2000.
- [103] S. Singamaneni and V. V. Tsukruk. Buckling instabilities in periodic composite polymeric materials. *Soft Matter*, 6(22): 5681-5692, 2010.
- [104] C. Harrison, C. M. Stafford, W. Zhang, and A. Karim. Sinusoidal phase grating created by a tunably buckled surface. *Applied Physics Letters*, 85(18): 4016, 2004.
- [105] C. M. Stafford, C. Harrison, K. L. Beers, A. Karim, E. J. Amis, M. R. VanLandingham, H. Kim, W. Volksen, R. D. Miller, and E. E. Simonyi. A buckling-based metrology for measuring the elastic moduli of polymeric thin films. *Nature Materials*, 3: 545-550, 2004.
- [106] A. J. Nolte, M. F. Rubner, and R. E. Cohen. Determining the Young's modulus of polyelectrolyte multilayer films via stress-induced mechanical buckling instabilities. *Macromolecules*, 38(13): 5367-5370, 2005.

- [109, 110] D. Eggenpieler. New paradigm to design micro and nano-patterned membranes. MSc Thesis, Massachusetts Institute of Technology. 2010
- [111, 112] J. F. Schumacher, C. J. Long, M. E. Callow, J. A. Finlay, J. A. Callow, and A. B. Brennan. Engineered nanoforce gradients for inhibition of settlement (attachment) of swimming algal spores. *Langmuir*, 24(9): 4931-4937, 2008.
- [113] K. Efimenko, J. Finlay, M. E. Callow, J. A. Callow, and J. Genzer. Development and testing of hierarchically wrinkled coatings for marine antifouling. *Applied Materials and Interfaces*, 1(5): 1031-1040, 2009.
- [114] W. Hamilton and W. G. Characklis. In structure and function of biofilms. Eds: Wiley: New York, 1989; pp 199-219.
- [115, 118] D. Cunliffe, C. H. Alarcon, V. Peters, J. R. Smith, and C. Alexander. Thermoresponsive surface grafted poly(N-isopropylacrylamide) copolymers: Effect of phase transitions on protein and bacterial attachment. *Langmuir*, 19: 2888-2899, 202.
- [116] M. E. Alf, T. A. Hatton, and K. K. Gleason. Insights into thin, thermally responsive polymer layers through quartz crystal microbalance with dissipation. *Langmuir*, 27: 10961-10968, 2011.
- [117] E. C. Cho, Y. D. Kim, and K. Cho. Thermally responsive poly(N-isopropylacrylamide) monolayer on gold: synthesis, surface characterization, and protein interaction/adsorption studies. *Polymer*, 45(10): 3195-3204, 2004.
- [119] L. K. Ista, and V. H. Perez-Luna, and G. P. Lopez. Surface-grafted, environmentally sensitive polymers for biofilm release. *Applied and environmental microbiology*, 165(4): 1603-1609, 1999.
- [120] P. Klemm, R. M. Vejborg, and M. Hancock. Prevention of bacterial adhesion. *Applied Microbiology and Biotechnology*, 88: 451-459, 2010.
- [122, 126, 129, 131, 133] K. K. Gleason et al. Chemical vapor deposition of conformal, functional, and responsive polymer films. *Advanced Materials*, 22(18): 1993-2027, 2010.

- [123] Y. Au, Q. M. Wang, H. Li, J. Lehn, D. Shenai, and R. G. Gordon. Vapor deposition of highly conformal copper seed layers for plating through-silicon vias (TSVs). *Journal of the Electrochemical Society*, 159(6): 382-385, 2012.
- [124, 127] W. E. Tenhaeff and K. K. Gleason. Initiated and oxidative chemical vapor deposition of polymeric thin films: iCVD and oCVD. *Advanced Functional Materials*, 18: 979-992, 2008.
- [125, 130] K. K. Gleason et al. Initiated chemical vapor deposition (iCVD) of polymeric nanocoatings. *Surface and Coatings Technology*, 201(22-23): 9400-9405, 2007.
- [128] M. Gupta and K. K. Gleason. Large-scale initiated chemical vapor deposition of poly(glycidyl methacrylate) thin film. *Thin Solid Films*, 515(4): 1579-1584, 2006.
- [132] W. S. O'Shaughnessy, M. Gao, and K. K. Gleason. Initiated chemical vapor deposition of trivinyltrimethylcyclotrisiloxane for biomaterial coating. *Langmuir*, 22: 7021-7026, 2006.
- [134] W. E. Tenhaeff and K. K. Gleason. Initiated chemical vapor deposition of alternating copolymers of styrene and maleic anhydride. *Langmuir*, 23(12): 6624-6630, 2007.
- [135] K. K. S. Lau and K. K. Gleason. Initiated chemical vapor deposition (iCVD) of poly(alkyl acrylates): An experimental study. *Macromolecules*, 39(10): 3688-3694, 2006.
- [136] M. Kim, B. Moon, and C. Hidrovo. Enhancement of the thermo-mechanical properties of PDMS molds for the hot embossing of PMMA microfluidic devices. *Journal of Micromechanics and Microengineering*, 23(9): 2013.
- [137] D. J. Campbell, K. J. Beckman, C. E. Calderon, P. W. Doolan, R. H. Moore, A. B. Ellis, G. C. Lisensky. Replication and compression of bulk surface structures with polydimethylsiloxane elastomer. *Journal of Chemical Education*, 76: 1999.
- [138] Y. Huang, Z. Yin, and Y. Xiong. Thermomechanical analysis of film-on-substrate system with temperature-dependent properties. *Journal of Applied Mechanics*, 77(4): 2010.

- [139] K. Efimenko, M. Rackaitis, E. Manias, A. Vaziri, L. Mahadevan, and J. Genzer. Nested self-similar wrinkling patterns in skins. *Nature Materials*, 4: 293-297, 2005.
- [140] J. Wang, A. Sutti, X. Wang, and T. Lin. Thermoresponsive hercosett/poly(N-isopropylacrylamide) films: a new, fast optically responsive coating. *Journal of Colloid and Interface Science*, 369(1): 231-237, 2012.
- [141] J. Dybal, M. Trchova, and P. Schmidt. The role of water in structural changes of poly(N-isopropylacrylamide) and poly(N-isopropylmethacrylamide) studied by FTIR, Raman spectroscopy and quantum chemical calculations. *Vibrational Spectroscopy*, 51(1): 44-51, 2009.
- [142] M. E. Alf, T. A. Hatton, and K. K. Gleason. Novel N-isopropylacrylamide based polymer architecture for faster LCST transition kinetics. *Polymer*, 52(20): 4429-4434, 2011.
- [143] X. Xu, A. V. Goponenko, and S.A. Asher. Polymerized PolyHEMA photonic crystals: pH and ethanol sensor materials. *Journal of American Chemical Society*, 130(10): 3113-3119, 2008.
- [146] M. Gupta and K. K. Gleason. Initiated chemical vapor deposition of poly(1H,1H,2H,2H-perfluorodecyl Acrylate) thin films. *Langmuir*, 22(24): 10047-10052, 2006.
- [144] K. Chan and K. K. Gleason. Initiated chemical vapor deposition of linear and cross-linked poly(2-hydroxyethyl methacrylate) for use as thin-film hydrogels. *Langmuir*, 21: 8930-8939, 2005.
- [148, 150, 151, 152, 156, 157] R. T. Hendricks and I. Lee. Wrinkle-free nanomechanical film: Control and prevention of polymer film buckling. *Nanoletters*, 7(2): 372-379, 2007.
- [153, 154] N. Bowden, W. T. Huck, K. E. Paul, and G. M. Whitesides. The controlled formation of ordered, sinusoidal structures by plasma oxidation of an elastomeric polymer. *Applied Physics Letters*, 75: 1999.

[155] W. T. Huck, N. Bowden, P. Onck, T. Pardoen, J. W. Hutchinson, and G. M. Whitesides. Ordering of spontaneously formed buckles on planar surfaces. *Langmuir*, 16(7): 3497-3501, 2000.